



BRNO UNIVERSITY OF TECHNOLOGY

VYSOKÉ UČENÍ TECHNICKÉ V BRNĚ

FACULTY OF CHEMISTRY

FAKULTA CHEMICKÁ

INSTITUTE OF MATERIALS SCIENCE

ÚSTAV CHEMIE MATERIÁLŮ

**RESEARCH OF COATINGS OF HYDRODYNAMICALLY
LUBRICATED SLIDING BEARINGS FOR COMBUSTION
ENGINES**

RESEARCH OF COATINGS OF HYDRODYNAMICALLY LUBRICATED SLIDING BEARINGS FOR
COMBUSTION ENGINES

DOCTORAL THESIS

DIZERTAČNÍ PRÁCE

AUTHOR

AUTOR PRÁCE

Ing. Martin Repka

SUPERVISOR

ŠKOLITEL

prof. Ing. Jaromír Havlica, DrSc.

BRNO 2017

Zadání dizertační práce

Ústav: Ústav chemie materiálů
Student: **Ing. Martin Repka**
Studijní program: Chemie, technologie a vlastnosti materiálů
Studijní obor: Chemie, technologie a vlastnosti materiálů
Vedoucí práce: **prof. Ing. Jaromír Havlica, DrSc.**
Akademický rok: 2016/17

Název dizertační práce:

Research of Coatings of Hydrodynamically Lubricated Sliding Bearings for Combustion Engines

Zadání dizertační práce:

Cílem disertační práce je studium nové formulace ložiskové vrstvy s pokročilými tribologickými vlastnostmi.

- Strukturní a tribologická charakterizace základní vrstvy PAI polymerního povlaku od Daido Metal
- Sledování možné interakce mezi mazivy a ložiskovými plochami, zejména v okrajových podmínkách
- Studium vlivu přísadky $\text{Ca}(\text{OH})_2$ na tribologické chování povrchu PAI kluzné vrstvy

Termín odevzdání dizertační práce: 30.5.2017

Ing. Martin Repka
student(ka)

prof. Ing. Jaromír Havlica, DrSc.
vedoucí práce

prof. RNDr. Josef Jančář, CSc.
vedoucí ústavu

V Brně dne 1.9.2016

prof. Ing. Martin Weiter, Ph.D.
děkan

ABSTRAKT

Hlavní náplní této dizertační práce je výzkum a vývoj nové povrchové vrstvy pro kluzná ložiska na bázi pevných lubrikantů v polyamid-imidové polymerní matrici se zlepšenými tribologickými vlastnostmi. Podklady pro materiálovou kompozici vzešly z expertízy komerčně dostupného povlaku, respektive jeho povrchovou analýzou v mezních operačních podmínkách. Charakterizace mazného oleje před a po tribotestování společně s detailní povrchovou analýzou dala podmínky pro vznik materiálové formulace. Další část práce se zabývá studiem přípravy a vývojem aplikačního nanášení s přípravou polymerní směsi. Nakonec je popsána studie vlivu sulfidu molybdeničitého a grafitu, jakožto pevných lubrikantů pro zlepšení třecích vlastností a hydroxidu vápenatého pro potenciální zlepšení ořezuvzdornosti výsledného povrchu pro palikaci kluzných ložisek.

ABSTRACT

The aim of this thesis is the research and characterisation of new sliding bearing overlay with advanced tribological properties based on the polyamide-imide matrix and solid lubricants. The background for the material composition came from the joint initial expertise of commercial coating layer, respectively its surface observation under boundary operational conditions which provided input for improved wear and friction characteristics. Oil characterisation before and after tribotesting and detailed surface chemistry analysis was performed to investigate polymer coating behaviour in stressed lubricated conditions. Further development of coating technique with preparation of newly formulated paint is introduced. Finally, the developed PAI coating with MoS₂ and graphite as lubricants for frictional improvement and calcium hydroxide as potential wear improvement additive were studied and evaluated for bearing application.

KLÍČOVÁ SLOVA

Kluzná ložiska, povlak, mazání, tribologické vlastnosti, opotřebení, tření.

KEYWORDS

Sliding bearing, coating, lubrication, tribological properties, wear, friction.

REPKA, M. *Research of Coatings of Hydrodynamically Lubricated Sliding Bearings for Combustion Engines*. Brno: Vysoké učení technické v Brně, Fakulta chemická, 2017. 113 s. Vedoucí dizertační práce prof. Ing. Jaromír Havlica, DrSc..

Declaration

I declare that the doctoral thesis has been worked out by myself and that all the quotations from the used literary sources are accurate and complete.

.....
student's signature

Acknowledgements

I would like to express my gratitude to doc. Ing. František Šoukal, Ph.D. for his time, knowledge and professional advice during my doctoral study and to prof. Ing. Jaromír Havlica, DrSc for supervising.

My sincere thanks goes to colleagues and whole company Daido Metal Co., Ltd. - organizační složka, The European Technical Centre for financial, material, technical and investigation support, AC2T research GmbH for cooperation in tribochemical feasibility study and Department of Tribology at Institute of Machine and Industrial Design, Faculty of Mechanical Engineering at Brno University of Technology for access to optical profilometer.

Last but not least, I would like to thank my parents and rest of family for their life long support and my girlfriend for being patient with me during the last months of finishing the thesis.

1 TABLE OF CONTENTS

| | | |
|-------|---------------------------------------|----|
| 1 | Table of contents | 5 |
| 2 | Introduction | 8 |
| 3 | Tribology of sliding components | 10 |
| 4 | Engine bearings | 10 |
| 4.1 | Materials | 11 |
| 4.2 | Material compositions | 18 |
| 4.2.1 | Tin and lead materials | 18 |
| 4.2.2 | Aluminium alloys | 19 |
| 4.2.3 | Copper alloys | 19 |
| 4.3 | Production of engine bearings | 19 |
| 4.3.1 | Sintering | 20 |
| 4.3.2 | Casting | 21 |
| 4.3.3 | Rolling process | 21 |
| 4.4 | Coatings | 22 |
| 4.4.1 | Electrochemical deposition | 24 |
| 4.4.2 | Sputter coating | 24 |
| 4.5 | Polymers in engine bearings | 25 |
| 4.5.1 | Nylon | 25 |
| 4.5.2 | Polytetrafluorethylene (PTFE) | 26 |
| 4.5.3 | Polyether ether ketone (PEEK) | 26 |
| 4.5.4 | Polyamide-imide (PAI) | 28 |
| 4.5.5 | Other polymers | 34 |
| 4.5.6 | Additives in polymers | 34 |
| 4.5.7 | Calcium hydroxide | 35 |
| 5 | Experimental | 36 |
| 5.1 | Goals of the dissertation | 37 |
| 5.1.1 | Subgoals | 37 |
| 5.2 | Overview of the used materials | 38 |
| 5.2.1 | Bearings | 38 |
| 5.2.2 | Polyamide-imide (PAI) | 38 |
| 5.2.3 | Solid lubricants | 40 |
| 5.2.4 | Calcium hydroxide | 41 |
| 5.3 | Preparation of paint | 42 |

| | | |
|-------|---|-----|
| 5.3.1 | Viscosity measuring..... | 42 |
| 5.3.2 | Application to the surface..... | 44 |
| 5.4 | Tribochemical analysis..... | 45 |
| 5.4.1 | Oil analysis | 45 |
| 5.4.2 | Surface characterisation | 47 |
| 5.4.3 | Tribotesting..... | 49 |
| 6 | Results and Discussion..... | 53 |
| 6.1 | Tribotesting..... | 53 |
| 6.2 | Lubricant analysis | 54 |
| 6.2.1 | Conventional oil analysis | 54 |
| 6.2.2 | Chemistry of fresh oil by advanced analysis | 56 |
| 6.2.3 | Chemistry of used oil | 58 |
| 6.3 | Surface characterisation | 61 |
| 6.3.1 | Non-destructive 3D microscopy | 61 |
| 6.3.2 | SEM-EDX analysis | 62 |
| 6.3.3 | XPS analysis | 65 |
| 6.3.4 | Surface chemistry by mass spectrometry | 69 |
| 6.4 | Implementation of results into surface layer formulation..... | 71 |
| 6.5 | PAI Characterisation..... | 72 |
| 6.5.1 | FTIR of PAIs | 72 |
| 6.6 | Coating preparation and characterisation..... | 74 |
| 6.6.1 | Shot blasting..... | 74 |
| 6.6.2 | Results of spraying | 75 |
| 6.6.3 | EDX analysis | 76 |
| 6.6.4 | Nanoindentation | 78 |
| 6.6.5 | Adhesion of polymer coatings..... | 80 |
| 6.7 | Tribotesting..... | 81 |
| 6.7.1 | Ball on disc | 81 |
| 6.7.2 | Block on ring testing | 82 |
| 6.7.3 | Surface characterisation of tested parts..... | 84 |
| 7 | Conclusion..... | 89 |
| 8 | Future work..... | 91 |
| 9 | APPENDIX | 92 |
| 9.1 | Appendix 1 Surface profile analysis | 92 |
| 9.2 | Appendix 2 Micro-scratch testing | 102 |

| | | |
|-----|--|-----|
| 9.3 | Appendix 3 Roughness on the counterparts | 106 |
| 10 | List of abbreviations | 108 |
| 11 | References..... | 109 |

2 INTRODUCTION

Automotive industry tends to more environmentally friendly and more efficient combustion engines. There are several approaches how to achieve this. One of the options is engine downsizing which goes along with high power densities resulting in substantially increased local contact pressures of rolling or sliding contacts and leading to enhanced danger of seizure [1]. Highly affected machine component by this trend are engine bearings. They are designed for increased fatigue loads but also conforming the variations in alignments [2]. Further needs for tribological requirements on the bearings include low friction, higher wear resistance, embeddability, conformability as well as corrosion resistance, etc. Therefore, research needs to compromise tribological properties, mechanical strength, and chemical performance of the material [3, 4, 5, 6, 7].

Recently, to satisfy the above needs for bearing material, resin overlays, where solid lubricant is dispersed in a resin binder, are being developed [8,9,10]. Due to the beneficial effect of solid lubricants on friction, wear is less likely to progress compared with conventional Al-Sn-Si based bearing alloys. Several inorganic materials (e.g., boron nitride, graphite) can provide excellent lubrication [11] from which MoS₂ is used in the studied resin overlay. The layer (which contains CaCO₃) helps to improve seizure properties of the bearing as well as good embeddability [12].

In tribotesting where loading is systematically applied to the lubricated bearing surface, some changes in material composition can occur resulting in different tribological performances of the surfaces. The changes refer to structural changes between the sliding surfaces which have effects on the tribological conditions [13]. Formed tribolayer can protect or contribute to the degradation of materials in contact [14] as well as influencing the resulting performances in the application. Rough surfaces formed in sliding contacts increase the local stress [15]. Tribo-chemical interactions, tribo-oxidation of formed tribolayers or debris can be formed which may cause material failures [16,17].

Understanding of mechanism and kinetics of the layer's formation, stability and tribological behaviour was important for further material study and research. Oil characterisation before and after tribotesting, together with surface chemistry analysis, was performed to find out degradation products and interactions towards tribolayer formation and material structure changes of the used bearing shell. The results led to understanding of several material phenomena and gave an input for material selection and further development of the bearing surface layer.

The goal of the dissertation was to study and research new potential for sliding bearing overlay with advanced tribological properties. Since the spectrum of the goal was not entirely specific and the direction was needed, joined expertise and past research in Daido Metal, the bearing producer has been done. Therefore, exchange of knowledge in product performance and subsequent analytical approach with the help of AC2T research GmbH (Austrian Competence Center for Tribology) in Austria was carried out to achieve the material knowledge base as a core feature in further development.

Initially the proposed methodology for the comprehensive description of the composition of tribolayers was generated by the operation of bearings lubricated with engine oil and evaluation was carried out on commercially available polymer coating. Detailed topography, morphology and chemistry of new and stressed surfaces of sliding parts on engine bearings were characterized by appropriate surface analytical tools. The findings served as a

feasibility study of the usefulness of analytical tools contributing to further material research on new developed coating and put the valuable inputs for formulating the new paint for coating.

The positive tribological effect of molybdenum disulphide was already confirmed and has been studied by many as a well-known solid lubricant [18]. That is the reason why it has been chosen as solid lubricant additive also for new studied coating. It has lamellar structures consisting of a stack of hexagonal sheets (planes) with strong covalent bonds and weak Van der Waals forces between the planes holding them together [19]. This lead to an idea to use Calcium Hydroxide and its hexagonal form of sheet plates in the polymer matrix of polyamide-imide (which is used for its heat resistance). The study covered the laboratory testing of resulting coating and preliminary formulation and preparation. The application method needed to be developed together with laboratory testing for tribological characteristics.

3 TRIBOLOGY OF SLIDING COMPONENTS

Tribology is in existence since recorded history, and there are well documented examples from history how early civilizations developed bearings and low friction surfaces [20]. The scientific study of tribology has the long period as well. Many laws of friction such as proportionality between normal force and limiting friction force were generally associated to Leonardo da Vinci in the late 15th century. On the other hand this multidisciplinary study is the domain of last two centuries and most of the knowledge is being gained since the Second World War.

Tribology is a science focused on friction, wear and lubrication of interacting surfaces in relative motion. The term is derived from the Greek word 'tribos' meaning rubbing or sliding.

Wear is the main reason of losing mechanical properties of material components. Therefore any reduction in wear could result in considerable savings. Friction is on the other hand cause of wear and energy dissipation. It results in easy implication that by friction control we can achieve a considerable saving. It is estimated that one third of the world's energy resources in present use is needed to overcome friction in one form or another. Lubrication is an effective tool for controlling wear and reducing friction. Tribology is a field of science which applies an operational analysis to problems of great economic significance such as reliability, maintenance and wear of technical equipment ranging from household appliances to spacecraft [21].

4 ENGINE BEARINGS

Engine bearings are the representatives of sliding bearings. Compared to the rolling bearings, sliding ones are easier to produce and therefore cheaper. The reason why they are used in engines is primarily in their ability to withstand high loading, dirt and especially vibration. Also important is that they can be assembled much more easily compared to the rolling bearings.

The engine bearings are loaded dynamically due to piston cycles in the engine. We are therefore talking about the hydrodynamic bearings (direction and size of load varies over time).

Hydrodynamic bearings are then distinguished according to the direction of force applied to the bearing:

- Radial – loading is applied perpendicular to the axis of bearing,
- Axial – enable to transfer the load in axial direction (to the axis of bearing),
- Combined – able to combine both the force directions (e.g. conic shape bearings).

From the design point of view we distinguish between bushings (unseparated bearing) and half shell bearings which can be seen also in Figure 1. The main focus of this dissertation is towards the connecting rod bearings (rod bearings) where the higher load is applied and special material is required.

Half shell engine bearings are a vital construction part of engines which help to convert reciprocating motion of the pistons into the rotary motion of the crankshaft. The main application is in the combustion engine [22]. The loading is generated by pressure of gases

in cylinder and inertial forces of reversible and rotating unbalanced masses. These dynamic forces have the main effect on the hydrodynamic oil film generation as well as on the fatigue of resulting material. The reasons of the separation into two half shells are mainly because of easy manipulation assembly and especially maintenance. Bushings in general are not that easy to dismantle from shaft and moreover, they are not recommended be used repeatedly [23].

There are several kinds of bearings used in engine (see Figure 1).

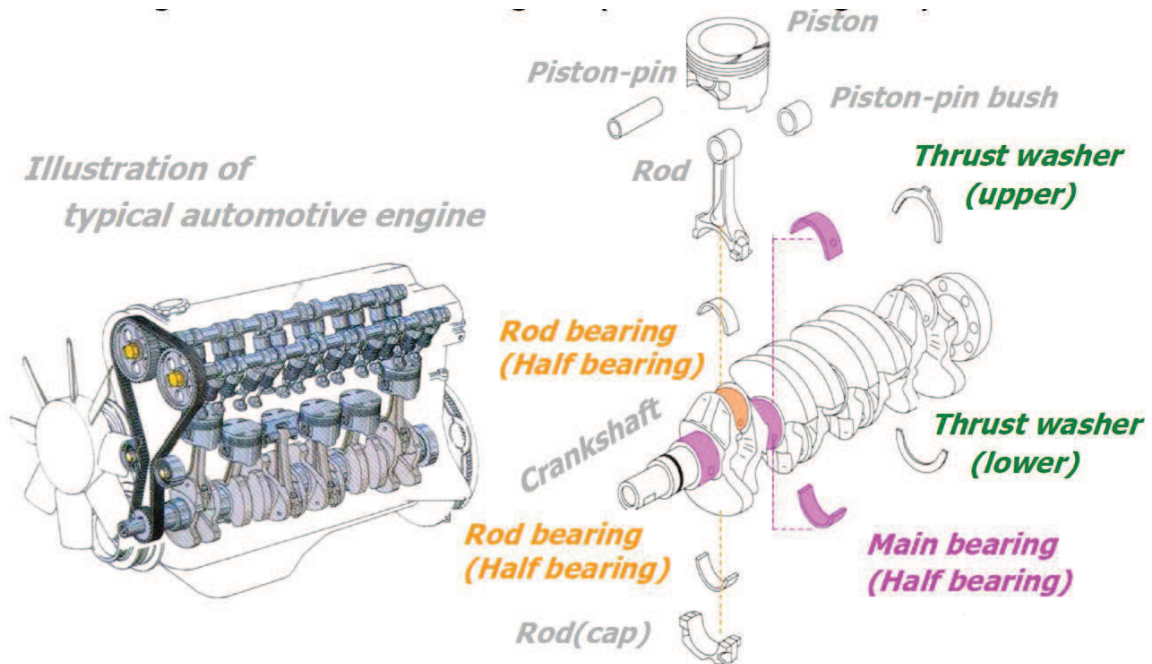


Figure 1 Illustration of typical engine bearings in automotive combustion engine part [24]

Considering the current trends of engine market, also increasing working cycles is among the targets. It results in increasing requirements on reliability and durability of sliding parts in higher rotation speeds and increased loading [25]. With increased sliding speed, maximum of hydrodynamic load bearing capacity is theoretically increased. On the other hand, it's also increasing the friction on the bearing, which generates temperature. This temperature has effect on the bearing as well as lubricant viscosity which is decreasing with increased temperature and that is what has effect on the load bearing capacity of hydrodynamic oil film. All of these phenomena result in the specific material selection on each engine bearing part separately calculated.

4.1 Materials

Bearing materials need to have special properties to operate successfully in machine parts. These materials depend on the type of bearing, type of lubricant and the environmental conditions. There is no single material satisfying all the applications [26].

There are several vital material properties for bearings. The overall need for strength and stability of the shape, the steel is considered the best material. As other unique properties like wear resistance, fatigue resistance, conformability, anti-seizure, and embeddability characteristics, etc. (described later) varies depending on the speed, size and changes in load, shaft (counterpart) materials, lubrication method and environmental factors such as

temperature and humidity. The important aspect in designing is therefore selecting proper sliding bearing material which can work in emergency conditions. It is a stage in the process where the system is running at low rotation speeds (mainly stop and start of the machine). Bearing is led into boundary lubrication regime, where thickness of oil/lubricant in the contact is low between the contacting areas, and localized contact of the counterparts (bearing and shaft) can appear and these phenomena can then lead to the seizure of bearing.

Good material therefore has to exhibit fatigue performance and compressive strength which will lead to sufficient load bearing capacity. Simultaneously, bearing has been conformable to certain surface deformation of parts which it is belonging to.

There are a lot of requirements whereas some of them are antagonistic and therefore the multi-layered material combinations have been developed in past decades. The key properties characterizing bearings are described below.

Compatibility

The operation is characterized by hydrodynamic regime when the shaft is separated from the oil by lubricant film. Starting and stopping the engine or even during the engine run, the shaft and the bearing come into the contact. The boundary or mixed lubrication regime occurs. Localized heating occurs during the contact causing some welding of parts and can lead to damage at these points. This phenomenon usually results in scoring damage to both the shaft and bearing materials. Compatibility leads to the ability of these material combinations to resist welding and scoring.

Embeddability

Engine operation causes wear of some constructing parts and forms wear debris which eventually comes into bearing clearance by the lubricant. Unfortunately, most often it is not possible to be removed by oil filter. The particles are still bigger than the minimum oil film thickness in lubricated components (e.g. crankshaft bearings). In order to operate successfully, the lubricated component must have a layer with ability to embed small hard particles into the surface without damaging the counterpart (in our case the shaft surface) as well as stopping to form scratches on its surface. The side effect due to hard particle pollutant is the increase in friction of the bearing which can eventually cause friction increase [27]. Ability of bearing surface to embed particles to the softer bearing material is essential in order to prevent possible scoring damages.

In Figure 2, the hard particle has produced an undesirable score on an aluminum/tin alloy surface. Generally, the embeddable layer (usually called overlay) is designed with a thickness close to the lubricant filter threshold. Overlay material property needs a low hardness but on the other hand high ductility and a high elastic modulus to avoid a forcing of the aggressive particles back to the contact. Such a problem is frequently encountered with hyper-elastic materials like elastomer seals.

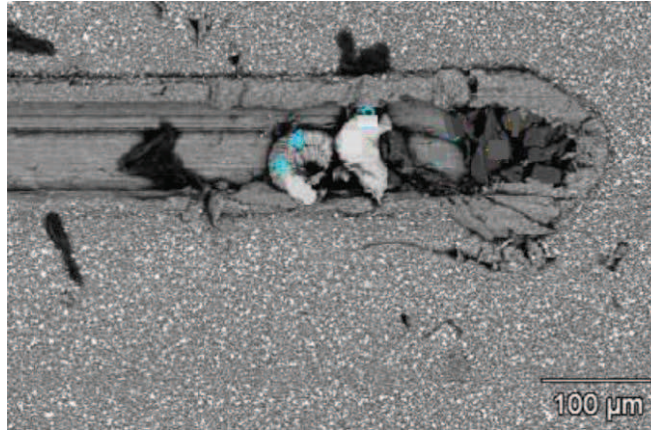


Figure 2 Particle embedded into the aluminium alloy [28]

Conformability

The ability refers to adjustment of bearing in conformal contacts. Bearing material needs to be able to misalign or deform easily between shaft and housing and challenge potential geometric inaccuracies caused by production of parts. Usually, bearing materials that have a low modulus of elasticity (low E) are readily conformable.

Corrosion resistance

Lubricant can represent aggressive conditions in which bearing has to be able to operate. Therefore the bearing material should be resistant to attack by lubricant as well as any other oxidation products produced during lubricant alteration or degradation. In most cases, lubrication oils are composed of additives covering also oxidation inhibitors. In the alteration process of the oil, these additives usually degrade and can produce organic acids, which invade and cause corrosion of certain bearing materials.

Fatigue resistance

The fatigue damages are a complex topic especially when we try to use approach similar to that of the classical material fatigue structural analysis. The overall target of fatigue analysis which is applied to the engine bearing material evaluation is to estimate the cycle number which generates microscopic nucleation in antifriction material.

Figure 3 and Figure 4 represent the three specific fatigue related scenarios based on the differences in materials. Figure 3 represents thick aluminium alloy bearing material where a vertical crack has formed down to the backsteel. It can be seen in Figure 3A that there is a horizontal crack in the adhesion layer to the backsteel as compared to the Figure 3B where no crack in adhesion layer is observed. Adhesion problems not always can be considered the reason. Problems are more complex to evaluate as it can come from several reasons (e.g. heavy load, faulty shape of shaft or housing, etc.)

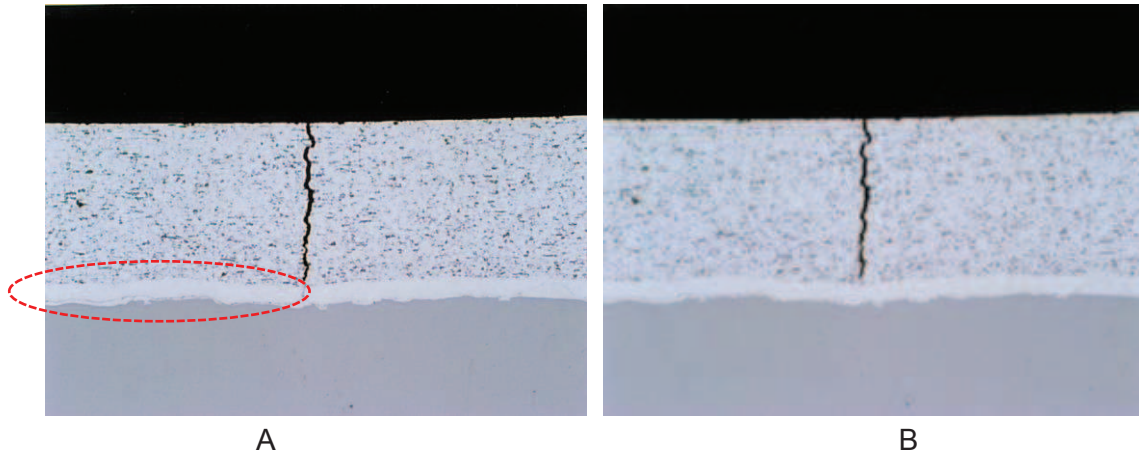


Figure 3 Thick layer with weak (A) and strong (B) bonding [24]

Figure 4 shows a different situation where only thin overlay is depressed, however, no problem is found in the alloy structure.

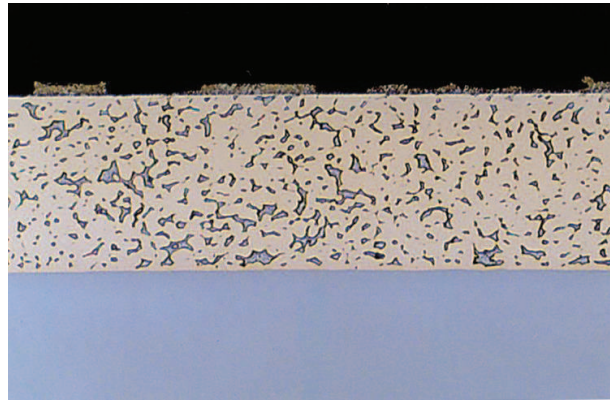


Figure 4 Thin layer fatigue [24]

In combustion engines, frequency and amplitude of loading is changing and depends also on the engine performance. Intensity usually varies cyclically. Fatigue failures can therefore be easily observed initially as cracks in the bearing surface. These cracks propagate usually in the lining of bearing bimetal, interconnecting with other cracks which can be observed. Apart from the loading, high temperature and inhomogeneity of material can cause the damage. This was not the problems of the figures above.

Bearing supplier had to come with simplification of the complexity resulting in an efficient fatigue analysis for bearing materials. They use specific pressure, or diametral pressure as a criterion. It is used formula where radial load F is divided by bearing length L and shaft diameter D .

$$P_{spec} = \frac{F}{LD} \quad (1)$$

Accurate fatigue resistance determination requires advanced measuring involving stress tensors, tridimensional fatigue analysis, using thermo-elasto-hydro-dynamic calculations, etc.

In general point, fatigue testing are expensive methods and therefore calculations usually are in place.

Experimental verification of calculations is done by application tests. Bearing manufacturers use rig tests which involve hydraulics for applying cycling load in high frequency and force until the moment when the crack is identified and measure maximum cycles which the material still can resist.

Wear resistance

Wear is as complex problem as fatigue. It is characterized as “a progressive destructive complex phenomenon which occurs during relative motion of two counteracting surfaces and deterioration of surfaces takes place in industrial operations” [29].

Regarding the bearing, we distinguish also different kind of wear associated with defects on the bearings:

Adhesive wear

During the running is the assurance of lubrication failure almost leading to sliding metals in contact where adhesion followed by wear is generated [30]. Adhesive wear (see Figure 5) is a surface damage and material removal which appears when counterpart smooth surface materials are in contact in an area of oil film breakdown. In these places, high local loading occurs which involves plastic deformations, elevated temperatures and local micro-weldings [31].



Figure 5 Detail of adhesive wear on engine bearing (AlSn20Cu1 alloy) [32]

Adhesive wear can exist as a form of seizure which corresponds to increased temperature even up to the melting point of sliding material. The faster the sliding speeds, the faster the seizure process results in changes of mechanical properties and structure in a range of 0.005 to 0.08 mm. Deeper changes leads to seizure of bearing.

Adhesive wear can be prevented by several measures:

- Precise geometric shape (roundness and roughness influence negatively number of local loading contacts, plastic deformation and temperature – lower possibility of junctions, micro-weldings).
- Counterpart material selection.
- Stability of oil film in boundary regime and formation of boundary layer (e.g. by chemical absorption).

Abrasive wear

When surface is loaded against particles from harder material, an abrasive wear occurs. Hard particles can be formed from counterpart where frictional effect causes ripping of some parts. Source of abrasive wear formation is also in particles attached to the surface of one counterpart and free particles coming to the contact with oil (damaging surfaces of both counterparts). The process is mechanical unless other aggressive conditions are in place. Harder material resist better to abrasive wear. On the other hand, embeddability of material can cause another potential elimination of hard particles. Particles can also be hardened from plastic deformations or oxidation in sliding contact.

The example of abrasive wear evolution is described on the mechanism in Figure 6 where microcuttings and fatigue due to counterbody's hard surface asperities or hard particles in the contact.

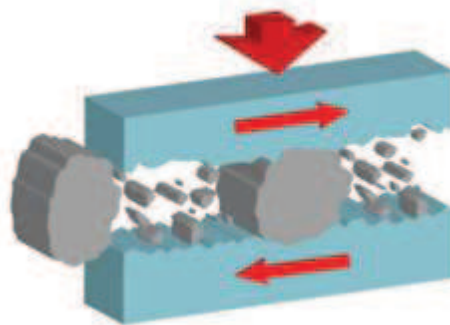


Figure 6 Mechanism of abrasive wear [33]

Tribochemical Reactions

In tribochemical reactions, the chemical reactions take place between the substrate material and counterpart because of the friction-induced activation in the main loaded area near surface zones with elements of the lubricant or ambient medium. Compared with the base body and counterbody, the reaction products exhibit changed properties and, after reaching a certain thickness, can be subjected to brittle chipping or even exhibit properties reducing friction and/or wear.

Seizure

Seizure is a failure of biggest importance for bearing design engineers. Seized bearings cause a serious damage in potential engines and materials and dimensions need to be chosen carefully to avoid it.

Theoretically, seizure occurs when the heat generation is higher than the heat dissipated by heat transfer and by lubricant flow. Practically, from experiences we know that seizure is mostly due to geometrical defects. It happens when the shaft directly contacts the bearing due to the lack of oil, startup, stoppage, uneven contact, etc., and severe overheating or surface flow results in even further heating causing adhesion or seizure. Too low clearance or too high clearance can generate high heat generation in bearings, which can induce seizure.

Illustration in Figure 7 represents the described phenomena. There are two domains of bearing seizure (red on figure) with respect to the clearance and the speed. For a large

clearance, seizure is induced by asperity contact. For a low clearance, seizure is due to clearance reduction by different thermal expansion between the shaft and the housing.

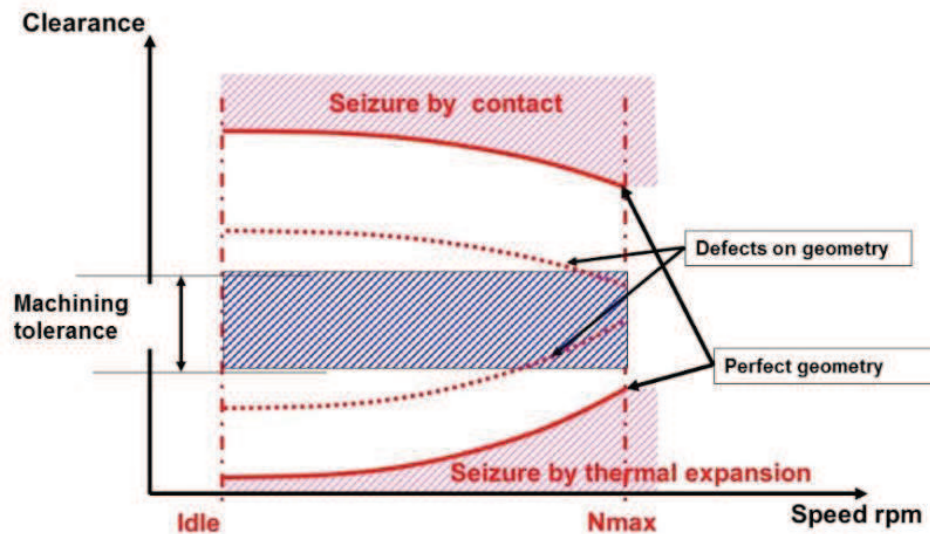


Figure 7 Seizure graph [34]

Bearing surface is machined (often using a process called boring) with some tolerances for the dimensions. The aim is to achieve clearance set by design engineers. Blue part of the graph is the variation for this machining in order to assess the seizure risk with respect to this machining tolerance. Shaft geometry or bearing geometry is not possible to machine perfectly. Therefore, local geometrical defects must also be taken into account to determine the seizure domain limits. The seizure areas will grow with respect to the geometrical defect amplitude. With the help of the red dot lines, it is possible to introduce worse geometrical defects to check if the clearance variation is still in a range to avoid seizure. Imply the blue rectangle must not cross the dotted red lines.

So, for new bearing designs, it is necessary to estimate the friction (mixed and hydrodynamic) for bearings with the largest geometrical defects associated with the bearing and shaft machining quality.

Practical example of improper machining quality of shaft can be seen in the Figure 8 where the seizure is observed around the centre of main bearing. Shaft ran-out and caused stop of the engine.

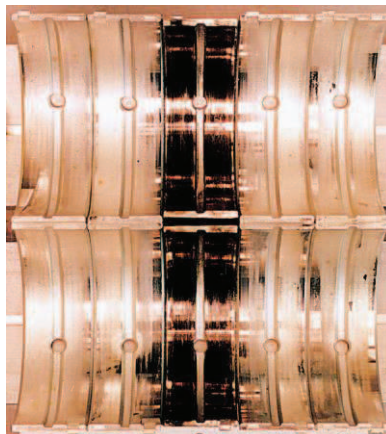


Figure 8 Seizure is observed on the centre of main bearing [24]

Thermal resistance

The thermal characteristics of the bearing material are difficult to approach. It has to be considered with regard to both heat dissipation and thermal distortion. The thermal conductivity is considered high to ensure maximum dissipation of the frictional heat generated in boundary and mixed lubrication regimes and has strong effect on seizure properties.

Further parameter which should be taken into account is linear thermal expansion coefficient. Bearing design has tough tolerances which could result in problematics in temperature variations.

Cavitation resistance

Cavitation erosion damage to bearing surfaces is a form of micro fatigue cracking initiated by the collapse of vapour cavities. Most commonly is observed near the oil hole where the oil enters the contact of bearing with shaft. Usual general knowledge is that lubrication conditions are necessary to change regarding the oil pressure or flow rate.

4.2 Material compositions

The composition of bearing material is usually concern of confidentiality for each bearing producer. Looking at the history of sliding bearings, probably the oldest one was made of wood (wheel connected to wooden housing). Further development especially in driving parts needed revolution in materials. Leonardo da Vinci recommended the tin for bearing [35] and before leaded bearings where the number one used component and still remained until today.

4.2.1 Tin and lead materials

Lead- and Tin base materials (also used to be called babbitts) still belong to the most widely used materials for hydrodynamically lubricated bearings offering perfect surface action between the bearing and journal surfaces. There is minimum damage of a steel journal under boundary lubrication conditions or in dirty lubrication and they exhibit excellent compatibility and anti-seizure characteristics. The softness of surface also provides perfect embeddability and conforms to geometric errors in machine construction and operation. They still have the majority of use as a material regarding engine bearings. Only automotive had to move from using of the lead based materials to the tin-based because of the European regulation (ELV).

It has relatively low load-carrying capacity which the industry solved by metallurgical bonding of these alloys to a stronger backing materials such as steel, cast iron, or bronze.

Babbitt linings are either still cast or centrifugally cast on the backing material. Fatigue strength is increased by decreasing the thickness of the babbitt lining.

Other materials are usually used only when higher load capacity is required and/or system is working under higher-temperature operation and/or requirements for fatigue life are higher than those of babbitt materials.

Regarding fatigue, basic problems have been improved by intermediate layer of a high strength fatigue-resisting material between a steel backing and thin babbitt surface layer. These composite bearings often eliminate the necessity for going to other bearing surfaces with poorer compatibility than is possible with babbitts.

4.2.2 Aluminium alloys

Usage of aluminium alloys in bearing industry is known for a very long time. Decent mechanical properties like anti-seizure, wear resistance, elongation and hardness scored caused massive extension of variety of these alloys in bearing applications. The usual compositions contained tin, copper, nickel and magnesium in different amounts and showed great potential to replace conventional tin base babbitts and leaded bronzes [36]. In the past, lead was cheaper option to tin whereas also more effective soft phase addition needed for aluminium.

Regarding European market, leaded aluminium alloys appeared as a problem as described in the sections above. Moreover conventional melting and casting of leaded alloys also caused some troubles regarding segregation of aluminium and lead phases based on the differences in density especially when the addition of Pb was above 1.5 % [37].

Steel-backed aluminium bearings have been found the biggest potential in crankshaft and big-end bearings in variety of compositional optimisations [38].

4.2.3 Copper alloys

Copper alloy materials for bearing applications can either be cast or wrought. However, the majority of the bearing materials such as high tin phosphor bronzes and leaded bronzes cannot be fabricated because of their special duplex structure, and bearings made from these alloys must be cast. Wrought materials are used where the bearings can be manufactured more economically by fabrication rather than by casting [39].

Bronzes are used in some applications as cast bearings without a steel backing (e.g. thrust washers of floating bearings for turbochargers).

Lead bronzes containing up to 25 % lead, provide higher load-carrying capacity and fatigue resistance and a higher temperature capability than the babbitt alloys. Tin contents up to about 10 % are used to improve the strength properties. Higher-lead bronze (70 % copper, 5 % tin, and 2-5% lead) can be used with soft shafts, but harder shafts (300 BHN) are recommended with the harder lower-lead bronzes, particularly under conditions of sparse lubrication.

Lead bronze bearings are used in pumps, diesel engines, railroad cars, home appliances, and many other applications.

Tin bronzes, which contain 9 to 20 % tin and small quantities of lead (usually < 1 %), are harder than lead bronzes and are therefore used in heavier-duty applications as well as turbocharged engines as the lead-free materials in automotive.

4.3 Production of engine bearings

As described earlier, the material for bearing production has to consist of several layers in according to fulfil the hard conditions in the engine. Production method of material consists of layer of an alloy with the desired characteristics bonded to a steel base (backsteel).

Strong bonding is required for the bimetal so that the steel and alloy layer do not separate after the bearing is mounted in the machine. The steel and alloy are basically attached by the bonding of metallic atoms. Technologies called sintering, roll bonding, and casting are used to attach the backsteel and bearing alloy at the atomic level at high temperature and pressure. One of these three techniques or mechanical bonding is selected according to the alloy type.

4.3.1 Sintering

Sintering is mainly used for copper alloy bimetal. Copper alloy powder is spread on the backsteel and bonded at high temperature. The production scheme is on the figure below (Figure 9).

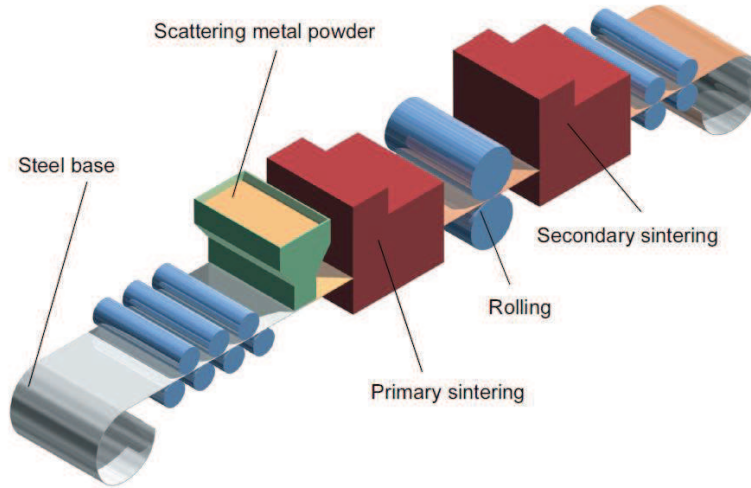


Figure3-4 Sintering process

Figure 9 Sintering process [24]

The basic raw material is bearing steel coil. It usually comes from the steel manufacturer. For the purposes of bearing, usually cold-rolled steel is produced. As from the hot-rolled coil, the cold reduction process produces closer dimensional tolerances which are required for bearing industry.

The steel strip is uncoiled levelled by series of cylinders before metal powder is spread to the surface. Washing of the strip is usually required so the bonding is maintained after the sintering process. Cleaning of steel coil can be done by either hot alkaline solution or mechanically.

The metal powder is added to tray with the prior controlled particle size and material composition quality. Spreading powder requires previous careful calculation based on experiences of necessary alloy thickness. This requires knowing the ratio between the densities of the powder and the sintered ally and elongation of the strip during the rolling.

Sintering process is know-how of each manufacturer. Sintering furnace is a continuous sleeve-type and several meters long where temperature reaches over 800°C depending on the alloy composition and is also result of research and development of bearing manufacturer. The atmosphere in the furnace is also controlled to be reduced. The reducing is necessary to convert all the surfaces of powder particle into the metallic state:



The particles are welded to each other and to the steel strip due to the mutual diffusion of their atoms.

The sintering process needs to be performed twice. Primary sintering to weld particles and bond them to steel coil and then re-sintering to eliminate closed pores formed between the joined particles. Re-sintering is conducted in a sintering furnace similar to that of the sintering stage with similar parameters as well as the process.

The ideal result is sintered structure of the copper alloy without any porosity with a similar structure as below on the picture (see Figure 10).

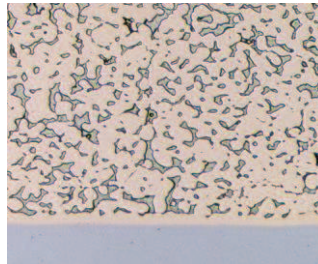


Figure 10 Structure of the Copper alloy [24]

The second phase (can be for example lead, bismuth, tin) is homogeneously distributed throughout the copper based matrix in form of small particles located between the copper grains.

4.3.2 Casting

Casting process is at the beginning same as the sintering process (see Figure 11). Steel coil is straightened and washed in alkaline solution and cleaned mechanically by cylindrical brushes. Strip edges are formed on the sides to keep melted copper alloy and prevent its side leakage.

Steel is preheated to about 1000°C in inert atmosphere preventing possible oxidation and melted copper alloy is poured onto the strip surface. Cooling is done by water.

Finishing process is composed of edge trimming by slitting the strip edges and polishing the surface. The strip is recoiled and follows to the further machining process for bearing production.

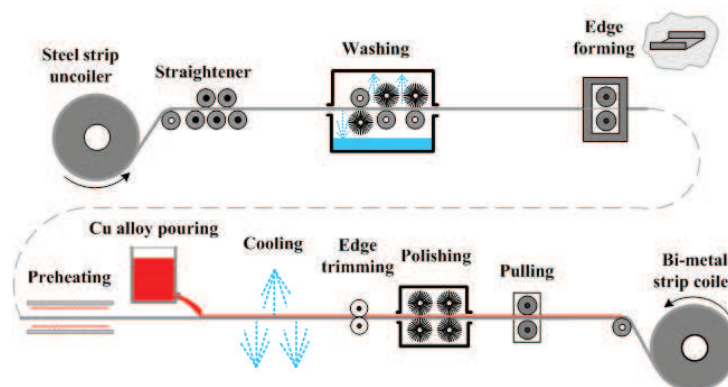


Figure 11 Casting process of copper based bi-metal strips[40]

4.3.3 Rolling process

Rolling process is usually used for aluminium alloy bimetal. The process can be seen in the figure below (see Figure 12).

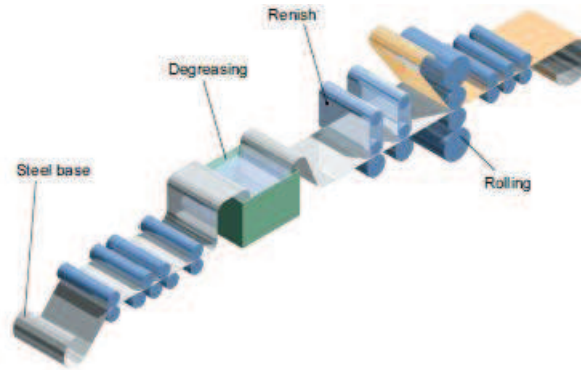


Figure 12 Roll bonding of aluminium bimetal [24]

Degreasing and mechanical cleaning is done for both the steel base and the prepared aluminium strip. Both strips enter rolling mill where they adhere to each other as a result of Solid State Welding. The pressure necessary for achievement of bonding is obtained at relatively high thickness reduction for on-pass rolling operation (4 rolling mills are used for bonding aluminium alloy with steel strip as seen).

4.4 Coatings

Although the material alloys and bimetals have been developed to meet requirements of the tribological properties, the complexity of mechanical and physical properties required coated surfaces as the combination in terms of hardness, elasticity, shear strength, fracture toughness, thermal expansion but especially adhesion to the substrate material.

It generally recognized four zones when applying surfaces where particular each zone must be considered different property (see Figure 13)

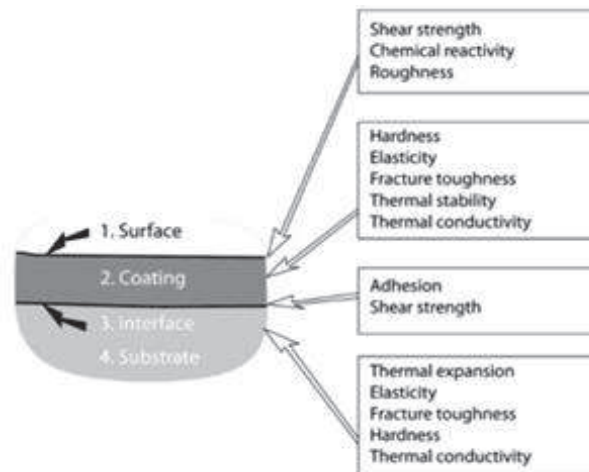


Figure 13 Material properties in different zones of the coated surface [41].

Substrate and coating material properties are generally determined by their composition and microstructure where porosity and homogeneity plays role. At the interphase, the mentioned adhesion and shear strength of the junction is important. The main focus on the surface of the coating is the study of chemical reactivity and surface roughness or preparation of surface artefacts together with the shear strength.

Also the coating design itself undergoes again in compromising of properties, such as good adhesion at the coating/substrate interface and no surface interactions with counterface,

or hardness versus toughness and obviously the cost of the preparation and application of the coating onto the product [21].

Holleck (scheme Figure 14) in his study characterized how aside from material selection, composition and also fabrication parameters determine the microstructure. In this sense the coating system usually represents a sort of composite system and bearings simultaneously benefit from this option as well as they become very dependent on the production.

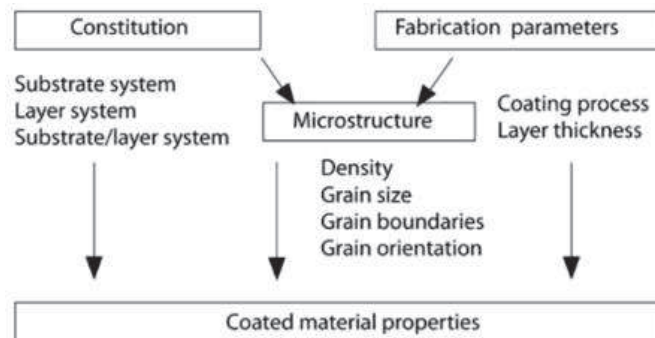


Figure 14 Examples of parameters influencing material properties of coated surfaces [42].

Expansion of tribological coating development started massively especially due to the availability of new coating methods which can control morphology and adhesion properties of coatings which were not available previously. The deposition techniques that have caused most of the interest in this field are primarily plasma and ion based methods.

Rickerby and Matthiew [43] classified the deposition processes into the following four categories:

- Gaseous state processes,
- Solution state processes,
- Molten or semi-molten state processes,
- Solid-state processes.

Solid-state processes are usually connected to thick coating. Therefore it was not gathered in the table (see below Figure 15). Regarding bearings, especially in engine plain bearings there is micrometer level range in which the material engineers can play.

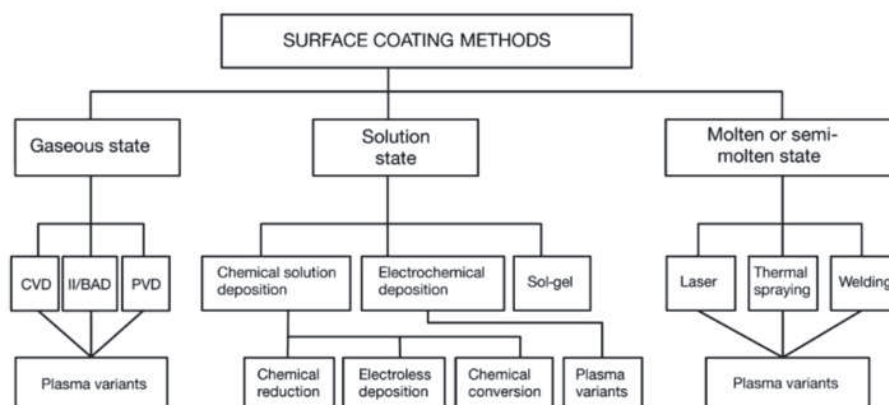


Figure 15 General classification of surface engineering method.

Each process can achieve different range in thickness which plays important role as had been pointed out. Figure 16 represents a scheme of approximate range for the coating thickness according to the technology and how it is vary as well as the deposition temperature. The temperature can influence the substrate material.

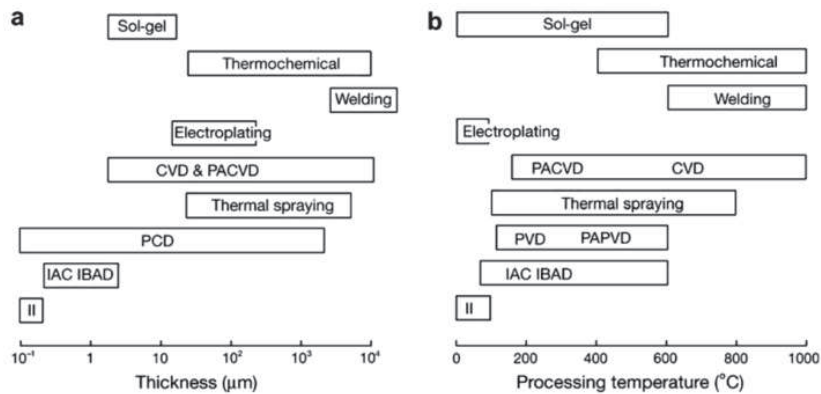


Figure 16 The typical range of coating thickness (a) and processing temperature (b) for coating technologies.

4.4.1 Electrochemical deposition

As requirements for bearing have increased, the functional top layers were introduced and electroplating has become one of the common process used for engine bearings. With Bi-metal bearings where the overlays is absent, tribological performance is determined by the bearing lining itself. There is a limitation to fulfil all the required properties in high loaded conditions.

Electroplated or galvanic coatings are widely used in the form of soft metals and since these overlays are rather thin, they have shortcomings in terms of mechanical strength [44].

Lead based PbSn(8-18)Cu(0-8) system is a commonly used material. These lead-based matrixes are reinforced by Cu and Sn, which form harder particles and improve also corrosion resistance. Additionally for some application, Indium is added to increase the fatigue and wear resistance [45].

When using tin, the diffusion is commonly appearing to the copper substrate from overlay resulting in lower performance of the overlay. Therefore an intermediate layer of Ni is applied between copper alloy lining and overlay [46].

ELV regulation of EU as mentioned earlier forced to implement Sn, Bi and Ag based systems [2]. These soft layers usually lack wear properties and therefore are doped with hard particles [47].

4.4.2 Sputter coating

Sputter bearings were developed already a decade ago to improve load carrying capacity and wear resistance of engine bearings because of turbocharged systems of engines. But the production came more recently. The reason was connected mainly with production scale of deposition processes. Main difficulties were connected to process control and electronic technologies with knowledge of plasma physics and chemistry.

The production technology using physical vapour deposition (PVD) processes commonly employ a method known as sputtering. The technique helps to produce material with fine grained structures. Atoms released from target material by ions, are deposited onto the

substrate material. A typical target material composition for this overlay is AlSn based alloy. The most widely used is the AlSn20 alloy. The deposited formed layers are much harder compared to the target material itself. These sputter coatings possess high fatigue strength, high load carrying capacity and high wear resistance combined with moderate sliding properties [48]. Hence, they find their use in highly loaded turbocharged diesel engines. One of the disadvantages of these coatings is their comparatively high costs. The reason for PVD technique is refinement of microstructure. This refinement influences strongly tribological performance of the layer. Example could be found in the work of Rosa et al. [49] who found the friction coefficient of thin film from AlSn20 deposited by magnetron sputtering which is lower than that of commercial Al–Sn alloy.

The sputter bearings have high fatigue resistance and exhibit high load carrying capacity and high wear resistance and therefore they found their use in highly loaded engine bearings. One of the disadvantages of these coatings is their high costs.

4.5 Polymers in engine bearings

In general, polymeric materials have had the greatest progress among triboelements of recent years and found its way in tribological applications. The main reason is the fact that polymers offer inherent properties such as light weight, ease of manufacturing and corrosion resistance. Moreover, by adding some reinforcements and lubricants they give better tribological properties, which are unreachable with metals, ceramics or neat polymers.

When we look at the engine bearings, it does not have the long term development. It came with introduction of high performance and thermal resistant polymers such as polyamide imide. Polymer based coatings are usually incorporated with solid lubricants predominately used as running-in layers. In certain cases, they are used as permanent layers as well. They are typically sprayed on the bearing surface and these layers improve the running-in behaviour as well as the geometrical adaptability. A widely used matrix material is polyamide-imide (PAI) with MoS₂ and graphite lamellae as filler material. As permanent layers, these composite materials reduce the friction to the rotating shaft when the lubricant film breaks down.

Regarding polymers, we are recognizing two categories: thermosetting and thermoplastic materials. Regarding thermosets, nonoriented fibers are generally set in phenolic resins. Regarding thermoplastics, nylon has been recognized as valuable bearing material aside of low-friction polymer polytetrafluoroethylene (PTFE).

The main focus of polymer overlays for crankshaft and conrod bearings was towards high performance polymers such as polyamide imide (PAI).

4.5.1 Nylon

Nylon has good abrasion resistance, a low wear rate, and good embeddability. Like most plastics, it has good anti-seizure properties. It has low thermal conductivity (0.24 W/m-°C), and failure is usually the result of overheating. Cold flow (creep) under load is one of its main disadvantages. This effect can be minimized by supporting thin nylon liners in metal sleeves. Nylon bearings are used in household applications such as mixers and blenders and for other lightly loaded applications [50].

4.5.2 Polytetrafluorethylene (PTFE)

PTFE is well known polymer in tribology. It exhibits low coefficient of friction in a contact with harder counterpart. The disadvantage is high wear rate which eliminates the application for higher load pressures and surface speeds.

PTFE exhibits poor wear and abrasion resistance, which can lead to early failure [51]. Regarding the bearings, PTFE is usually used as an additive to wear protective matrices in case of bushings. The wear resistance can be increased also by implementing proper fillers [52].

Regarding our work, PTFE has been excluded from study since it was established that PTFE exhibits significantly low coefficient of friction when sliding against steels. The low coefficient of friction results from the ability of its extended chain linear molecules, $-(CF_2-CF_2)_n-$, to form low shear strength films upon its surface and mating counter-faces during sliding [53].

Recently, GGB has patented a sliding layer for production of multilayer self-lubricated bearing based on PTFE [54]. They added 10 to 20 vol. % sphalerite ($ZnFeS$) as a lubricant which allows the sliding layer to be self-lubricated. Then approximately 10 vol. % secondary lubricant - graphite and antimony oxide is added to improve frictional properties.

Bickle et al. patented⁵⁵ low frictional bearing composite material based on PTFE where they used 10-25 vol. % zinc sulphide with smaller particle size than $1\text{ }\mu\text{m}$ and 1.5-3.5 vol. % carbon fibres and 1-7 vol. % PFA. It is claimed that Zinc sulphide support homogeneous distribution of carbon fibres in the composite. Particles of ZnS are wetting the surface of carbon fibres and which includes bonding of carbon fibres to the PTF substrate material. Carbon fibres are claimed of 10-20 μm and length 100-200 μm and used as additive to decrease friction of resulting material.

4.5.3 Polyether ether ketone (PEEK)

PEEK is a semicrystalline thermoplastic with excellent mechanical and chemical resistance properties that are retained to high temperatures. The processing conditions used to mold PEEK. It can influence the crystallinity, and hence the mechanical properties [56]. It is also common material as a polymer matrix material for several engine bearing manufacturers, especially in the production of bushings.

The real advances in parameters are coming from filling the PEEK matrix by other additives in according to improve the material properties for different application. PEEK itself from the tribological viewpoint has relatively high friction coefficient especially during unlubricated sliding conditions but the wear rates are remarkably low and therefore became popular.

Rodriguez et al. compared the tribological behaviour of solid lubricants in a polyetheretherketone (PEEK) polymer matrix under different contact pressures and sliding speeds on dry reciprocating conditions with a 100Cr6 steel as a countersurface. They have finalized the lowest coefficient of friction was achieved by the PEEK material using PEEK with 10 wt. % of PTFE, 10 wt. % graphite and 10% wt. of short carbon fibres. According to the researchers, the main reason was the self-lubricant effect of PTFE. The formation of a transfer film (secondary layer) was mainly observed by them with neat PEEK where the adhesion provided a protective effect to damage with better wear resistance. They also have observed abrasion with dominant wear mechanism in materials filled short carbon fibers (SCF), PTFE and graphite. Graphite and PTFE are known for reducing adhesion between

polymer materials and steel countersurfaces. This was according to scientists attributed to the soft nature of PTFE which is poorly adhered to the countersurface and is rapidly removed as wear debris [57].

K.A. Laux et. al [58] had investigated what is the surface temperature of PEEK polymers in sliding conditions on steel and sapphire counterparts. As for our case, we are not considering sapphire counterparts in future for engine bearings. Interesting conclusion on the outcome is that the PEEK debris were found adhered to the steel surface as well as iron oxide residue on the PEEK wear scars and this phenomena was not observed on sapphire. The PEEK transfer film on steel countersurface is highly oriented which suggests its formation process is similar to drawing or extrusion of polymers at high temperature. The transfer film formation processes are the one which influence the friction and surface temperature.

Kalin et.al from University of Ljubljana [59] investigated effect of the material type and the morphology of well-known solid lubricant nanoparticles on the tribological properties of PEEK composites. They used WS_2 (Tungsten (IV) sulfide) fullerene-like (WS_2F), WS_2 needle-like (WS_2N), carbon nanotubes (CNT) and graphene nanopowder (GNP).

The WS_2 -based nanoparticles increased the wear performance as classically the carbon based composites are known for as compared to PEEK, WS_2F improved the wear rate by 10% and the WS_2N by 60%, while the carbon-based particles deteriorated the wear behaviour by 20% (CNT) and as much as three times in the case of the GNP. The addition of WS_2F nanoparticles and the CNT resulted in a lower coefficient of friction compared to the WS_2N particles and the GNP. The resulting diagram seems do mistake in description but probably WS_2F is around 0,4 (see Figure 17).

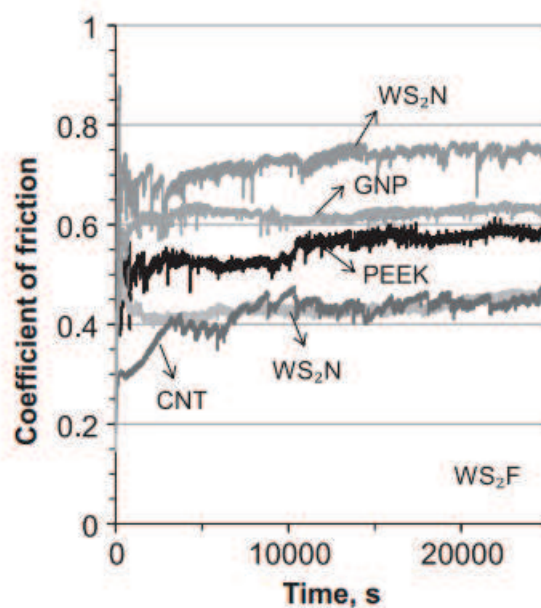


Figure 17 The representative friction–evolution curves as a function of sliding time [59].

One of the main applications of PEEK materials regarding engine bearings are toward bushings used for fuel injection pumps. The lubrication of these elements is rarely reported. Zhang et al. [60] have studied performance of PEEK materials under fuel and engine oil lubrication conditions. Even very small quantity of diesel decreases obviously the friction coefficient and wear rate of pure PEEK. The same was observed with PEEK filled with multiple fillers, i.e. short carbon fibers, solid lubricants and ceramic particles. They believed

that tribofilm produced with diesel lubrication block the material transfer of solid lubricants towards the surface of PEEK and any other tribolayer formation on the surface of bearing. Therefore the frictional results for dry conditions and lubricated are of the significant difference (see Figure 18).

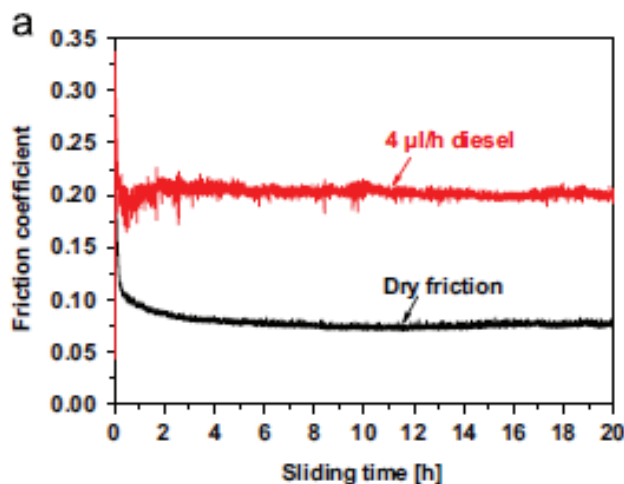


Figure 18 Friction coefficient evolutions of PEEK-Com under dry friction condition and with 4 $\mu\text{L/h}$ diesel "lubrication" [60].

4.5.4 Polyamide-imide (PAI)

Polyamide-imide (PAI) has been commercially available for several decades. The synthesis, properties and applications have been extensively described in past in a similar attractively as polyamides and polyimides. Their superior mechanical, thermal and oxidative properties have made them suitable for various applications [61] and therefore have found the interest also in engine bearing producers.

Although PAI is an amorphous thermoplastic, it requires a post cure after application to surfaces in order to increase its molecular weight, which increases the chemical and thermal stabilities of PAI. The chemical degradation of PAI matrix can be created only by hot steam and high pH. The neat PAI's compressive strength and its impact strength are higher compared to other high-performance polymers (see Table 1).

Table 1 Comparison of the Compressive Properties and the Impact Strengths of Selected High-Temperature Thermoplastics

| | Compressive Strength (MPa) | Compressive Modulus (GPa) | Impact Strength (Izod, Notched) (Jcm^{-1}) |
|--------------------------|----------------------------|---------------------------|---|
| Torlon 4203 (PAI) | 166 | 3.3 | 1.06 |
| Temppalux PEI | 151 | 3.3 | 0.53 |
| Techtron PPS | 148 | 3.0 | 0.23 |
| Ketron PEEK | 138 | 3.5 | 0.53 |

At the beginning, the PAI have been developed as an alternative material to polyimides and polyamides to keep the balance of thermal stability with good processability. PAIs combine the superior mechanical properties associated with the amide group, and the high thermal stability of the imide ring in the same material, thus making the material even

stronger. In addition, the synthetic route to PAIs offers the possibility of incorporating specific functionalities between the amide and imide groups. It was found that synthetic modification of PAIs by addition of flexible linkages or by incorporation of variety of functional groups reduces the crystallinity and enhances the solubility of the polymers [62]. Some example of the list is below:

- fluorene, phthalide or phthalimidine group [63],
- cinnamoyl and azobenzene [64],
- phenoxy phenylene [65],
- methoxy-substituted triphenylamine [66],
- oligoether spacers or bulky pendent groups [67].

The first successful result of PAI synthesis forming into patent was probably the one by Frosch [68]. His synthesis was based on the reaction of 1,2,3-benzenetricarboxylic acid and aliphatic diamines. The reaction was firstly formed polyamic acid, then by thermal cyclization they formed PAI. The thermal stability of these polymers was lower due to the aliphatic diamine precursors which resulted in commercial unattractiveness. The main start was due to DuPont with development of aromatic PAIs around the end of Second World War (therefore references are missing).

Later in seventies, Amoco Chemicals produced Torlon from trimellitic anhydride chloride (TMAc) and 4,4'-diaminodiphenylmethane [69]. The polymer exhibited very high strength, stiffness, creep resistance and displayed good performances at moderately high temperatures. They followed in development. Since then, a lot of chemical and structural modifications have been done on Torlon resulting in spread portfolio of products. Till today, it still remains one of the well-established commercially available PAIs and therefore it was also chosen for this thesis.

The Solvay Advanced Polymers L.L.C is currently manufacturer and trademark owner of Torlon polymers. Torlon® PAI (polyamide-imide) combines the unique performance of thermoset polyimides with the melt-processing advantage of thermoplastic PA. In general, they produce 2 categories of polymer grades:

1. Wear-resistance grades which offers unsurpassed performance in both dry and lubricated environments.
2. High-strength grades retain their toughness, high strength and high stiffness up to 275 °C, making PAI the industry's highest performing thermoplastic. Its broad chemical resistance includes strong acids and most organics.

The resulting comparison diagram of the Torlon PAIs is in Figure 19 below.

The real advantage of the polymer and its use for bearing application is high creep resistance and an extremely low coefficient of linear thermal expansion (CLTE) resulting in excellent dimensional stability. This is important for the bearing industry where micrometer precision is required.

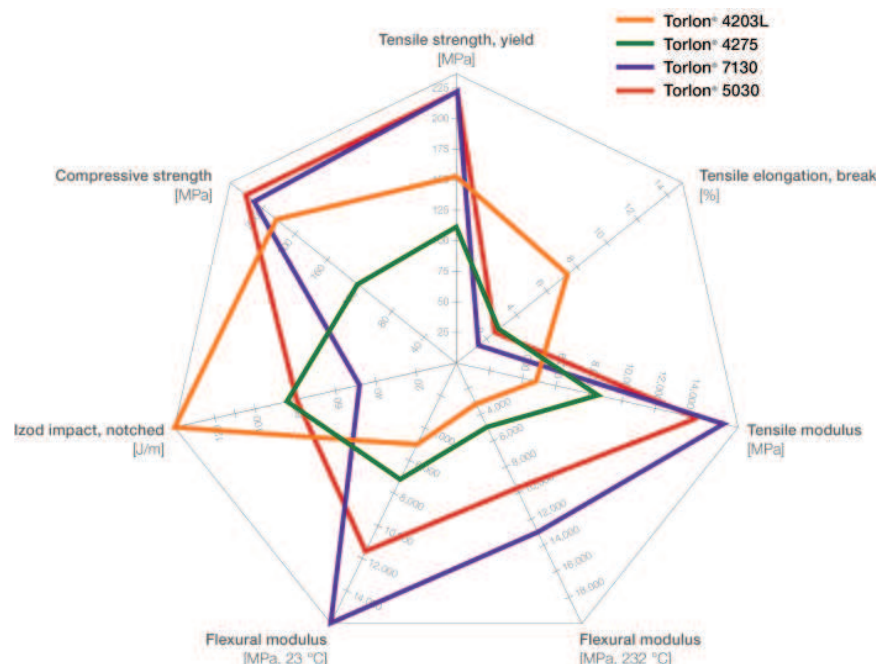


Figure 19 Comparison of Torlon® PAI grades [70]

Torlon PAIs are generally used for molding and all the grades above are also used for it. The tensile strength and tensile modulus of high-strength grade Torlon 4203 reach 152 MPa and 4.48 GPa, respectively. The tensile strength of Torlon 5030 and Torlon 7130 grades, which are glass-fiber and carbon-fiber PAI composites, respectively, reaches 221 MPa. The high-strength grades retain their toughness and strength up to 275 °C which makes them suitable for engine applications.

Applications

A wide range of PAIs have been investigated for applications in filtration, high temperature adhesives, electronic wire enamels, injection-molding techniques, integrated optics and biomedical applications [63–68].

Already several research with application of PAI has been implemented in past. Chitose et al. from Taiho Kogyo company [71] presented a concept of the bearing based on the PAI with MoS₂ solid lubricant. They have achieved 40% less coefficient of friction, 25% less starting torque and 65% less bearing wear in comparison to the conventional aluminium alloy bimetal bearing without overlay under close to the start-stop lubrication conditions by testers.

The testing was done using ball on plate test as well as bearing tester with static loading conditions mainly for wear and frictional results.

Shabanian et al. from Faculty of Chemistry and Petrochemical Engineering, Standard Research Institute in Iran [72] implemented new composite based on a semi-aromatic polyamide (PA) reinforced by multiwall carbon nanotubes (CNTs) was prepared by a solution mixing method. PA was synthesized through a direct polycondensation between azelaic acid and bis(3-amino phenyl)phenyl phosphine oxide. The effect of the CNT addition was mainly for the flame retardancy.

Gebretsadik et.al. from the Luleå University of Technology [73] looked at the Pb-free bearing materials in according to study them and compare the friction and wear behaviour

under mixed and boundary lubrication conditions. The friction and wear evaluation was performed using block-on-ring test configuration. Different rotational speed was used for investigation running-in friction in mixed and boundary lubrication regimes for these materials. Also longer tests were used for state-friction behaviour and wear characteristic results. The findings show a positive effect of PAI based overlay containing MoS₂ and graphite especially at lower sliding speed where has better wear resistance than Pb-based and Al–Sn based materials.

Recently, Federal Mogul company released application for patent of sliding coating based on PAI to piston rings as well (their well-known application of this coating is for engine half bearings as mentioned before). The additives are ferrous oxides with MoS₂ or other solid lubricants for mainly wear and anti-seizure modifier of the coating [74].

Daido Metal company leads also several patents over the world relating to the PAI base overlays. In USA, they patented [75] the composite layer based on PAI with addition of solid lubricant based on PTFE and MoS₂ for lowering the frictional abilities together with hard particles based on metal oxides for increasing in wear. According to their knowledge, less than 1 wt % of the hard particles cannot improve the wear resistance. On the other hand, if the hard particles are more than 50 wt %, the coating layer is oppositely worse in wear resistance.

According to the invention, the polyamide used for the realization of the sliding surfaces may be advantageously crosslinked, e.g. chemically or by irradiation, thus allowing to increase its maximum operating temperature, mechanical strength and modulus of elasticity compared to the a polyamide that is not crosslinked. Crosslinking of the material also allows to obtain a higher surface hardness and to increase wear resistance and dimensional stability in view of high operating temperatures.

Fortune Construction Engineering Ltd. patented the low-friction polymer material based on cast polyamide 6 which they crosslinked with lubricants on a liquid state thus allowing to keep good frictional properties and increased mechanical properties, especially compression resistance in compare to the fluoropolymers. The crosslinking allowed to increase the molecular weight of the polymer and to form the intermolecular bond which can further influence the material properties [76].

A composite material for sliding surface bearings based on the aromatic polyamide fibers (0.02 to 0.1 mm in diameter and have a length of ≤ 0.3 mm in a volume ratio 1.5 to 15%) was claimed in US patent US4847135 A of Kolbenschmidt Aktiengesellschaft [77] where as the matrix they used a polymer selected from the group consisting of polytetrafluoroethylene, polyvinylidene fluoride, polyethersulfone, polyetheretherketone, polyetherimide, polyphenylenesulfide, polyacetal and polyimide in volume ratio 5 to 35 % and in mixture of the two of them.

Miba Gleitlager Austria patented [78] sliding layer based on PAI of 60-80 vol. %. Molybdenum sulfide (15-25%) and graphite (5-15%) used as an additive for frictional properties. The proportion of polyimide resin was preferably calculated for the amount of solvent to be removed. The disadvantage of this solution was mainly in strength and possible use in highly loaded plain bearings. Therefore they recently patented [79] sliding layer composed of the PAI based with the same solid lubricant particles as in previous patent but with mixture of alumina powder. They claim that further improvement in wear performances of the surface layer, hexagonal boron nitride was used in the range of 5-25 %.

Another similar structural bearing material as for the layer was patented by Mahle [80]. The cross-sectional image of the bearing material is on Figure 20.

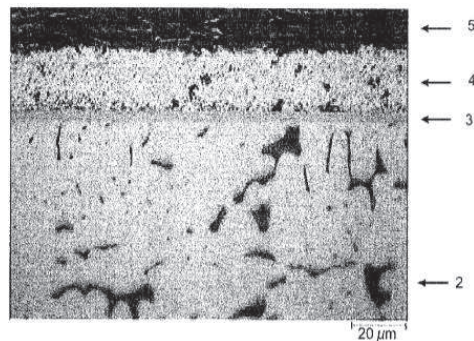


Figure 20 Sliding bearing patented composite

The base material is bearing steel onto which applies a primary layer of bronze alloy (2) with composition of 4-8 % tin, 1-4 % bismuth, 1-3 % nickel with balance to copper in thickness 150-400 μm . They claim that in according to sputter the layer (4), the bonding layer has to be implemented (3) to increase the bonding forces. The bonding layer comprises from nickel and chromes in a range of thickness 1-5 μm . The sputtered layer (4) comprises 1-40 % tin, 1 % silicon, 1% copper, 2% iron with balanced of aluminium in thickness 3-20 μm .

The sliding polymeric layer (5) based on PAI matrix provided with a 1-14 % of soft metal (aluminium powder – 5 μm particle size), 5.7 % fluoropolymer (PTFE or fluorinated ethylene-propylene) mainly for lubrication properties and 4.8 % silane-based material.

Silane material (as claimed gamma-aminopropyltriethoxy-silane) was used as a material to increase stability of matrix. Further important function is in adhesion properties to the sputtered layer, as claimed in the patent. The multilayer system exceeded the load capacity 150 MPa which makes it interesting for potential high loaded engine systems. There is obviously also significantly higher cost as compared to classical bearing systems.

Synthesis of PAIs

Synthesis and chemistry of PAIs itself is complicated covering a large variety of existing monomers such as anhydrides, carboxylic acids, diacyl chlorides and diamines, and diverse procedures. The physical, chemical and mechanical properties of these materials can be adjusted or modified by changes in the chemical structure of the monomers or the reaction conditions. Several approaches have been successfully applied for the preparation of PAIs [81,82].

One of the oldest approaches for the synthesis of high molecular weight PAIs is the direct polycondensation of imide-containing dicarboxylic acids with aromatic diamines by phosphorylation which was introduced by Yamazaki et al. [83] in 1975. Later, this method was successfully modified by many researchers [84, 85].

The most convenient way is synthesis by:

- amide-imide forming reactions,
- reactions involving amide or imide-containing monomers.

Amide-imide forming reaction

This forming method produces PAI by reacting trimellitic anhydride (TMA) or trimellitic anhydride chloride (TMAc) with diamine [86] or with diisocyanate [87].

Avella et al. [88] modified the PAI synthesis and by the direct polycondensation of flexible aromatic diamines with monoesters of isomeric tricarboxylic acid anhydrides with aryloxy group or with monoesters of TMA (see Figure 21) in a single pot system. The method uses triphenylphosphite (TPP) and pyridine as condensing agents to form amide bonds from aromatic diamines and a mixture of isomeric 1,2,4-benzenetricarboxylic acid monoethyl esters. They claimed that these polymers exhibited higher thermal stability compared to those derived from TMA.

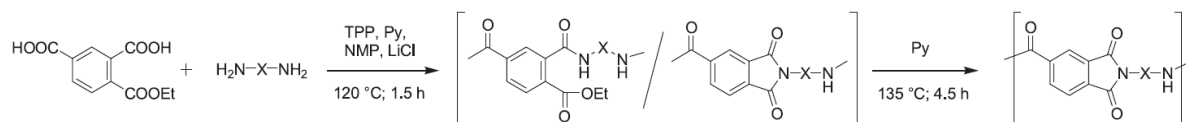


Figure 21 Two-step polymerisation method for synthesis of PAIs by single-pot.

The above methods for PAIs synthesis are producing viscous polyamic acid as an intermediate. Water is released as the by-product during the imidization of the polyamic acid. It results in low yields of polymers (hydrolysis of the polyamic acid). Its synthesis requires very pure monomers and extremely anhydrous reaction conditions to achieve high molecular weights. To overcome these drawbacks, many research groups used diisocyanates as a substitute for diamines. The diisocyanates evolving CO_2 gas bubbles out of the reaction system during polymerization process more easily but reactivity of ANCO group makes the pot life of diisocyanate very short which complicates the whole reaction.

Reactions involving imide or amide-containing monomers

Synthesis where imide-containing monomers are used, a diimide dicarboxylic acid (DIDA) or imide-containing dicarboxylic acids reacts with various diamines to synthesize a series of PAIs. Alternatively, imide- or diimide-containing dicarboxylic acid chlorides can be used instead of the acids. This synthesis has several advantages compared to the conventional polyamic acid type. The final polymers are linear, soluble, and as most important, high molecular weight.

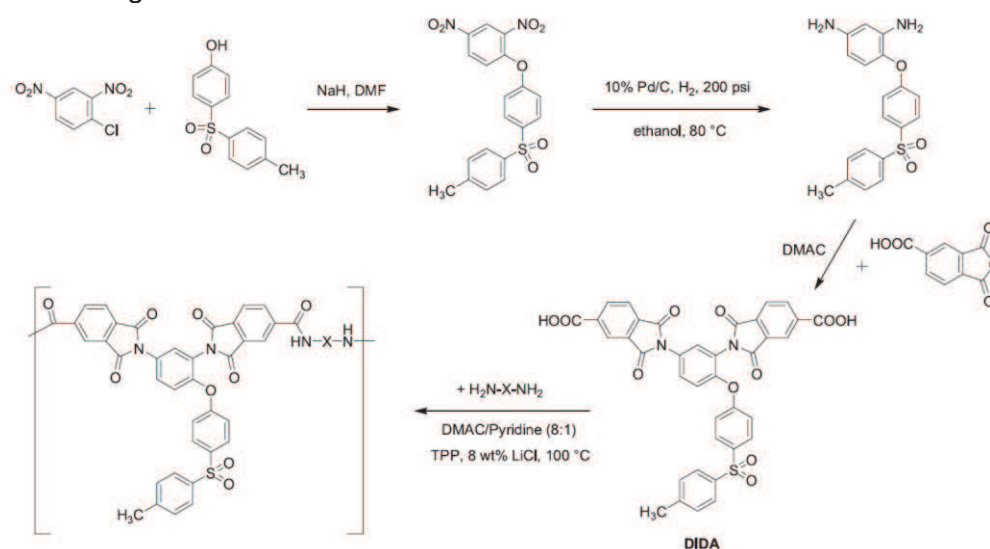


Figure 22 Synthesis of PAI from diimide dicarboxylic acid.

Good example of this work is from Patil et al. from 2007 [89]. They used 4-{4-[(4-vinylphenyl) sulphonyl]}-1,3-bis-trimellitoimido benzene containing sulfone and bulky pendent group as a PAI building block. They obtained high-molecular-weight polymers by direct polycondensation of the DIDA with various diamines by means of triphenyl phosphite (TPP) and pyridine (see Figure 22).

Lately, a lot of novel techniques of production has been developed (microwave irradiation, sol-gel process, ultrasonic irradiation method, chemical crosslinking, etc.). These methods and other PAI synthesis options were not studied since the synthesis of PAI was not part of the thesis. On the other hand, it is evident that there had been a significant progress in designing the structure of PAIs, their precursors, and developing new preparation/modification methods, to improve their thermo-mechanical properties as well as processibility. Interest for PAI is growing due to their high performance polymer properties.

4.5.5 Other polymers

Dixon Corporation patented [90] a composition combining PTFE resin and polyimide resin which can be shaped into the bearing bushing with exceptional resistance to frictional wear and hence which is satisfactory as a dry bearing material even against soft metals. They claim that the co-polymer has unusual synergistic behaviour especially because neither the component alone, neither PTFE resin or polyimide resin, has satisfactory bearing resistance when moving against a soft metal such as brass. Thus, their invention also provides a method of increasing the abrasion resistance of PTFE resins.

4.5.6 Additives in polymers

Nanoparticles

It has been generally accepted that smaller particles have better performance than larger particles in improving the tribological properties of polymers under sliding wear conditions [91], especially in a nanoscale. There was variety of work to verify the theory of polymer nanocomposites.

Rong et al. studied TiO₂ nanoparticles and mainly their distribution effect on wear resistance of epoxy resin matrix when sliding against smooth steel nanocomposite [92]. Xue et al. [93] studied SiC particles in PEEK where the comparison of the dimensions of SiC particles influence the friction and wear of the PEEK composites. He found out that the wear rate of PEEK filled with 10.0 wt.% nanosized whisker SiC was almost unaffected.

The performance of nanocomposites is normally attributed to the large interface area between nanoparticles and the polymer matrix, which potentially leads to better bonding between different phases, and therefore to a better property profile than that achieved with conventional polymer composite [94]. Researches have demonstrated that inorganic nanoparticles can simultaneously improve different mechanical properties of polymer composites, whereas traditional micro-sized particles normally increase some properties, e.g. stiffness, but may have a detrimental effect on others, e.g. toughness and strength [9–11].

Toshihiro Kobayashi et.al patented [95] an addition of vitreous carbon as the additive which can increase tribological properties of conventional bearing material composites. Further, when carbon is blended to the plastic, the manufacturing cost can be reduced as well as weight. Bearing material has less wear, long life, no risk of seizure, improved slidability and heat resistance, and less dimensional changes due to temperature change.

Company Taiho Kogyo patented [96] resin overlay with solid lubricant (MoS_2 , PTFE, graphite, WS_2 , h-BN, and B_2O_3) with hard material (such as SiC , Al_2O_3 , TiN , AlN , CrO_2 , Si_3N_4 , ZrO_2 , and P) in resin which can again vary (PAI and PI resin, an epoxy resin, a phenolic resin, a polyacetal resin, a polyetheretherketone resin, or a polyphenylene sulfide resin).

Different concept was released recently when company Mahle implemented and patented idea of polymer overlay for start-stop application [97]. They described 2 layer polymer overlay for enhanced seizure and scuff resistance under boundary lubrication conditions where both layers have the same composition but different curing temperatures. Matrix was based on polyamide/imide resin, acrylate resin, epoxy resin, phenolic resin or fluoropolymer with dry lubricant as fluoropolymer, Mo_2S , or graphene.

First polymer layer curing at 190 - 240 degrees provided enhanced load carrying capacity and second polymer layer as top layer was cured at 120-180 degrees provided enhanced resistance to seizure and scuffing [98].

Very recently, Federal Mogul applied for the patent [99] where invention is related to the anti-friction coating based on PAI with zinc sulphide and barium sulfate as additives. They claim that tribological properties (specifically load carrying capacity and wear resistance) are significantly improved compare to those containing either only zinc sulfide or barium sulfate. According to their results, the peak load capacity at the crankshaft bearings could be increased up to 120 MPa. This is a value which otherwise is achieved only by aluminum-based sputter coatings.

As the application was used crankshaft bearing where they claim that mixture increase effectivity of lubricant film whereby the increase of the wear rate with the specific bearing load is reduced. This increases the load limit, which in turn significantly increases the operational reliability of the bearing at load beneath the load limit.

4.5.7 Calcium hydroxide

The thesis focuses on the addition of calcium hydroxide to the PAI matrix. There are no literature records on the addition of calcium hydroxide to the polymer. The original idea is coming from generally published articles where inorganic clay minerals consisting of layered silicates in polymer matrices helped with significant improvement on mechanical properties [100, 101]. It was showed that stiffness or Young's modulus can be improved by adding either micro- or nano-particles since rigid inorganic particles generally have a much higher stiffness than polymer matrices [102,103].

It is generally known that the mechanical properties of particulate–polymer composites depend strongly on the particle size, particle–matrix interface adhesion and particle loading [104]. Particle size has a certain effect on the mechanical properties. As an example connected to the baseline coating material, smaller calcium carbonate particles provide higher strength. Smaller particle size of CaCO_3 yields also higher fracture toughness for calcium carbonate filled high density polyethylene (HDPE) [105]. Particle–matrix interface adhesion and particle loading are two important factors that also affect mechanical properties [106].

Regarding Ca(OH)_2 , it can be formed of different particle sizes and shapes. For this work was considered the hexagonal plates which can be found in cement paste usually with needles of ettringite [107]. The formation could play significant role as a laminate filler in the matrix of PAI and increase the toughness of the surface.

5 EXPERIMENTAL

Experimental work on the thesis was combination of feasibility study on benchmark material followed by material research of new coating formulation. Feasibility study researched coating overlay and its effect on additives.

Improvement of tribological properties on material in terms of low friction and low wear require surface characterisation which helps to gather knowledge on how the involved benchmark component interacts in tribosystem. The tribosystem of engine bearing is the bearing itself together with an engine oil and the counterpart (a shaft). The aim was to study aspects regarding the stability of MoS_2 (solid lubricant additive) in PAI, reactions of MoS_2 and its potential degradation products in the tribocontact, reactions of CaCO_3 in the tribocontact and with acids formed in oil degradation, etc. All of these aspects were systematically investigated and evaluated before the material formulation and preparation of new coating. Moreover, the impact of engine oil degradation in the long run was considered as an interesting input. Therefore the investigation was carried out on the new fresh oil as well as on the used oil from testing.

All of the knowledge from this initial study put a base to further development stage of coatings used for engine bearings. The target properties and role of each material component led to information for further research.

Finally, the PAI base coating was chosen for new coating formulation. The reason was not only investigation outcome, but also currently most expanding trend of surface treatment for engine bearings. Concerning the tribological characterisation and investigation, the target evaluation parameters were considered wear and friction.

It was working with the same polymer as was during the tribological study, PAI from Hitachi Chemical. The overall experimental design can be seen on the picture below (see Figure 23). It started with the comparative study of paint from Hitachi Chemical (refers to Hitachi) and European available Torlon (refers to Torlon). Difference in paint supplier followed by the preparation of coatings and characterisation with different additives based on literature review and internal company documents and past expertise from Daido Metal was further input for resulting formulation.

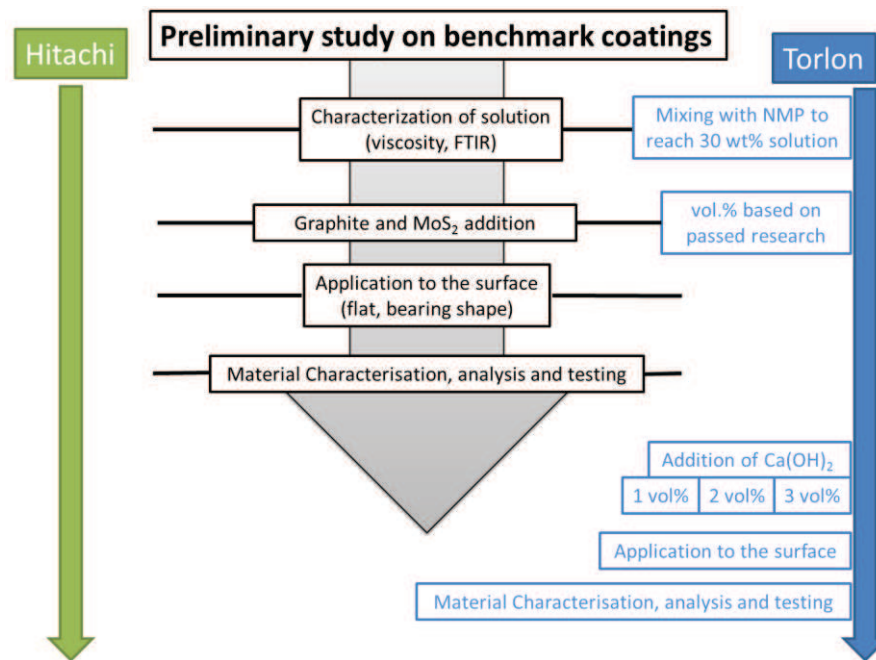


Figure 23 Diagram of experimental work flow

5.1 Goals of the dissertation

The goal of the dissertation was to study new formulation of bearing overlay with advanced tribological properties.

5.1.1 Subgoals

Following sub-goals have been defined to reach the target:

- Analyze the base coating polymer overlay from Daido Metal and provide subsequent characterisation.
- Determine possible interaction between lubricants and bearing surfaces especially under boundary conditions and provide input for improved wear and friction characteristics.
- Study the effect of Ca(OH)₂ addition to PAI matrix on resulting tribological behaviour of the surface

The initial investigation within this dissertation was to join the expertise and past research in Daido Metal. Therefore, exchange of knowledge in product performance (Daido Metal) and analytical approach with the help of AC2T research GmbH (Austrian Competence Center for Tribology) in Austria was done in according to achieve the material knowledge base as a core feature in further development.

Initially the proposed methodology for the comprehensive description of the composition of tribolayers generated by the operation of bearings lubricated with engine oil was evaluated. Detailed topography, morphology and chemistry of new and stressed surfaces of sliding parts on engine bearings were characterized by appropriate surface analytical tools. The findings served as a feasibility study of the usefulness of analytical tools contributing to the overall goal characterized in the introduction.

5.2 Overview of the used materials

5.2.1 Bearings

Benchmark engine bearings were chosen from the company Daido Metal Co., Ltd. It was decided the part of conrod half shell bearing made of standard bimetal material: bearing steel as a support material on which the conventional Al-Sn-Si alloy was lined. The bearing was machined to resulting shape and dimensions according to the typical automotive supplier requirements and surface was treated by application of polymer coating by spraying process.

Result of such a bearing can be seen on the Figure 24.

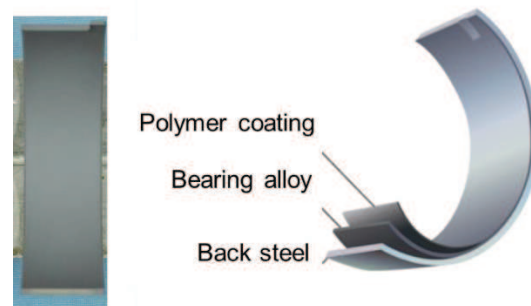


Figure 24 Bearing half shell structure

The initial research study was proceed to evaluate the current surface layer (patented polymer overlay of Daido Metal Co. Ltd. [108]) under different running conditions.

The overlay composition was composed of polymer matrix and solid lubricants. Used polymer is high temperature resistant polyamide-imide (PAI) because it exhibits superior mechanical properties compared to other polymers besides excellent temperature resistance. The filler combines solid lubricant molybdenum sulphide MoS_2 to achieve frictional performances and calcium carbonate CaCO_3 additive which is incorporated in according to achieve increased seizure resistance. Thickness of the layer was approximately $6\text{ }\mu\text{m}$.

5.2.2 Polyamide-imide (PAI)

The experiments were using two commercial PAI products as mentioned above. The first one was already prepared solution from company Hitachi Chemical including 30 wt. % of PAI. The solvent was NMP with Xylene. This polymer was also used for bearing overlay in feasibility study and therefore was included as benchmark. Torlon company was chosen as another candidate for PAI mainly because of European production and sales. The difference was on the chemical as well as origin phase. Torlon was in original powder and needed to be mixed in solvent first and then characterized.

Hitachi

Sample was measured for viscosity on rheometer ARES-G2 from TA Instrument at constant laboratory conditions. Viscosity was measured with the changing shear rate. Results can be seen in Figure 25. The sample's viscosity was determined to be 93.1 mPa.s .

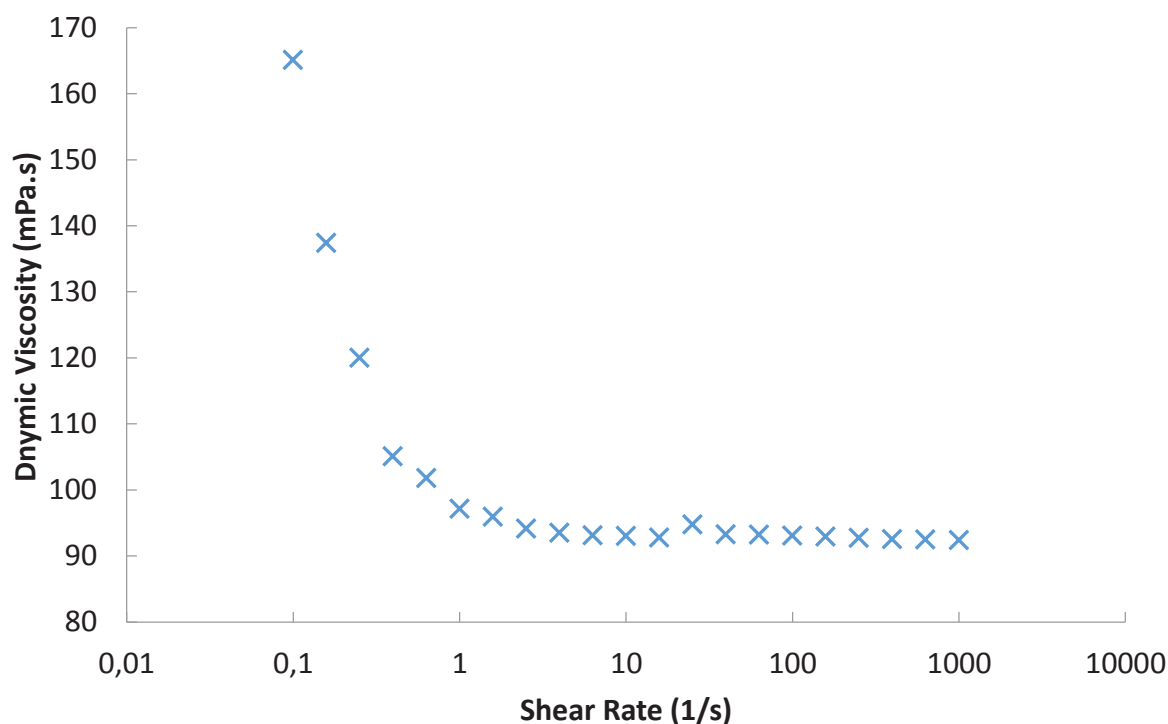


Figure 25 Dynamic Viscosity of tested PAI sample solution from Hitachi Chemical

Torlon

PAI Torlon was delivered as a powder form and therefore was needed to be dissolved in solvent. The grade of Torlon PAI was chosen according to possibility to make solution with other additives. According to supplier information, the PAI grade was soluble in dipolar aprotic solvents such as dimethylacetamide (DMAC), dimethylsulfoxide (DMSO) and dimethylformamide (DMF). N-Methyl-2-pyrrolidone (NMP) was chosen as one of the less toxic from the list.

In order to understand and evaluate the technology of dispersion, the particles size distribution was essential. It was analysed by HELOS Particle Size Analysis.

Results are in the figure below (see Figure 26). The distribution of particle size is in a range of 2 to 20 μm where the median is 7.67 μm .

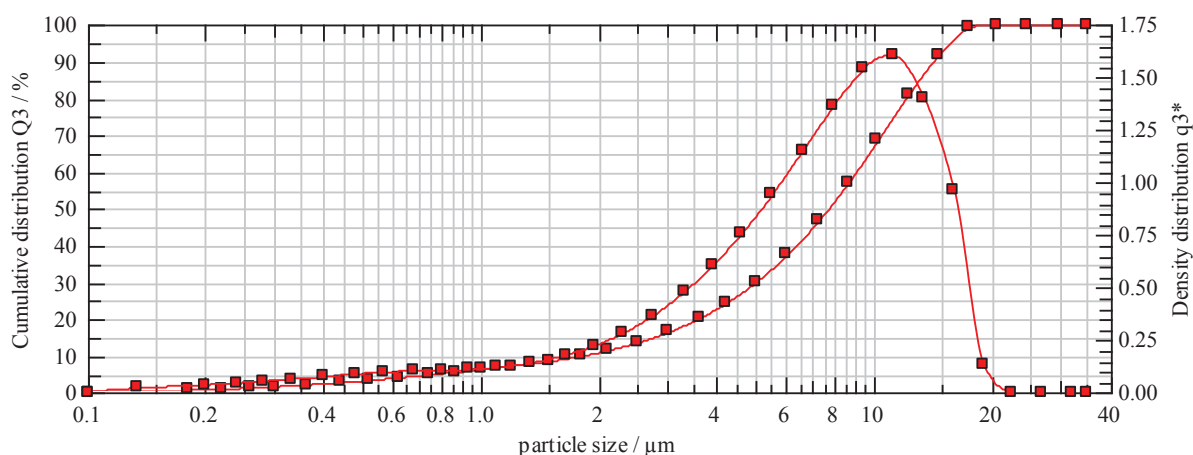


Figure 26 Distribution diagram of Torlon particle size

For the experiment and solution, dimethylacetamide was checked if there are changes regarding mechanical properties of resulting coating but originally the experiment was started with NMP. In each mixing and dissolving and viscosity was measured each time. The reason was in ability to be then applied sufficiently to the surface.

Spraying was chosen as application method to form the coatings. It was necessary to develop the spraying unit to be able to form layer in micron preciseness and methodology to keep good adhesion of the coating. The methods are described later.

5.2.3 Solid lubricants

Molybdenum disulphide

Molybdenum disulphide was chosen in form of commercially available lubricant product Mogul Molyka R from company Paramo, a.s. The percent concentration of MoS_2 in the lubricant is 95 %. Mogul Molyka R was used as additive to PAI solution and therefore also particle size distribution was tested. The resulting distribution curve of the powder form is in Figure 27. The mean for particle is $4.8 \mu\text{m}$ which makes the MoS_2 hard to implement without surface roughness issues. Therefore an effort had to be taken for development suitable preparation technique.

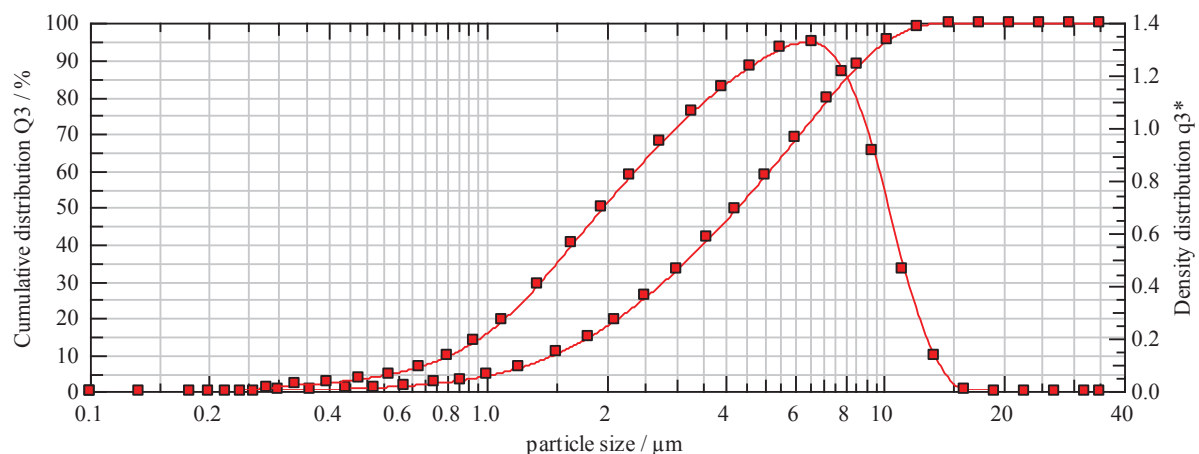


Figure 27 Distribution diagram of MoS_2 particle size

Graphite

The other solid lubricant was tried graphite as based on the literature overview outcome. Commercial classical powdery form with purity level 99.5 % was used. Certainly the particle size needed to be measured in advance as well. The resulting distribution curve is on the following Figure 30. As can be seen from the result, the particle size was too large for our type of coating. It was considered a milling before using.

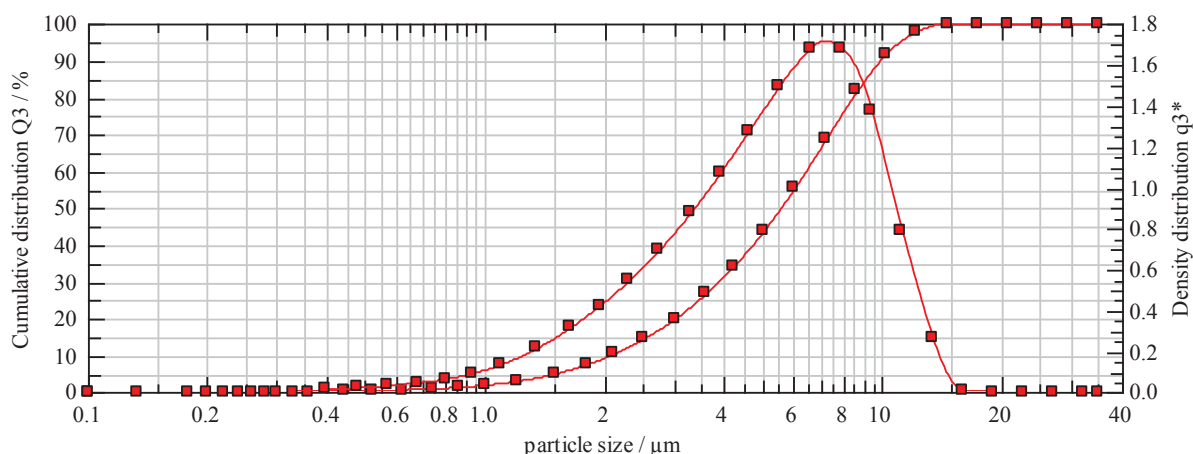


Figure 28 Distribution diagram of Graphite particle size

5.2.4 Calcium hydroxide

Calcium hydroxide was used as filler to increase the toughness of the coating to protect bearing surface in higher specific loads. There was no commercial supplier and therefore it was prepared in laboratory conditions. The preparation was based on past work of Taglieri and Daniele with nanolime [109,110,111].

Anhydrite of calcium chloride (CaCl_2) together with sodium hydroxide (NaOH) was used without further purification. It started from two aqueous solution of calcium chloride (0.3 M) and sodium hydroxide (0.6 M) maintained at the temperature of about 90°C ; the alkaline solution of NaOH (used as precipitator) was added from burette by drops (approx. 4mL/min) to the CaCl_2 one, both in volumes of 50 mL. After about 24 hours two distinct phases were reached, a white precipitated phase in liquid solution. It was necessary to remove NaCl first. Several deionised water washings have been performed through the filtration process. Aqueous nanolime suspension (with a $\text{Ca}(\text{OH})_2$ concentration of 10 mg/ml) was defined as resulting additive. The sample was then characterized.

Structure is represented by the SEM image below (please see Figure 29). The hexagonal structured plates are clearly visible in the image.

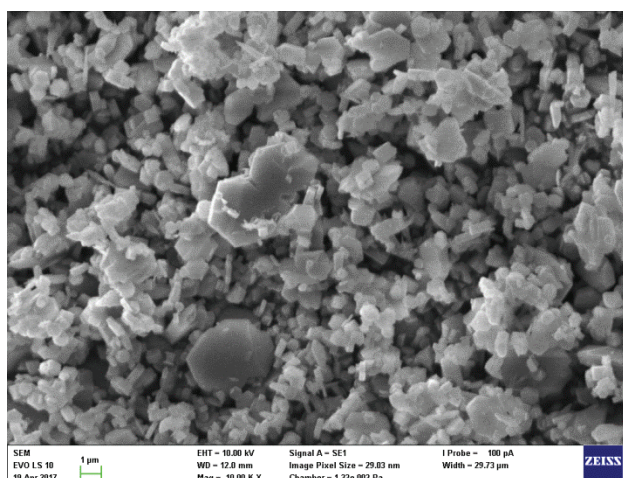


Figure 29 SEM image of hexagonal structure of $\text{Ca}(\text{OH})_2$ magnified 10000x.

The particle size distribution is shown on the curve below (see Figure 30). The main concentration of particles were around 2 μm (mean was 2.07 μm). Originally the lower particle size was expected (based on the literature). However, for the target thickness of the coating, it was sufficient.

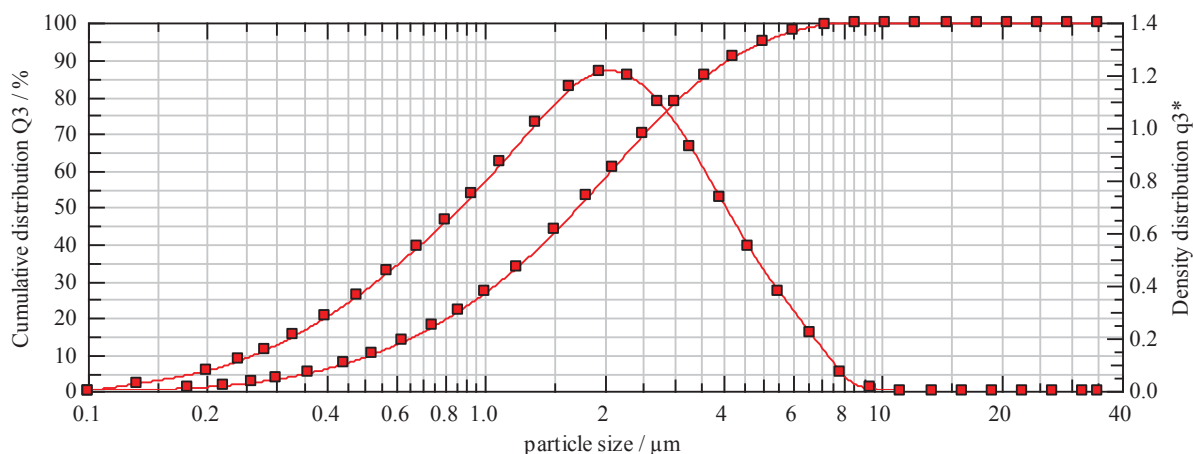


Figure 30 Distribution diagram of Calcium hydroxide particle size

5.3 Preparation of paint

Target solution was undergone by development of mixing method. Small particle size of additives tends to agglomerate when mixed into a solution. The same happened with PAI powder and NMP solvent. It was searched for effective method of de-agglomerating and dispersing of polymer part in solvent to overcome the bonding forces after wetting the powder. For this reason the dispersing device for homogenization and suspensions was chosen. It was used innovative system of gyroscopic mixing of the initial powder form into the solutions and then improved the dispersion and homogeneity of PAI in NMP by dispersing technology on rotor-stator principle. Due to the high circumferential speed of this device, the medium processed is drawn axially into the dispersion head and then forced radially through the slots in the rotor-stator arrangement. The high speed and minimal gap between the rotor and stator produced shear forces resulting in better dispersion.

After the dispersion, the system was characterised from the chemical point of view to analyse the differences between benchmarked and newly prepared PAI solution.

The infrared spectrometry (FTIR) was used to analyse the organics, especially the differences in amide and imide functional groups in each system.

Results of analysis were contrasted against each other to reach if any change occurred in the system.

5.3.1 Viscosity measuring

Viscosity plays a significant role in the preparation of the coating and therefore every dispersion had to be checked for the viscosity. As been mentioned, rheometer ARES-G2 at constant laboratory temperature condition was initially used. As the method needed to be used in each sample preparation, substitutional methodology needed to be carried out.

The comparison testing to rheometer was used TQC Viscosity Cup Immersion Ford according to ASTM D1200. Cup was made of titanium anodised aluminum, with fixed nozzle, orifice No. 4 (see on the picture below Figure 31).



Figure 31 Viscosity cup ASTM D1200, type Ford DIP

Ford viscosity cups are simple gravity devices. The principle is in measuring timed flow of a known volume of liquid through an orifice located at the bottom. When considered ideal conditions, this rate of flow would be proportional to the kinematic viscosity depending on the specific gravity of the draining liquid. Units are expressed in stokes and centistokes. However, it is difficult to maintain conditions all the time ideal. On the other hand, the results were sufficiently used for further analysis. Table 2 below represents the conversion of time flow to resulting viscosity in Centistokes (cSt).

Table 2 Conversion table of Ford viscosity cup results in Centistokes (cSt)

| Time (seconds) | DIN | BS | | | | | ISO | | | | | FORD / ASTM | | | | | ZAHN | | | | | SHELL | | | | | |
|-------------------|-----|------|-----|-----|----|-----|------|------|------|-----|-----|-------------|---|-----|-----|-----|------|-----|------|------|------|-------|------|-----|-----|-----|------|
| | | 4 | 2 | 3 | 4 | 5 | 6 | 3 | 4 | 5 | 6 | 1 | 2 | 3 | 4 | 1 | 2 | 3 | 4 | 5 | 1 | 2 | 3 | 4 | 5 | 6 | |
| 15 | 35 | 6.4 | | | 19 | 40 | 234 | | | 35 | 66 | | | 19 | 40 | | 4 | 99 | 148 | 322 | | | 20 | 48 | 91 | 235 | |
| 16 | 45 | 6.8 | 3 | | 24 | 48 | 262 | | | 39 | 75 | | | 22 | 46 | | 7 | 99 | 163 | 345 | | | 21 | 52 | 96 | 251 | |
| 17 | 51 | 7.3 | 5 | 28 | | 56 | 290 | | | 43 | 84 | | | 24 | 48 | | 11 | 111 | 176 | 368 | | | 23 | 56 | 104 | 267 | |
| 18 | 57 | 7.7 | 7 | 32 | | 64 | 317 | | | 47 | 93 | | | 26 | 52 | | 14 | 123 | 192 | 391 | 1.1 | 7.5 | 24 | 59 | 111 | 284 | |
| 19 | 63 | 8.1 | 9 | 36 | | 72 | 343 | | | 51 | 101 | | | 1 | 59 | 56 | 18 | 135 | 207 | 414 | 1.4 | 8.1 | 26 | 62 | 117 | 300 | |
| 20 | 69 | 8.6 | 11 | 39 | | 79 | 369 | | | 55 | 110 | | | 3 | 61 | 60 | 21 | 146 | 222 | 437 | 1.6 | 8.6 | 27 | 66 | 124 | 316 | |
| 21 | 74 | 9.0 | 13 | 43 | | 86 | 395 | | | 59 | 118 | | | 4 | 63 | 64 | 25 | 158 | 237 | 460 | 1.8 | 9.2 | 29 | 69 | 130 | 332 | |
| 22 | 80 | 9.4 | 15 | 47 | | 93 | 420 | | | 62 | 126 | | | 6 | 66 | 67 | 28 | 170 | 252 | 483 | 2.0 | 9.8 | 30 | 72 | 137 | 348 | |
| 23 | 85 | 9.8 | 17 | 50 | | 100 | 445 | 1 | | 66 | 134 | | | 7 | 68 | 71 | 32 | 181 | 266 | 506 | 2.3 | 10.4 | 32 | 76 | 143 | 365 | |
| 24 | 91 | 10.3 | 18 | 54 | | 107 | 470 | 2 | | 70 | 142 | | | 9 | 40 | 76 | 35 | 193 | 281 | 529 | 2.5 | 10.9 | 33 | 79 | 150 | 381 | |
| 25 | 96 | 10.7 | 20 | 57 | | 114 | 494 | 3 | | 73 | 150 | | | 10 | 43 | 79 | 39 | 205 | 296 | 552 | 2.7 | 11.5 | 35 | 83 | 156 | 397 | |
| 26 | 101 | 11.1 | 22 | 60 | | 120 | 519 | 4 | | 77 | 157 | | | 12 | 45 | 83 | 42 | 216 | 311 | 575 | 2.9 | 12.1 | 36 | 86 | 163 | 413 | |
| 27 | 107 | 11.5 | 23 | 64 | | 127 | 543 | 4.5 | | 80 | 165 | | | 13 | 47 | 87 | 46 | 228 | 326 | 598 | 3.2 | 12.7 | 38 | 90 | 169 | 429 | |
| 28 | 112 | 12.0 | 25 | 67 | | 133 | 567 | 5 | | 84 | 173 | | | 14 | 49 | 91 | 49 | 240 | 340 | 621 | 3.4 | 13.2 | 39 | 93 | 176 | 446 | |
| 29 | 117 | 12.4 | 26 | 70 | | 140 | 591 | 5.5 | | 88 | 180 | | | 16 | 52 | 94 | 53 | 252 | 355 | 644 | 3.6 | 13.8 | 41 | 97 | 182 | 462 | |
| 30 | 122 | 12.8 | 28 | 73 | | 146 | 614 | 6 | 34.5 | 91 | 188 | | | 17 | 54 | 98 | 56 | 263 | 370 | 667 | 3.8 | 14.4 | 42 | 100 | 189 | 478 | |
| 31 | 127 | 13.3 | 30 | 77 | | 153 | 638 | 6.6 | | 95 | 196 | | | 19 | 56 | 102 | 60 | 275 | 385 | 690 | 4.1 | 15.0 | 44 | 104 | 195 | 494 | |
| 32 | 132 | 13.7 | 31 | 80 | | 159 | 662 | 7.3 | 37.5 | 98 | 203 | | | 20 | 59 | 106 | 1 | 63 | 287 | 400 | 713 | 4.3 | 15.6 | 45 | 107 | 202 | 510 |
| 33 | 137 | 14.1 | 33 | 83 | | 165 | 685 | 8.6 | 39.0 | 102 | 210 | | | 22 | 61 | 110 | 4 | 67 | 298 | 414 | 736 | 4.5 | 16.1 | 47 | 110 | 208 | 527 |
| 34 | 142 | 14.5 | 34 | 86 | | 171 | 709 | 9.2 | 41.0 | 105 | 218 | | | 23 | 63 | 114 | 6 | 70 | 310 | 429 | 759 | 4.7 | 16.7 | 48 | 114 | 215 | 543 |
| 35 | 147 | 15.0 | 35 | 89 | | 177 | 732 | 9.8 | 42.0 | 109 | 225 | 24 | | 66 | 117 | 7 | 74 | 322 | 444 | 782 | 5.0 | 17.3 | 50 | 117 | 221 | 559 | |
| 36 | 152 | 15.4 | 37 | 92 | | 184 | 755 | 10.4 | 44.0 | 112 | 233 | | | 26 | 68 | 121 | 8 | 77 | 333 | 459 | 805 | 5.2 | 17.9 | 51 | 121 | 228 | 575 |
| 37 | 157 | 15.8 | 38 | 96 | | 190 | 778 | 11.0 | 45.2 | 115 | 240 | | | 27 | 70 | 125 | 9 | 81 | 345 | 474 | 828 | 5.4 | 18.4 | 53 | 124 | 234 | 591 |
| 38 | 162 | 16.3 | 40 | 99 | | 196 | 801 | 11.6 | 47.0 | 119 | 247 | 1 | | 29 | 73 | 129 | 10 | 84 | 357 | 488 | 851 | 5.6 | 19.0 | 54 | 126 | 241 | 608 |
| 39 | 167 | 16.7 | 41 | 102 | | 202 | 825 | 12.1 | 48.0 | 122 | 254 | 2 | | 30 | 75 | 133 | 11 | 88 | 369 | 503 | 874 | 5.9 | 19.6 | 56 | 131 | 247 | 624 |
| 40 | 172 | 17.1 | 43 | 105 | | 208 | 848 | 12.7 | 50.0 | 126 | 262 | 2 | | 32 | 77 | 137 | 12 | 91 | 380 | 518 | 897 | 6.1 | 20.2 | 57 | 135 | 254 | 640 |
| 41 | 176 | 17.5 | 44 | 108 | | 214 | 871 | 13.3 | 51.2 | 129 | 269 | 3 | | 33 | 80 | 141 | 13 | 95 | 392 | 533 | 920 | 6.3 | 20.7 | 59 | 138 | 260 | 656 |
| 42 | 181 | 18.0 | 45 | 111 | | 220 | 893 | 13.8 | 53.0 | 133 | 276 | 4 | | 35 | 82 | 144 | 14 | 98 | 404 | 548 | 943 | 6.6 | 21.3 | 60 | 141 | 267 | 672 |
| 43 | 186 | 18.4 | 47 | 114 | | 226 | 916 | 14.4 | 54.0 | 136 | 283 | 4 | | 36 | 84 | 148 | 15 | 102 | 415 | 562 | 966 | 6.8 | 21.9 | 62 | 145 | 273 | 689 |
| 44 | 191 | 18.8 | 48 | 117 | | 232 | 939 | 14.9 | 56.0 | 139 | 291 | 5 | | 37 | 86 | 152 | 17 | 105 | 427 | 577 | 989 | 7.0 | 22.5 | 63 | 148 | 280 | 705 |
| 45 | 196 | 19.2 | 50 | 120 | | 238 | 962 | 15.5 | 57.0 | 143 | 298 | 5 | | 39 | 89 | 156 | 18 | 109 | 439 | 592 | 1012 | 7.2 | 23.0 | 65 | 152 | 286 | 721 |
| 46 | 200 | 19.7 | 51 | 123 | | 244 | 985 | 16.0 | 59.0 | 146 | 305 | 6 | | 40 | 91 | 160 | 19 | 112 | 450 | 607 | 1035 | 7.5 | 23.6 | 66 | 155 | 293 | 737 |
| 47 | 205 | 20.1 | 52 | 126 | | 250 | 1008 | 16.6 | 60.0 | 149 | 312 | 6 | | 42 | 93 | 164 | 20 | 116 | 462 | 622 | 1058 | 7.7 | 24.2 | 68 | 159 | 299 | 753 |
| 48 | 210 | 20.5 | 54 | 129 | | 255 | 1030 | 17.1 | 62.0 | 153 | 319 | 7 | | 43 | 96 | 168 | 21 | 119 | 474 | 636 | 1081 | 7.9 | 24.8 | 69 | 162 | 306 | 770 |
| 49 | 215 | 21.0 | 55 | 132 | | 261 | 1053 | 17.6 | 63.5 | 156 | 326 | 7 | | 45 | 98 | 171 | 22 | 123 | 486 | 651 | 1104 | 8.1 | 25.3 | 71 | 166 | 312 | 786 |
| 50 | 219 | 21.4 | 56 | 135 | | 267 | 1076 | 18.2 | 64.5 | 160 | 334 | 8 | | 46 | 100 | 175 | 23 | 126 | 497 | 666 | 1127 | 8.4 | 25.9 | 72 | 169 | 319 | 802 |
| 51 | 224 | 21.8 | 58 | 138 | | 273 | 1099 | 18.7 | 66.0 | 163 | 341 | 8 | | 48 | 103 | 179 | 24 | 130 | 509 | 681 | 1150 | 8.6 | 26.5 | 74 | 173 | 325 | 818 |
| 52 | 229 | 22.2 | 59 | 141 | | 279 | 1121 | 19.2 | 67.5 | 166 | 348 | 8 | | 49 | 105 | 183 | 25 | 133 | 521 | 696 | 1173 | 8.8 | 27.1 | 76 | 176 | 332 | 834 |
| 53 | 234 | 22.7 | 60 | 144 | | 285 | 1144 | 19.7 | 69.0 | 170 | 355 | 9 | | 50 | 107 | 187 | 26 | 137 | 532 | 710 | 1196 | 9.0 | 27.6 | 77 | 179 | 338 | 851 |
| 54 | 238 | 23.1 | 62 | 147 | | 291 | 1166 | 20.2 | 70.0 | 173 | 362 | 9 | | 52 | 110 | 191 | 28 | 140 | 544 | 725 | 1219 | 9.3 | 28.2 | 79 | 183 | 345 | 867 |
| 55 | 243 | 23.5 | 63 | 150 | | 297 | 1189 | 20.7 | 71.5 | 176 | 369 | 10 | | 53 | 112 | 194 | 29 | 144 | 556 | 740 | 1242 | 9.5 | 28.8 | 80 | 186 | 351 | 883 |
| 56 | 248 | 24.0 | 64 | 153 | | 302 | 1212 | 21.2 | 73.0 | 180 | 376 | 10 | | 55 | 114 | 198 | 30 | 147 | 567 | 755 | 1265 | 9.7 | 29.4 | 82 | 190 | 358 | 899 |
| 57 | 253 | 24.4 | 66 | 156 | | 308 | 1234 | 21.7 | 75.0 | 183 | 383 | 11 | | 56 | 116 | 202 | 31 | 151 | 579 | 770 | 1288 | 9.9 | 30.0 | 83 | 193 | 364 | 915 |
| 58 | 257 | 24.8 | 67 | 159 | | 314 | 1257 | 22.2 | 76.0 | 186 | 390 | 11 | | 58 | 119 | 206 | 32 | 154 | 591 | 784 | 1311 | 10.2 | 30.6 | 85 | 197 | 371 | 932 |
| 59 | 262 | 25.2 | 68 | 162 | | 320 | 1279 | 22.7 | 77.0 | 190 | 397 | 12 | | 59 | 121 | 210 | 33 | 158 | 603 | 799 | 1334 | 10.4 | 31.1 | 86 | 200 | 377 | 948 |
| 60 | 267 | 25.7 | 70 | 165 | | 326 | 1302 | 23.2 | 79.0 | 193 | 405 | 12 | | 60 | 123 | 214 | 34 | 161 | 614 | 814 | 1357 | 10.6 | 31.7 | 88 | 204 | 384 | 964 |
| 65 | 290 | 27.8 | 76 | 179 | | 354 | 1414 | 26 | 86.0 | 210 | 440 | 15 | | 68 | 135 | 233 | 40 | 179 | 673 | 888 | 1472 | 11.8 | 34.6 | 95 | 221 | 416 | 1045 |
| 70 | 313 | 29.9 | 83 | 194 | | 383 | 1526 | 28 | 93.0 | 226 | 475 | 17 | | 75 | 147 | 252 | 45 | 196 | 731 | 962 | 1567 | 12.9 | 37.4 | 103 | 236 | 445 | 1126 |
| 75 | 337 | 32.1 | 89 | 208 | | 412 | 1638 | 31 | 100 | 243 | 510 | 20 | | 82 | 158 | 271 | 51 | 214 | 790 | 1036 | 1702 | 14.0 | 40.3 | 110 | 255 | 481 | 1207 |
| 80 | 360 | 34.2 | 96 | 223 | | 441 | 1750 | 33 | 108 | 260 | 545 | 22 | | 89 | 170 | 291 | 56 | 231 | 848 | 1110 | 1817 | 15.1 | 43.2 | 118 | 273 | 514 | 1288 |
| 85 | 383 | 36.4 | 102 | 237 | | 469 | 1861 | 35 | 115 | 276 | 580 | 25 | | 96 | 181 | 310 | 61.6 | 249 | 907 | 1154 | 1932 | 16.3 | 46.1 | 126 | 290 | 546 | 1369 |
| 90 | 406 | 38.5 | 108 | 252 | | 498 | 1973 | 38 | 122 | 293 | 615 | 27 | | 104 | 193 | 329 | 67 | 266 | 965 | 1258 | 2047 | 17.4 | 49.0 | 133 | 307 | 579 | 1450 |
| 100 | 452 | 42.8 | 121 | 280 | | 554 | 2195 | 42 | 135 | 326 | 684 | 32 | | 118 | 216 | 368 | 76 | 301 | 1082 | 1406 | 2277 | 19.7 | 54.7 | 148 | 342 | 644 | 1612 |
| 110 | 499 | 47.0 | 134 | 309 | | 611 | 2418 | 47 | 149 | 355 | 754 | 37 | | 132 | 239 | 405 | 89 | 336 | 1199 | 1554 | 2507 | 21.9 | 60.5 | 163 | 376 | 709 | 1774 |
| 120 | 545 | 51.3 | 146 | 338 | | 668 | 2640 | 51 | 162 | 383 | 823 | 42 | | 147 | 262 | 445 | 100 | 371 | 1316 | 1702 | 2737 | 24.2 | 66.2 | 178 | 411 | 774 | 1939 |
| 130 | 591 | 55.6 | 159 | 366 | | 724 | 2862 | 555 | | | | | | | | | | | | | | | | | | | |

5.3.2 Application to the surface

In any of bearing design handbook can be read that the minimum value of the oil film thickness may reach down to a value of a human hair diameter. Such a small gap between the bearing and the journal surfaces demonstrates the importance of keeping the dimensions, shapes and the surface quality of the parts at very tight tolerances.

When applying the coating, the possible thickness variation had to be considered. For this reason, procedure for precise application of paint to the surface was developed. The automatic spraying system was used for experimental production (see below on Figure 32 Polymer spraying unit).

This system works with pressurized pot in which the paint is mixing and through pressure valve transferred towards the automatic spraying gun with nozzle of certain diameter on extension system. The extension allowed spraying multiple bearings fixed on the rotary stage. The diameter of nozzle was chosen according to the paint mixture, used additives as well as the target thickness. We have started with minimum thickness to keep the oil clearance for testing. The rotation of the rotary stage was set to the maximum rotation speed to keep the maximum distribution on the surface in horizontal direction. Speed of the nozzle in vertical direction as well as paint volume input sprayed was optimized based on the experimental results of the resulting paint.



Figure 32 Polymer spraying unit

In order to increase the adhesion of the paint to aluminium surface, it had to be develop system for increasing the surface area and cleaning the substrate for oxidized layer which could influence the adhesion forces. On the same time it was necessary to keep the thickness of bearing unchanged. Based on the development started in Daido Metal, it was considered to follow in the same direction. Sandblasting was chosen as a pre-treatment method for preparation of polymer spraying. The system can be seen on the picture below (see Figure 33).



Figure 33 Sandblasting Unit

Sandblasting unit was purchased from commercial distributor. There was needed additional design since the design of cabin was used only for the hand sandblasting with no option for automatic pre-treatment. It was important to eliminate any differences within the samples to accurately observe the quality of final coating. The design consisted of arm holding the jig with bearing. The arm was designed for movement in X and Y axis and with option for rotation. The rotation was important for the quality of surface treatment of bearing shapes. The process and working parameters were developed by adjusting the speeds of movements and pressure of sandblasting. Roughness and thickness on the bearing was measured and final check for adhesion was carried out.

5.4 Tribochemical analysis

5.4.1 Oil analysis

Optical Emission Spectrometer with Inductively Coupled Plasma (OES)

Optical emission spectrometer with inductively coupled plasma (ICP-OES) was applied for the qualitative and quantitative determination of the elemental composition of the fresh and

used oil. The device was a Vista MPX (Varian, Australia) optical emission spectrometer. Before ICP OES analysis, the samples were prepared by acidic digestion in a microwave device (Multiwave 3000, Anton Paar, Austria) to transform the present metallic and non-metallic compounds into water soluble salts and to avoid undesired matrix effects of the oil which could disrupt the measurement. The obtained aqueous solutions were directly introduced to the ICP OES device for analysis.

Fourier Transform Infrared Spectroscopy (FTIR)

Infrared spectra in the mid-infrared range (400 to 4000 cm^{-1}) were obtained by a FTIR Tensor 27 (Bruker, Germany). Transmission spectra were prepared with a ZnSe cuvette having a path length of 100 μm . Spectrum interpretation was based on identification of base oil and additive specific absorption bands.

Oxidation and nitration of oil samples were determined according to DIN 51453. Therein, the extinction is determined at the wavelength of 1710 cm^{-1} with baseline endpoints at 1970 cm^{-1} and 580 cm^{-1} . Similarly, the nitration is determined by the extinction measured at the wavelength of 1630 cm^{-1} with baseline endpoints at 1645 cm^{-1} and 1615 cm^{-1} . Per definition, unused oils have no oxidation or nitration.

Stabinger viscometer

Viscometrical data (according to ASTM D 7042) and densities were determined by a Stabinger viscometer (SVM 3000 Anton Paar, Austria). In comparison to conventional capillary viscometers, the Stabinger viscometer requires only a small quantity of oil (about 3 mL). The kinematic viscosity and the density of the oil samples were measured at 40°C and 100°C. The viscosity indices (VI) according to ISO 2909 and densities at 15°C and were calculated from the measuring values at 40 and 100°C.

Total Base Number (TBN)

TBN is a measure for the ability of the oil to neutralize acids. It was determined by potentiometric titration in glacial acetic acid using perchloric acid according to standard DIN ISO 3771. The level of base reserve is expressed in mg KOH/g oil.

Neutralisation Number (NN) by Colorimetric Titration

Neutralisation number is a measure for the acids in oil. The amount of oil acidification was determined by manual colorimetric titration according to DIN 51558. The oil samples were dissolved in a mixture of toluene, isopropanol and small amounts of water. The sample solutions were then titrated with methanolic potassium hydroxide (KOH) with a concentration of 0.1 mol/L using alkali as indicator. The level of acidification is expressed as neutralisation number (NN) in mg KOH/g oil.

Advanced oil analysis

High-resolution and accurate mass spectroscopic measurements of the fresh and used oil samples – the latter obtained from the fatigue test machine – were performed in positive and negative ion mode using a LTQ Orbitrap XLTM hybrid tandem mass spectrometer (Thermo Fisher, Bremen, Germany) equipped with an IonMax atmospheric pressure interface (API) ion source that carries the electro-spray ionisation (ESI) probe and the atmospheric pressure chemical ionisation (APCI) probe (Thermo Fisher scientific, Germany). For qualitative

analyses, a methodology proposed by Pisarova et al. has been modified [112]: the oil samples were dissolved in a 7:3 chloroform-methanol mixture, with a dilution factor of 1:1000 and injected via direct infusion into the mass spectrometer using the ESI and APCI probe.

In the next step, selected additives were semi-quantified by normal phase liquid chromatography (NPLC) that was performed using an Accela pump (Thermo Fisher scientific) coupled with APCI and the LTQ Orbitrap XL tandem mass spectrometer. The mobile phase was a mixture of n-hexane, ethyl acetate and 2-propanol in the ratio 93:5:2 applied with a flow rate of 400 $\mu\text{L}/\text{min}$. As stationary phase, a Luna NH2 5 μm 150 x 2.00 mm from Phenomenex was selected. Before injection, the oil samples were diluted in n-hexane with a dilution factor 1:1000. The resulting chromatograms were processed with Xcalibur 2.0.7 software (Thermo Fisher scientific).

5.4.2 Surface characterisation

Characterisation of Surface by Profilometers

Regarding the initial tribochemical preliminary study of benchmark coating experiments, the measurements of the topography was performed with Alicona InfiniteFocus G5 focus variation microscope with 5x objective. After rinsing the bearing half shells with petroleum ether, the images were measured and built from 10 lines and 8 columns (calculation from 80 individual images) for the new surface and surface from bench test as well as 10 lines and 7 columns (calculation from 70 individual images) for the surface from the metal (rig) test.

Topographic measurement by focus variation was performed by determining the best focus position of the optical sensor elements. This focus position was related to a certain distance between the objective lens and the sample. Therefore, the sample is vertically scanned at different distances or focus positions, respectively. The best focus position was calculated by determining the contrast between each pixel and its respective neighbours in the CCD array. Additionally to the topography, the device simultaneously provided the true colour image of the sample. This technique allows surveys of machine parts and components regarding wear and geometrical changes of high resolution in reasonable time.

For further characterisation of the coating, a Bruker Contour Elite™ X was used for its advanced metrology functions where we were able to measure the surface wear scars in nanometer range.

Roughness measurement

For surface roughness measurement, the parts were cleaned from residues of oils and dirt. The testing system was Zeiss surfcom 530A. There are many different roughness parameters in use, but R_a seems so far as the most common and therefore was considered here as well. The measuring distance was 4 mm with step of measuring 0.5 μm and speed 0.150 mm/s.

SEM analysis

For the documentation of the general condition of the cleaned bearing half shells, a stereomicroscope was applied without prior cutting of the cleaned specimens.

Morphology and elemental composition was provided by high resolution scanning electron microscope (HR-SEM) Supra VP40 (Carl Zeiss AG, Germany) equipped with an electron field emission gun (Schottky thermal field emitter) and an energy-dispersive X-ray

spectroscopy (EDS) detector for elemental analysis. The cleaned bearing half shells were analysed without prior cutting.

For the further material characterisation was used Zeiss Evo LS 10 equipped with the detector of secondary electrons, detector of backscattered electrons as well as the detector of secondary electrons for variable pressure and Energy-Dispersive X-Ray Analyser for the analysis and mapping of elements.

And at the final resolution imaging and analysis on the coating, a JEOL JSM-7600F was used equipped with an electron field emission gun (Schottky thermal field emitter) and an energy-dispersive X-ray spectroscopy (EDS) detector for elemental analysis.

X-ray photoelectron spectroscopy (XPS)

For XPS characterisation bearing half shells were cut by rotary jars. Detailed analysis of the surface chemistries regarding elemental composition and binding states of the elements was obtained by XPS using a Theta Probe (Thermo Fisher Scientific, East Grinstead, UK) with a monochromatic Al K α X-ray source ($h\nu = 1486.6$ eV). The base pressure during the measurements was consistently at 3×10^{-9} mbar. Analytical spot resolution for the survey spectra was $400 \mu\text{m}$ at a pass energy of 200 eV. For the detail spectra, the pass energy was reduced to 50 eV. For the investigation of smaller surface features, the spot resolution was set to $50 \mu\text{m}$. Depth profiles were acquired by Ar $^{+}$ etching. An area of $2 \times 2 \text{ mm}^2$ was sputtered with an acceleration voltage of 3 kV at a sputter current of $1 \mu\text{A}$. The surface was sputtered for 0, 10, 20, 50, 80, 110, 210 and 260 seconds. The depth was calculated according to the average sputter rate of $0.2 \text{ nm/s}/\mu\text{A}/\text{mm}^2$. All acquired spectra were referenced to the C1s peak at 284.6 eV. The resulting analytical data were processed with the Avantage Data System software (Thermo Fisher Scientific, East Grinstead, UK) using Gaussian/Lorentzian peak fitting. Prior analysis, the bearing half shells have been cut in specimens of each approximately 2 cm and were cleaned with petroleum ether by 10 min ultrasonication.

Laser desorption ionisation mass spectrometry (LDI-MS)

The cut specimens for XPS analysis were further analysed by LDI-MS by procedure developed in AC2T research GmbH¹¹³. The atmospheric pressure (AP) matrix assisted laser desorption ionization (MALDI) and LDI mass spectrometric measurements were performed on a LTQ Orbitrap XLTM hybrid tandem mass spectrometer (Thermo Fisher, Bremen, Germany). AP MALDI/LDI MS experiments were conducted using an AP MALDI PDF+ ion source from MassTech (Columbia, MD, USA). The wavelength of the all-solid-state triple frequency Nd:YAG laser source was 355 nm operated at a repetition rate of 10 Hz. Laser pulse width was 3-5 ns (FWHM) with pulse energy of 200 μJ . Pulse delay for pulsed dynamic focusing (PDF) was set to 25 μs to optimize ion signals. Temperature of the transfer capillary was set to 275°C, and the automatic gain control (AGC) of the LTQ Orbitrap XL was turned off to secure equal acquisition time for each single scan event. Overall acquisition time for all AP MALDI experiments was set to 0.5 min. The samples were analysed without (LDI) and with matrix (MALDI) applied onto the surface where the matrix served as promotor of ionisation. For MALDI measurements, the matrix solution was prepared of α -cyano-4-hydroxycinnamic acid (CHCA) with a concentration of 10 mg/mL in a mixture of acetonitrile and water (1:1, v/v).

Nanoindentation

Nanoindentation was the only option to characterize some of the mechanical properties of the coating. The system used was Anton Paar Nanoindentation NHT and the testing parameters are in the Table 3. The parameters were adjusted according to preliminary testing and expertise on similar coatings.

Table 3 Testing parameters for Nanoindentation

| Scratch parameters | |
|------------------------------|---|
| Acquisition Rate : 10.0 [Hz] | Advanced Approach distance : 2000 nm |
| Linear Loading | Approach speed : 2000 nm/min Retract speed : 2000 nm/min |
| Max load: 10.00 mN | |
| Loading rate: 20.00 mN/min | |
| Unloading rate: 20.00 mN/min | |
| Pause : 10.0 s | |
| Indenters | |
| Type : Berkovich | |
| Material : Diamond | |

Scratch testing

Scratch testing is a widely used technique to characterize the practical adhesion failure of thin films and coatings. For testing the adhesion of developed coatings, Micro Scratch Tester from Anton Paar was used. The test parameters are in the table below. It was chosen on the basis of the experimental results and considering the hardness and thickness of the coating.

Table 4 Testing Parameters for Scratch Test

| Scratch parameters | |
|---------------------------|------------------------------|
| Linear Scratch | + RST S/N: 01-05468 settings |
| Type: Progressive | Fn contact : 1 N |
| Begin Load (N): 1 | Fn Speed : 5 N/s |
| End Load (N): 30 | Fn Remove speed : 10 N/s |
| Loading rate (N/min): 60 | Approach speed : 2 %/s |
| AE Sensitivity: 7 | |
| Indenters | |
| Type : Rockwell | Material : Diamond |
| Radius (µm) : 200 | |

5.4.3 Tribotesting

The experimental verification of all samples was performed by applying variety of stresses towards the surface by running on small tabletop systems with low load and contact area. Big

bearing evaluation systems were possible to reach from outsource testing in Daido Metal with preliminary study on benchmark coatings.

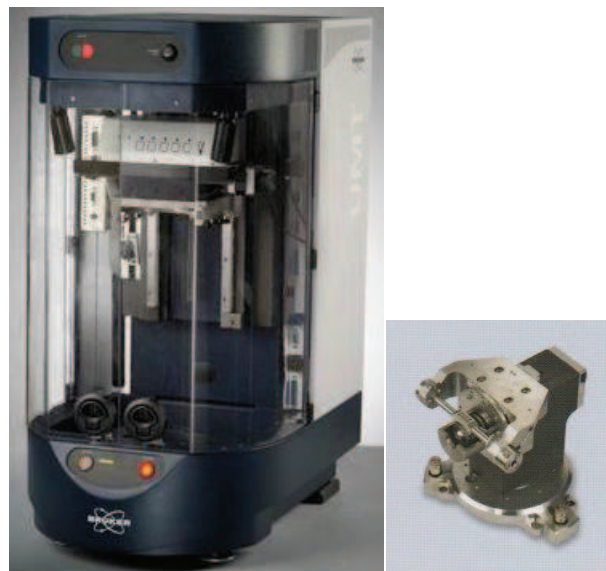
Analysis and investigation of the surface and characterisation of coating was applied after the each test and failure mechanisms and tribological properties were studied.

Block on ring

The system based on a Bruker Universal Mechanical Test (UMT) platform with precision control of load, speed, and position was used for specific frictional and wear characteristics of newly developed polymer coating. Its complementarity to prediction of tribological behaviour of developed paint was able to decrease the amount of samples needed to be tested on fatigue test of big and expensive tribometer.

The machine consists of single motor to cover full torque (up to 5Nm) and speed range (0.1 to 5000 rpm).

Block on ring configuration as the drive module was chosen since this setting allows pure sliding conditions very much similar to application of the halfbearings. The machine is pictured on Figure 34 below.



a) b)
Figure 34 UMT Tribolab system (a) with Block-on-ring drive (b)

Configuration was chosen because the configuration simulates typical sliding conditions similar to the configuration in the real engine bearings.

As the ring was used Timken A4183, \varnothing 35 where surface roughness was measured and controlled below 0.1. Load was adjusted to 40N and controlled by load sensor. Speed for the ring was adjusted to the sequences 10,20,50,100,200,400,700,1000,1500 rpm with intervals for each speed 10s and 6s for speeds 1000 and 1500 min^{-1} .

As the lubricant was used mineral oil in the viscosity grade VG22 in the laboratory temperature. Test was repeated 3 times from low speed to highest and vice versa (total 6 cycles). The overview of the testing parameters is in the Table 5.

Table 5 Testing parameters for Bruker UMT Tribolab system

| | Dimensions | Units |
|------------------------|--|---------------------------------|
| Sample | 9x5xT1.5 | mm |
| Counterpart | ring, carbon steel $R_z \leq 0.09$, diameter 35 mm | μm |
| Loading | 4 | Kg |
| Speed | 10-1500 | rpm |
| Test Duration | 7 | min |
| Lubrication | Renolin GP 22 | |
| Oil Temperature | 20 | °C |

Ball on disc

A Mini traction machine (MTM) is conventional ball-on-disk configuration tribo-tester. Its advantage is simple contact conditions. Therefore it is also valuable system for friction and wear testing options. Our main target was the study of boundary and mixed lubrication regime on developing samples.

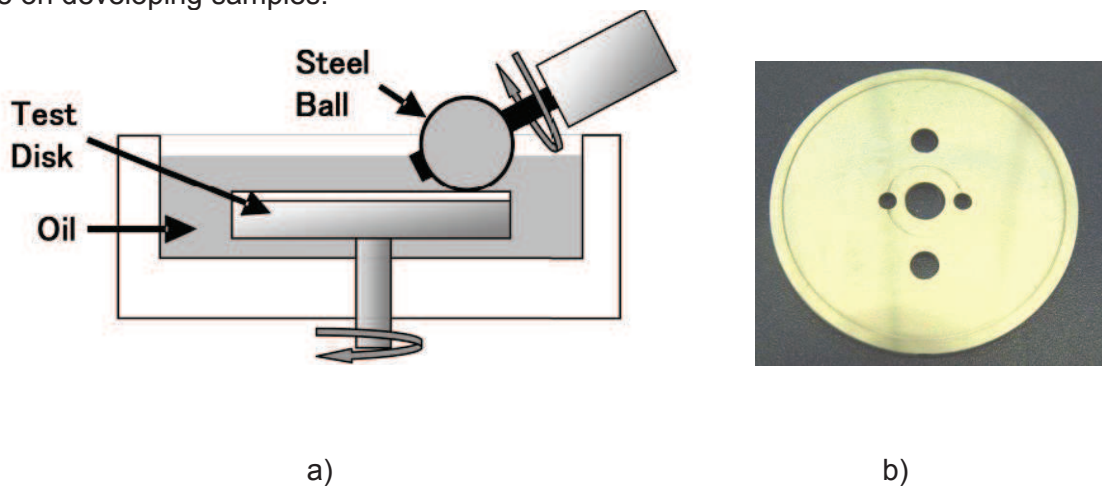


Figure 35 MTM ball-on-disc configuration (a) and test specimen (b)

Big disadvantage of the system is the point contact as well as the stationary ball which made system difficult for softer plain bearing materials. The configuration can be seen on the Figure 35.

The tests were performed for various entrainment velocities under fixed relative sliding velocity as the new experimental method by controlling the ball rotational speed and the test disk independently.

Testing conditions:

The disc in diameter 46 mm was used which was prepared from our target developing material. Regarding the ball, used material was JIS SUJ2, equivalent to the bearing steel 100Cr6 used conventionally in standard MTM tests and ball size 19.05 mm.

Sliding velocity was 0.5 m/s and entertainment speed was varied between 1 to 2350 rpm. The ball was loaded against disc by load of only 1N to prevent hard hertzian contact (in our case only cca 190 MPa).

The tests were running in lubricated conditions with oil Renolin GP 22. They are the base oils without additives and heated to 60°C during the test.

The overall conditions are on the presented in Table 6.

Table 6 Conditions of MTM tests

| Items | Conditions | Unit |
|----------------------------|--------------------|------|
| Disc Diameter | 46 | mm |
| Ball size | 19.05 | mm |
| Ball material | JIS SUJ2 (100Cr6) | - |
| Sliding velocity | 0.5 | m/s |
| Entertainment speed | Varied 0-11 | m/s |
| Test load | 1.0 | N |
| Test oil | Renolin GP 22 | - |
| Oil Temperature | 60 | °C |

Tribotesting for benchmark evaluation

For benchmark pre-evaluation procedure, two kinds of experiments were chosen. One set of bearing specimens were assessed in an engine bench test, and another set was evaluated in a laboratory tribometer (half bearing rig test machine) of Daido Metal. The engine bench test covered short-term tests on a 3.5 L V6 gasoline engine according to the internal methodology of a car manufacturer.

Laboratory machine system of Daido Metal allows the application of more severe conditions in the tribosystem bearing-oil-shaft. A dynamic loading was applied to the connecting rod with a mounted test bearing. The loading pattern was sinusoidal where the specific load was 60 MPa with a frequency of 200 Hz. The shaft was made of steel JIS S55C with roughness Rz below 0,1 µm and connected to the driving unit. A torque meter was installed between the shaft and a motor to monitor torque during the test. Thermocouples were used to measure the temperature on the outer side of the test bearing to detect seizure and fatigue on the bearing. Engine oil was pumped via an inlet above the upper bearing half shell into the tribocontact. Tests were stopped when the temperature on the backside of the bearing raised rapidly as a response to crack initiation. Otherwise, the test bearing passes the fatigue test if no critical temperature increase happens within 19,7 mil cycles. Bearings and the engine oils were sampled and subjected to surface and lubricant analysis, respectively.

6 RESULTS AND DISCUSSION

The results are divided according to the goals which were introduced in experimental part of this dissertation. It was started with the description and characterisation of tribochemistry on our benchmarked materials. The oil which came into the contact when testing to characterize for wear particles as well as the degradation processes. These results helped with understanding and description of bearing lubrication – interaction between lubricants and bearing surfaces especially under boundary conditions and provided necessary input for further polymer layer development. Further, the wear and fatigue performance of material was studied and compare the developed testing method with classical engine bearing production. Based on these results, new mixture was formulated and applied to the same surface material and tested again.

6.1 Tribotesting

The benchmark bearing set of commercial bearing of Daido Metal with polymer overlay which was assessed in the engine bench test passed without any difficulties and significant damage as can be seen in C. Although considerable surface modifications, compared to the newly produced bearing half shells (Figure 36), were observable, no complete removal of the coating of these bearings occurred. Accordingly, the presence of abrasive wear scars did not negatively influence reliability of the coating.

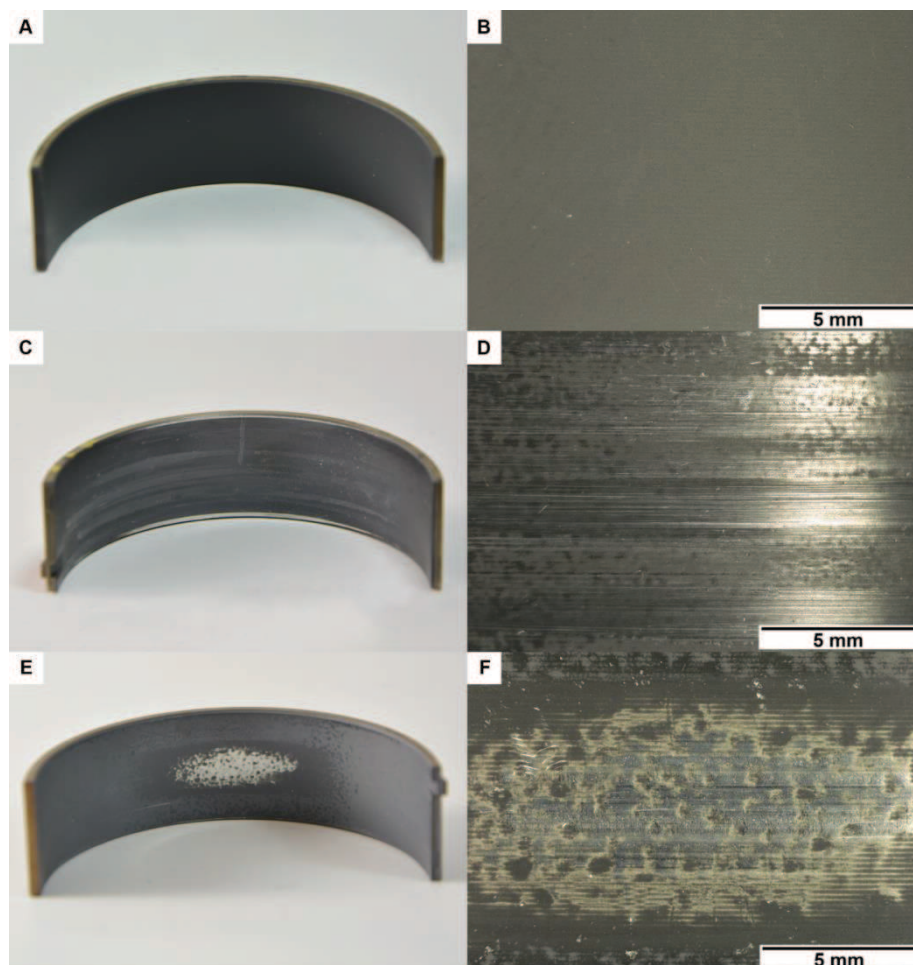


Figure 36 Appearance (A) and stereomicroscopic image (B) of a newly produced engine bearing. Appearance (C) and stereomicroscopic image (D) of the loaded bearing half shell

after the engine bench test. Appearance (E) and stereomicroscopic image (F) of the loaded bearing half shell after the fatigue experiment.

A complete loss of the coating was observed on samples from laboratory tribometer of Daido Metal where 19,7 mil cycles were applied. Wear observed is attributed to the mainly loaded area where the bearing surface is operating in the boundary lubrication regime. Under such conditions, abrasive wear on the surface can often be observed. Worn surfaces are discussed in more detail later.

6.2 Lubricant analysis

6.2.1 Conventional oil analysis

As to the proper interpretation of the surface chemistries, prior compilation of oil analytical data was necessary. The differences between the fresh oil compared to the one from fatigue experiment were already detectable visually: the used oil showed indication of darkening, hence signs of degradation. Minor differences between the fresh and the used oil are also observable for the carried out elemental analysis by ICP-OES, see Table 7. The used oil from fatigue experiment contained iron in a concentration of 32 ppm which can be assigned to wear particles. Elements from additives can be attributed to the antiwear additive zinc dialkyldithiophosphate (ZDDP), an additive based on molybdenum acting as antioxidant, friction modifier and/or wear protecting additive, a detergent based on calcium and a boron-containing additive. Copper typically found in non-ferrous bearing materials and silicon typically found in antifoam additives appeared only in very low concentrations. The decrease of Ca, Mo, S and Zn are not necessarily related to additive degradation, because these changes are in the range of measuring inaccuracy.

Table 7: Elemental analysis of 0W-20 GF5 unused and used oil by ICP OES, Yellow: wear related alteration, green: no alteration

| Sample | Concentration (ppm) | | | | | | | | |
|-----------|---------------------|------|-----|----|-----|-----|------|-----|-----|
| | B | Ca | Cu | Fe | Mo | P | S | Si | Zn |
| Fresh oil | 240 | 1970 | <5 | 1 | 690 | 710 | 1960 | <10 | 640 |
| Used oil | 240 | 1880 | <10 | 32 | 680 | 710 | 1860 | <10 | 630 |

The presence of ZDDP was also confirmed by the FTIR spectra of the oils (Figure 37), which shows a significant absorption band at 900 to 1100 cm⁻¹.

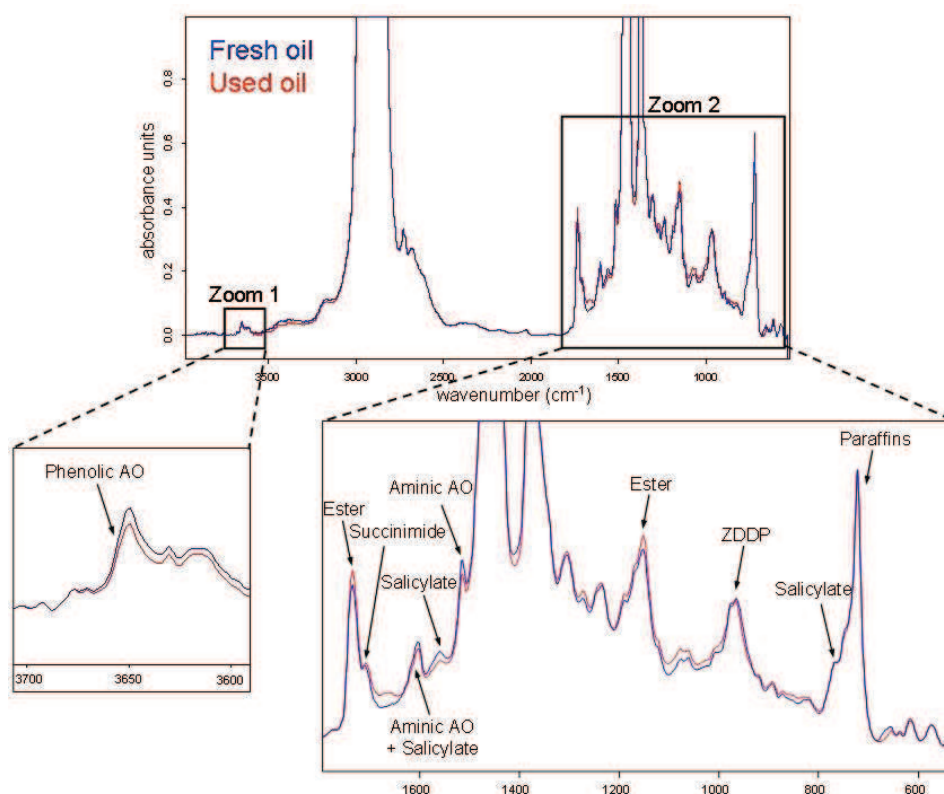


Figure 37: Detailed evaluation of the FTIR spectra of 0W-20 GF5 unused and used oil showing basic structures of base oil and additives. 'AO' is the abbreviation for antioxidant.

Further absorption bands characteristic to phenolic and aminic antioxidants ('Phenolic AO' and 'Aminic AO') could be assigned as well as salicylates (detergents) and succinimides (dispersants). Oxidation and nitration level of the used oil were also determined by processing the respective FTIR spectra according to DIN 51453. In the case of the oxidation level, a moderate increase was elucidated for the used oil. For the nitration, no change compared to the fresh oil was observable as expected because nitration can be found in engine oils stressed to combustion processes but not in tribometers due to lack of a combustion process.

Furthermore, the base oil could be elucidated as a group 3 hydrocrack oil. As VI improver, polymethylacrylate (PMMA) can be suggested by means of the FTIR spectra (as analysed earlier). It is noted that ICP-OES and FTIR provide substantial information about the composition of fresh and used lubricants. However, elements by ICP-OES and functional groups by FTIR cannot evidence the exact structure of the lubricant components as it is possible by mass spectrometry.

As a consequence of tribological stress, the viscosity has significantly changed. The results of the measurements with the Stabinger viscometer are shown in Table 8.

Table 8: Viscosity parameters and density of the 0W-20 GF5 unused and used oil.

| Sample | Viscosity at 40°C (mm²/s) | Viscosity at 100°C (mm²/s) | VI (-) | Density at 15°C (g/cm³) |
|-----------|---------------------------------|----------------------------------|-----------|-------------------------------|
| Fresh oil | 37.0 | 8.49 | 218 | 0.8451 |
| Used oil | 31.4 | 6.97 | 193 | 0.8473 |

The used oil viscosity at 40 and 100° C decreased significantly in comparison with the fresh oil. Accordingly, the viscosity index which is 218 for the fresh oil decreased to 193 for the used oil. VI decrease can be explained by higher shear stress in the fatigue experiment that causes substantial degradation of the VI improver polymer added to achieve lower temperature dependency of the engine oil viscosity.

Oxidation typically indicates base oil degradation and is accompanied by viscosity increase. However, as oxidation took place at a low level, oxidation-induced viscosity increase can be neglected for the used oil.

Also in the case of the total base number and the neutralisation number, a significant alteration was observed between the unused and the used oil (see Table 9). However, the degradation of the used oil is not in a range where it would cause failure during operation.

Table 9 Base reserve (TBN) and acidification (NN) of 0W-20 GF5 unused and used oil.

| Sample | TBN [mg KOH/g] | NN [mg KOH/g] |
|------------|-------------------|------------------|
| Unused oil | 8.93 | 1.85 |
| Used oil | 8.51 | 2.26 |

6.2.2 Chemistry of fresh oil by advanced analysis

By applying ESI-MS and APCI-MS, several oil additives could be determined in the engine oil 0W-20 GF5. The additive structures elucidated are illustrated in Table 10.

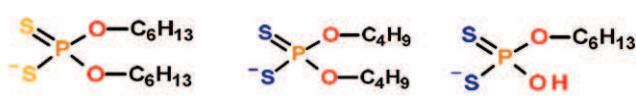
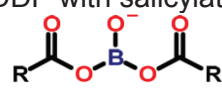
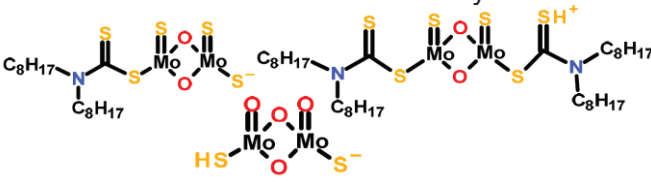
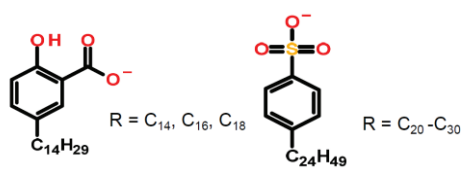
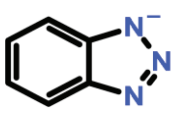
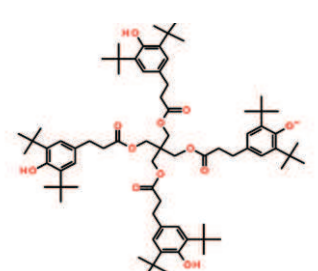
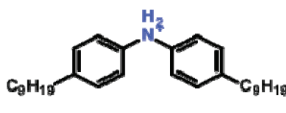
The presence of ZDDP as anti-wear additive was already confirmed by ICP-OES and FTIR measurements. MS measurements provided more structural information which is based on the interpretation of the mass-to-charge ratios (m/z) that refers to molar masses of the charged molecules. The characteristic main peak of ZDDP was detected at 297.11 m/z . To this ion mass, a ZDDP structure with two C_6 side chains can be assigned. Other masses detected can also be attributed to ZDDP and the differences in m/z compared to the main peak can be explained by variations in the alkyl side chain lengths, exemplarily: ZDDP with two C_4 (butyl) side chains was detected at 241.05 m/z ; the ion 213.02 m/z can be assigned to a ZDDP with a single alkyl chain of C_6H_{13} . As second anti-wear agent, molybdenum dialkyldithiocarbamates was identified. This finding conforms to the results obtained by ICP-OES where molybdenum was unambiguously determined. It is known that the combination of organic molybdenum compounds and ZDDP can lead to a significant reduction of the friction coefficient of the lubricant by a synergistic mechanisms [114]. As third anti-wear additive, borate esters were identified. This finding is also in good agreement with the ICP-OES results. These borate esters are also known to be effective anti-oxidants [115].

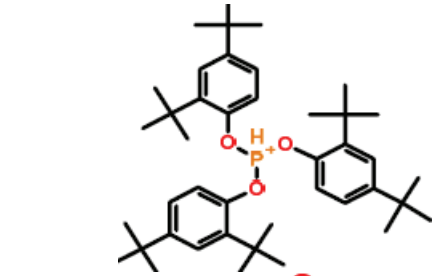
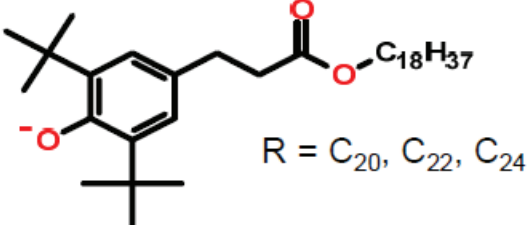
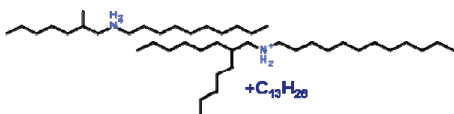
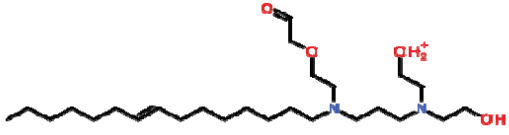
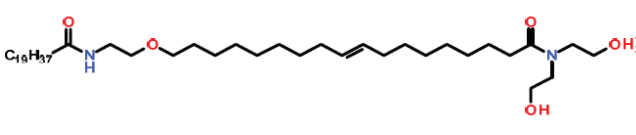
Alkylsalicylic acid was detected in the oil as detergent additive. The side chain lengths vary from C_{14} , C_{16} to C_{18} corresponding to 333.24 m/z , 361.27 m/z , and 389.30 m/z . A second detergent, alkylbenzenesulfonic acid was identified with a main peak at 493.37 m/z which corresponds to a side chain of C_{24} . The side chain distribution of this detergent ranges from C_{20} to C_{30} .

The mass of the ion 118.04 m/z detected was assigned to benzotriazole which is applied as corrosion inhibitor. As antioxidant additives, four different structures were determined.

From the class of aromatic amines useful as primary antioxidant, diphenylamine was identified at 422.38 m/z. Furthermore, a phosphorus-based antioxidant, tris(2,4-di-tertbutylphenyl) phosphite and two phenolic structures, pentaerythrol tetrakis(3-(3,5-di-tert-butyl-4-hydroxyphenyl)propionate) and (3,5-di-tert-butyl-4-hydroxyphenyl)propionate were detected in the oil. Phosphites are known to eliminate hydroperoxides, peroxy and alkoxy radicals, retard the darkening of lubricants over time and also reduce photo-degradation.

Table 10 The summary of chemistry identified by ESI MS in unused oil can be found in here:

| Application | Chemical structure | Name of additive |
|---------------------|---|---|
| Anti-wear |  | Zinc dialkyldithiophosphate |
| | <p>ZDDP with salicylates</p>  | Borate ester |
| | <p>Borate ester with salicylates</p>  | Molybdenum dialkyldithiocarbamate |
| | | |
| Detergent |  | Alkylsalicylic acid, alkylbenzenesulfonic acid |
| Corrosion inhibitor |  | Benzotriazole |
| Antioxidant |  | Pentaerythritol tetrakis(3-(3,5-di-tert-butyl-4-hydroxyphenyl)propionate) |
| |  | Alkylated diphenylamine |

| | | |
|--------------------|--|---|
| |  | Tris(2,4-di-tert-butylphenyl)phosphite |
| |  | Tris(2,4-di-tert-butylphenyl)phosphite (3,5-di-tert-butyl-4-hydroxyphenyl)propionate |
| |  | Amines |
| Alkalinity control |  | Tallow amines |
| Friction modifier |  | Modified fatty acids |

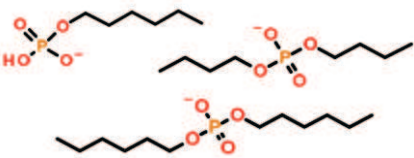
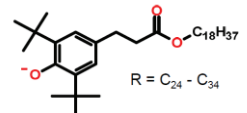
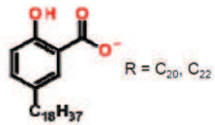
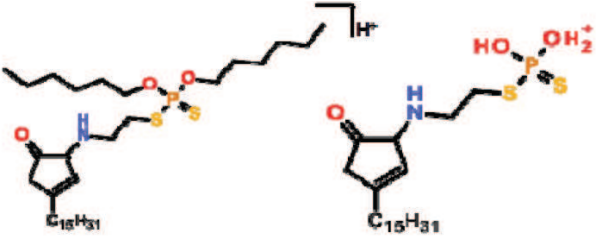
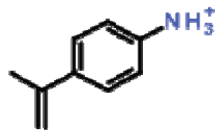
6.2.3 Chemistry of used oil

In the used oil, all additives detected in the fresh oil were still present. But contrary to ICP-OES and FTIR measurements, some distinct variations between the fresh and used oil could be elucidated by applying high resolution mass spectrometry.

It should be noted that the possibility of contamination of the engine oil is not considered in the result discussion. The reason is pragmatic. First of all, the tribosystem was cleaned before the start of the test. It works in laboratory conditions where the cleanliness is necessary factor of performing quality testing. The foreign particles or other possible foreign additives from the test could be implemented only from running and wear on the contacting parts.

All compound structures, which were possible to determine in the used oil in addition to the additive compounds found in the unused oil, are illustrated in the below Table 11.

Table 11 Structures of degradation products exclusively detected in 0W-20 GF5 used oil by ESI MS.

| Chemical structure | Name of degradation product |
|---|---|
|  | Alkylphosphates (ZDDP degradation product) |
|  | (3,5-di-tert-butyl-4-hydroxyphenyl)propionate |
|  | Alkylsalicylic acid |
|  | ZDDP degradation product |
|  | 4-propen-1-yl-aniline |

In two cases, it was possible to identify products with longer side chains in the used oil compared to that of the additives in the unused oil. The alkyl side chain of the alkylsalicylic acid detergent was prolonged by C_2H_4 and C_4H_8 (now side chain length up to C_{22}). The same occurred in the case of the (3,5-di-tert-butyl-4-hydroxyphenyl)propionate antioxidant where the side chain was prolonged by C_6H_{12} to $C_{16}H_{32}$ (now side chain length up to C_{34}).

Two degradation products could be directly related to ZDDP anti-wear additive. In Figure 38, the comparison between the fresh and used oil illustrates that additional ions were detected in used oil. These ions 181.06 m/z, 209.09 m/z, and 265.16 m/z can be assigned to alkyl phosphate structures. The alkyl phosphates identified in the used oil, were also detected by LDI-MS on the surface of the bearing half shell stressed in the fatigue experiment. Furthermore, phosphorus with a binding energy related to a phosphate structure was detected on the same surface by XPS. This means that these alkyl phosphates which are most probably ZDDP degradation products are effective in the tribological contact.

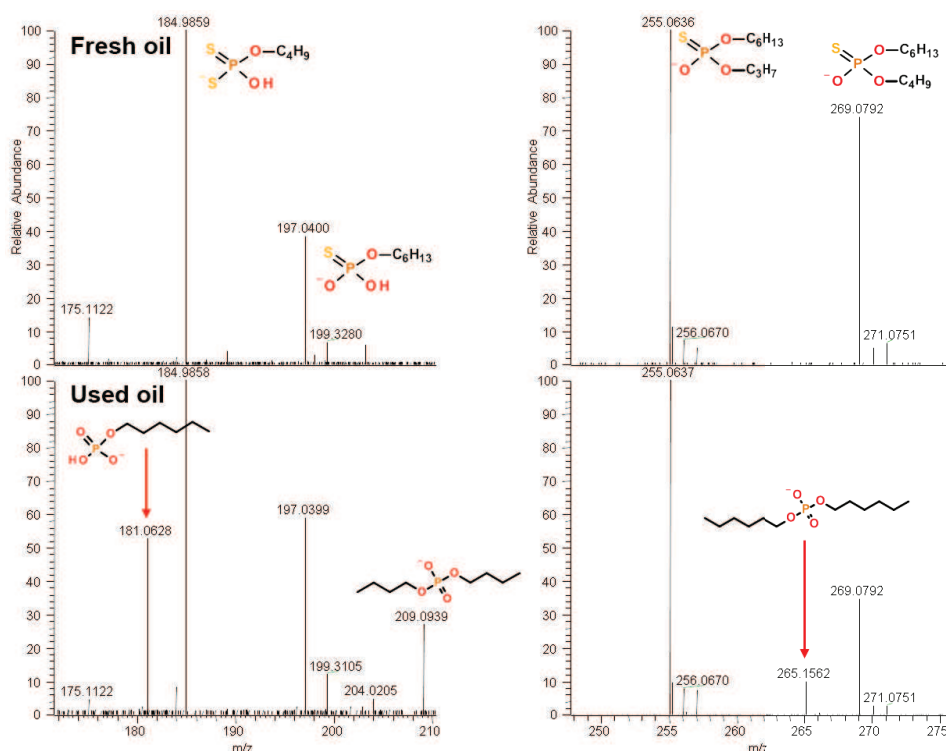


Figure 38 Alkyl phosphate degradation products of ZDDP found in 0W-20 GF5 used oil by ESI MS.

By applying normal phase liquid chromatography (NPLC) APCI-MS, it was further possible to reveal that the tris(2,4-di-tertbutylphenyl) phosphite additive was significantly depleted in the used oil compared to the fresh oil. According to the evaluation of the peak area of the extracted ion chromatogram at 647.45 m/z, the concentration of the phosphite antioxidant was reduced by approximately 50% in the fatigue experiment.

By applying NPLC APCI MS, it was further possible to reveal that the tris(2,4-di-tertbutylphenyl) phosphite additive was significantly decreased in the used oil compared to the unused oil. According to the evaluation of the peak area of the extracted chromatogram, the concentration of the phosphite antioxidant was reduced by approximately 50% by the operation in the tribotester (see Figure 39).

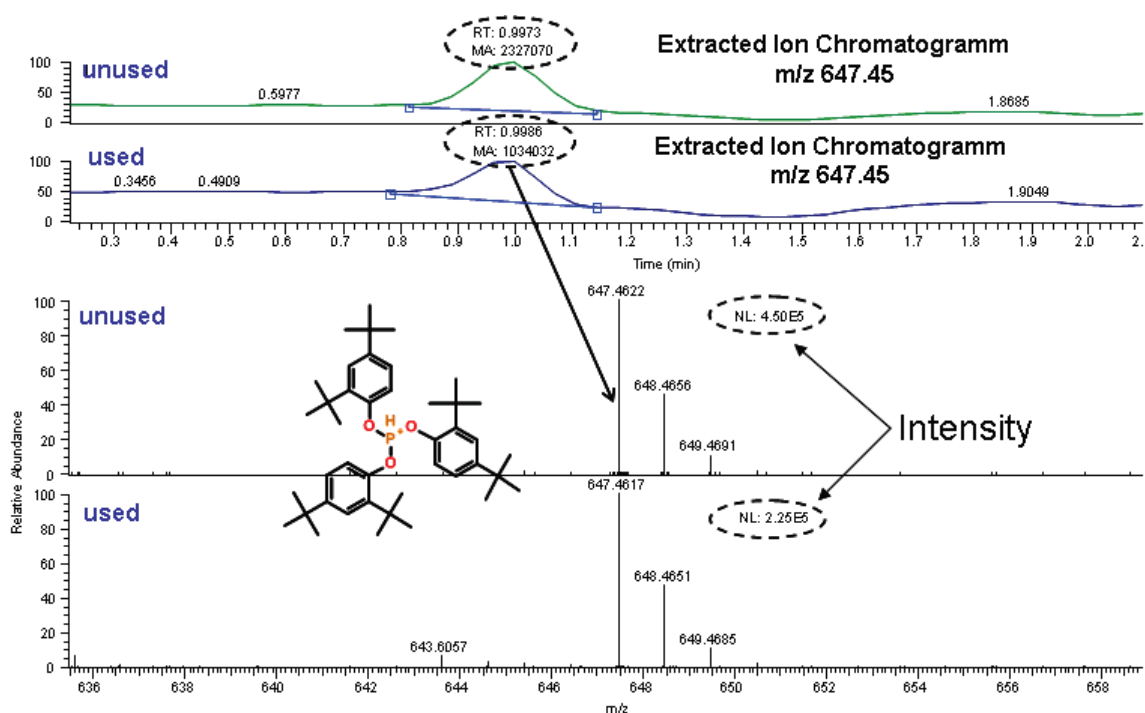


Figure 39 Comparison of antioxidant content of tris(2,4-di-tert-butylphenyl)phosphite in the unused and used oil by NPLC APCI MS analysis.

6.3 Surface characterisation

6.3.1 Non-destructive 3D microscopy

Figure 40 – Figure 42 show characteristic topographies as well as profiles along the width of the wear scars. While the newly produced bearing shell exhibits – as expected – homogeneous profile or roughness, respectively, the appearance of the wear scars of the surfaces from engine bench test and laboratory test can be clearly differentiated. Especially in the middle of the profile of the sample from engine bench test and the edges of the profile of the sample from laboratory test, pronounced grooves could be detected.

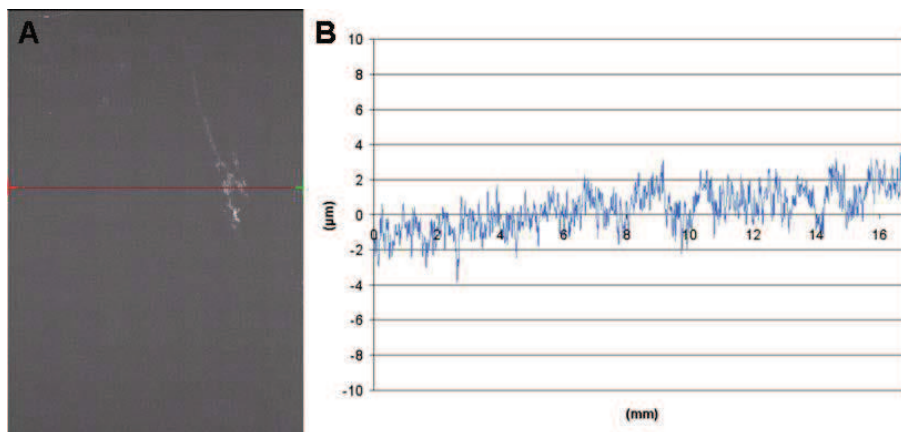


Figure 40 Topography measurement on the newly produced bearing shell. The red line in (A) assigns the area of the line scan performed for the profile measurement. (B) shows the profile over the width of the bearing shell.

Basically, significant increase of knowledge can be gained from topography measurements compared to light microscopy. In particular in larger test series, important surface parameters such as roughness (dependent on measuring direction) and wear volumes can be determined for a differentiation of the individual tests.

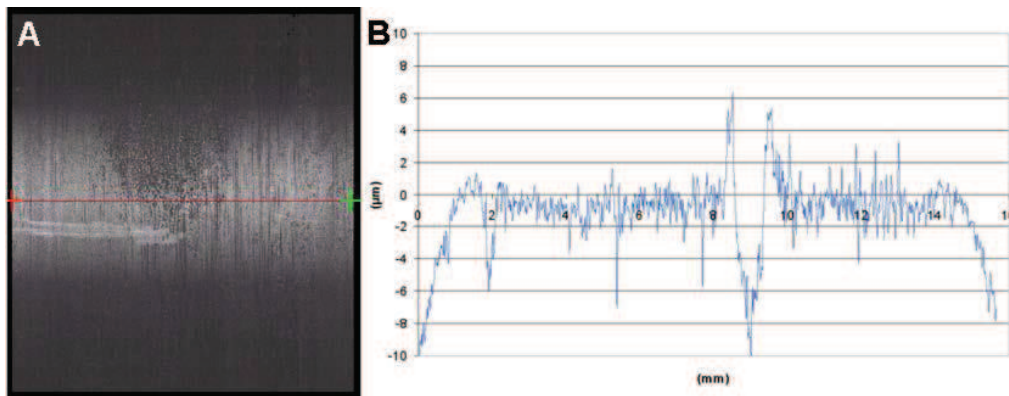


Figure 41 Topography measurement on the bearing shell after the engine bench test. The red line in (A) assigns the area of the line scan performed for the profile measurement. (B) shows the profile over the width of the bearing shell.

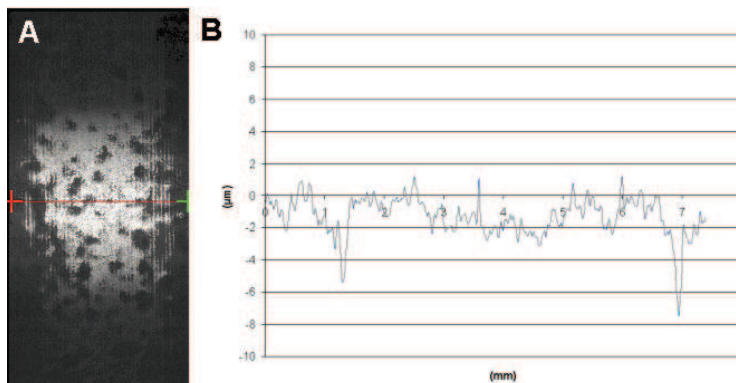


Figure 42 Topography measurement in the wear zone (area with the exposed substrate material) on the bearing shell after the laboratory test. The red line in (A) assigns the area of the line scan performed for the profile measurement. (B) shows the profile over the width of the bearing shell.

6.3.2 SEM-EDX analysis

SEM-EDX characterisation of the newly produced bearing shell showed a homogeneous polymer layer (Figure 43). Nitrogen, incorporated in the PAI structure had too weak response in the EDX to be clearly detected. All other elements expected were found, in particular molybdenum (MoS_2), sulfur (MoS_2) and calcium (CaCO_3).

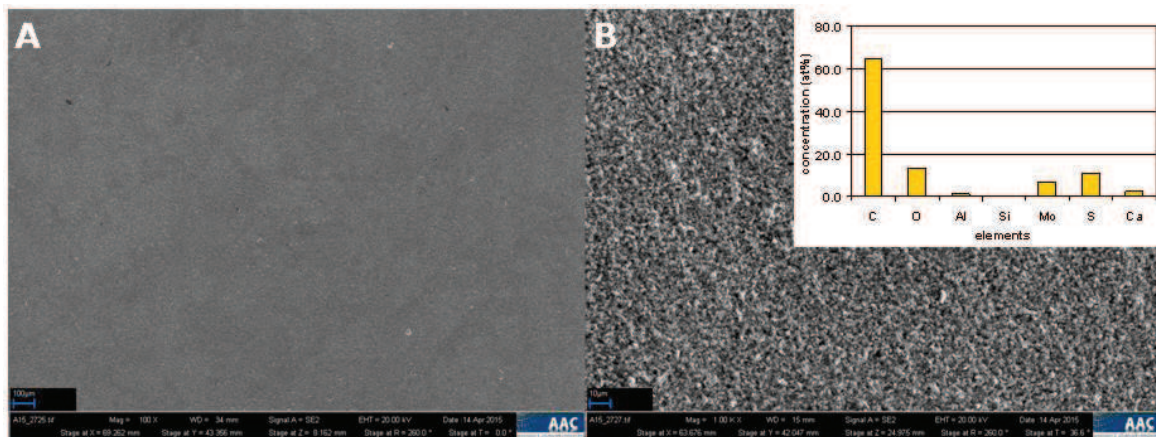


Figure 43 SEM image of the reference surface of newly produced bearing shell. (A) magnification 100 x (B) magnification 1000 x with EDX analysis.

On the bearing half shell after the engine bench test, wear scars are clearly visible. Already at the lower magnification (A), the grooves from abrasive wear are obvious (Figure 44). In (B) of, two different areas are marked. Area 2 shows approximately the same morphology as the reference surface but with a smoother surface. Area 1 is different due to even more pronounced smoothing than in Area 2.

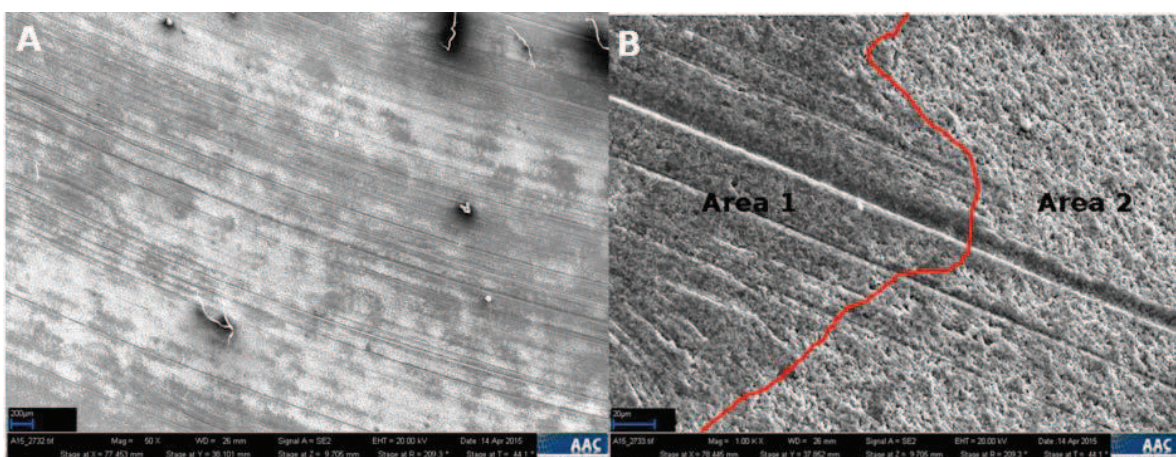


Figure 44 Wear on the bearing half shell after the engine bench test. (A) magnification 50 x, (B) magnification 1000 x

However, these topographical and morphological differences are not reflected in the chemical composition of the surface. Both areas exhibit the same chemical composition which is equal to the reference surface of the newly produced bearing shell.

Spot analysis inside deeper grooves as shown in Figure 45(A) spot 1128 clearly exhibit that depth exceeds the thickness of the polymer coating. This can be concluded from the significant increase in aluminium and tin content inside these grooves. As shown in Figure 45 (B), grooves are not the only mode of depletion of the polymer coating. Such grooves observed have an abrupt onset and an abrupt end. This indicates that a wear particle was first pressed into the polymer and then scratched over the surface until it was released from the surface. Deep holes, generated by disruption of the coating, uncover the substrate

material of the bearing half shell. It was also possible to identify wear particles on the surface consisting most probably of SiO_2 as shown in Figure 45(A) spot 1127.

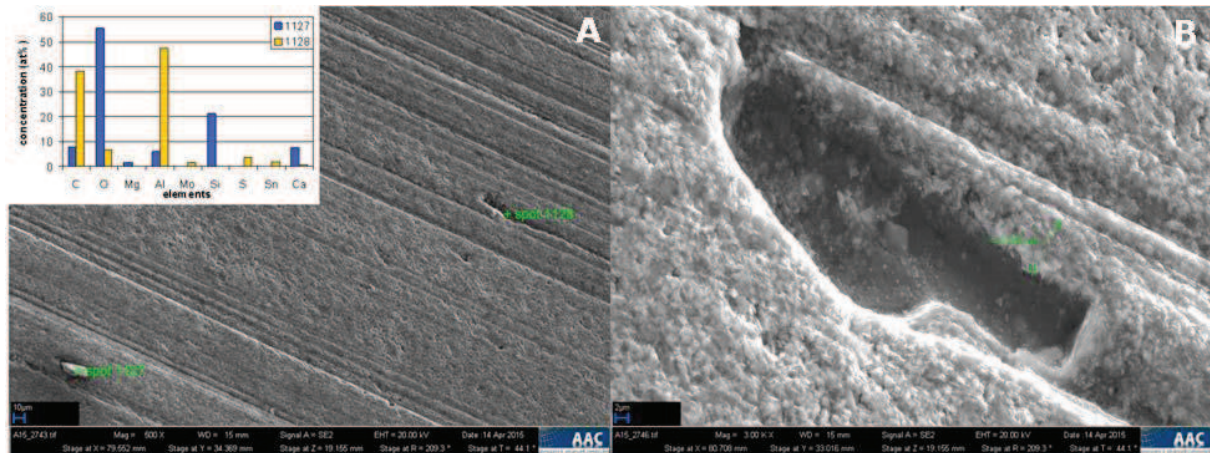


Figure 45 (A) Abrasive wear (spot 1128) and wear particle (spot 1127) on the bearing half shell after the engine bench test. (B) Disruption of the polymer surface (spot 1128) through the bench test.

A different wear mechanism can be observed in the case of the half shell tested on the tribometer (laboratory test). Pattern shown in Figure 46 (A) revealed manufacture scars of the substrate material. In the case of the bearing shell after the laboratory test, the polymer layer was smoothly abraded. In the area of the highest strain, i.e. in the middle of the half shell, the complete layer was rubbed off there and substrate material was uncovered. Figure 46 (B) depicts the area bottom right in (A) with locally present and absent polymer layer, respectively. This is evidenced by EDX analysis in Figure 46 (B) area 1129 and area 1130. In spot 1131, neat substrate material is detected with aluminium and tin.

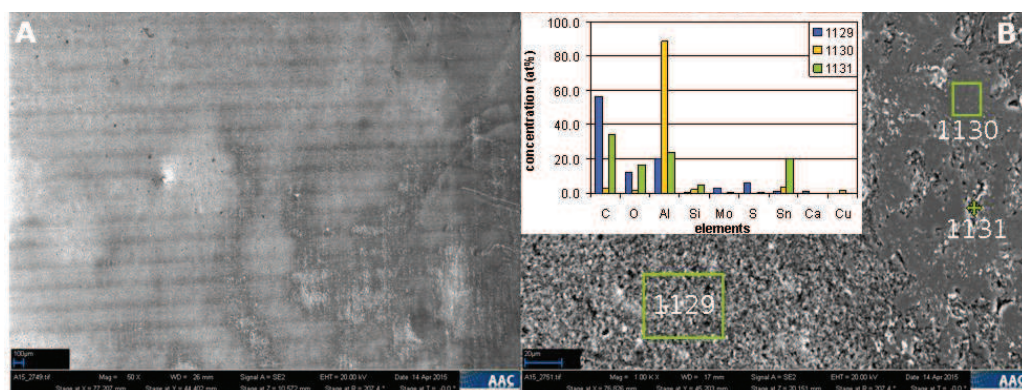


Figure 46 (A) Worn polymer surface after the laboratory test with (50 x); (B) 1000 close up of the borderline between substrate material and polymer.

A close up of the wear zone of the uncovered substrate material is shown in Figure 47. EDS analysis on different morphological apparitions revealed distinctly different compositions.

Spot 1134, defined in the smooth area, exhibit the composition of the substrate material. The particle investigated with spot 1132 exhibited a high copper content and traces of

phosphorus and sulfur which can be related to oil additives. The bright particle represented by spot 1133 is mainly composed of tin, oxygen, nitrogen and carbon – so highly probably tin oxide with polymer residues.

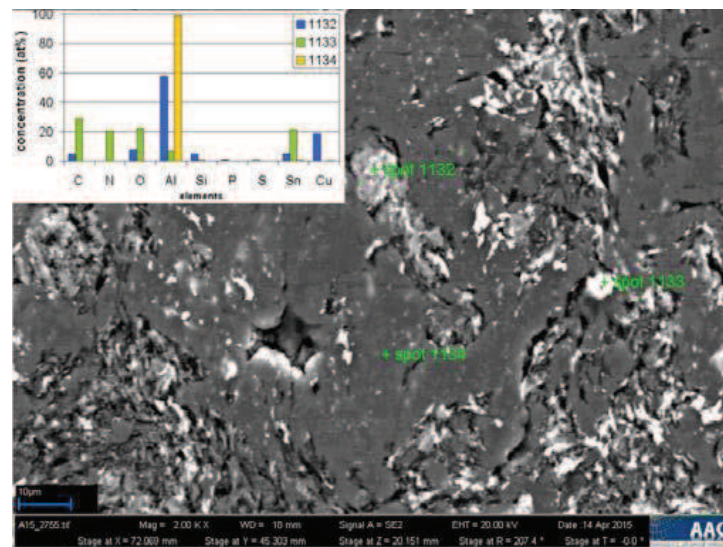


Figure 47 Close up of the substrate material after rubbing off the polymer coating.

6.3.3 XPS analysis

The specimens were investigated by XPS to characterise the polymer coating on the newly produced bearing shell and to reveal the impact of tribological stress on the respective assessed polymer surfaces on the nano-scale.

The newly produced bearing shell was analysed by XPS in a region where the original surface condition was still ensured, i.e. characterised by lack of small scratches. The results of the reference measurements on the newly produced bearing shell correlate with the available information about the composition of the polymer coating.

In Figure 48, the survey spectrum in this region of the newly produced bearing shell shows the expected composition of the polymer coating. Neglecting the possible content of contamination on the surface, carbon, oxygen and nitrogen can be related to the polyamideimide coating.

Calcium on the top surface was detected with a binding energy of 348.9 eV, which can be clearly attributed to calcium carbonate (CaCO_3) incorporated into the polymer coating. In the detail spectrum of carbon C1s, a binding energy of 288.8 eV was elucidated, which can be also assigned to a carbonate binding state. For molybdenum, a binding energy of 229.3 eV was detected which corresponds to MoS_2 . Slight oxidation of molybdenum could be elucidated by assigning the binding energy of 233.0 eV to MoO_3 .

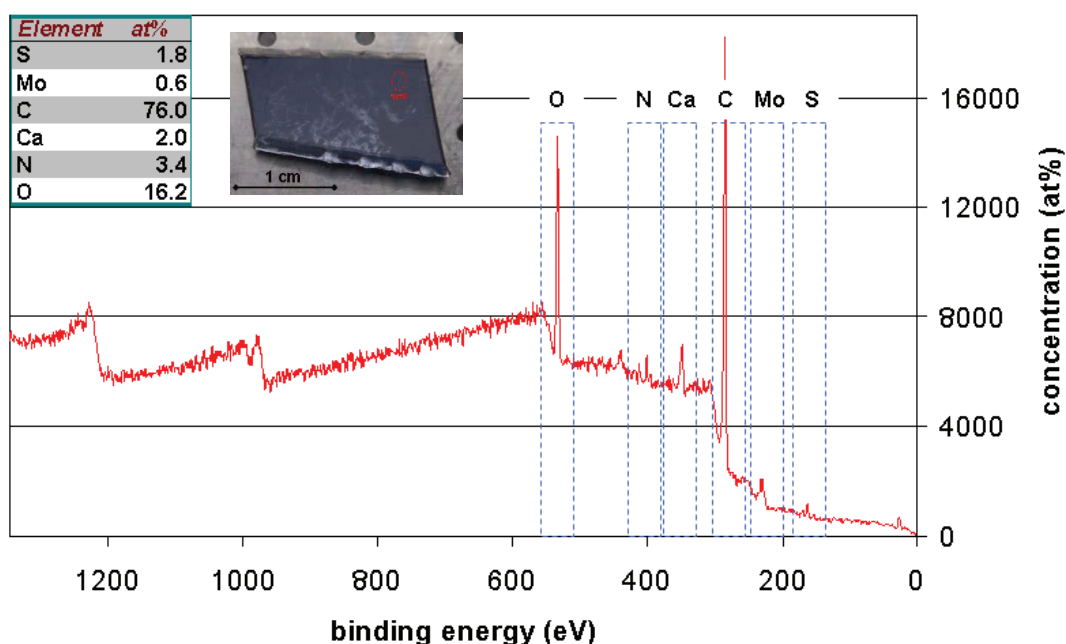


Figure 48 Survey spectrum of the measurement spot defined on the newly produced bearing shell. Table top left shows the elemental composition.

Accordingly, two binding states were obtained for sulphur in MoS_2 as shown in the detail spectrum in Figure 49: the sulfidic binding state (MoS_2) with a binding energy of 162.0 eV and oxidized sulphur (sulphate) with a binding energy of 169.2 eV. This finding indicates that MoS_2 on the surface exhibits some sensitivity towards oxidation even without tribological stress.

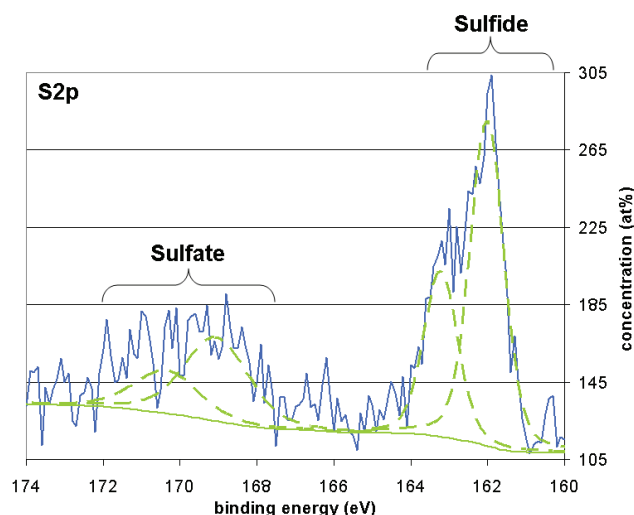


Figure 49 Detail spectrum of the sulphur ($\text{S}2p$) on the newly produced bearing half shell.

Based on the knowledge gained by light and scanning electron microscope, different regions of interest were investigated on these samples with XPS spot analysis. In particular, the morphology of the polymer surface significantly varies depending on the tribological strains introduced in the engine bench test and laboratory test (tribometer). The measuring spots defined for XPS are shown next to the particular spectra measuring.

On the surface of the bearing shell stressed in the engine bench test, two morphologically different regions could be elucidated by visual inspection. In these regions, two

corresponding measurement spots were defined. Except zinc, which appeared in traces only in spot 2, no other elements were detected compared to the reference. The respective spectra are shown in Figure 50.

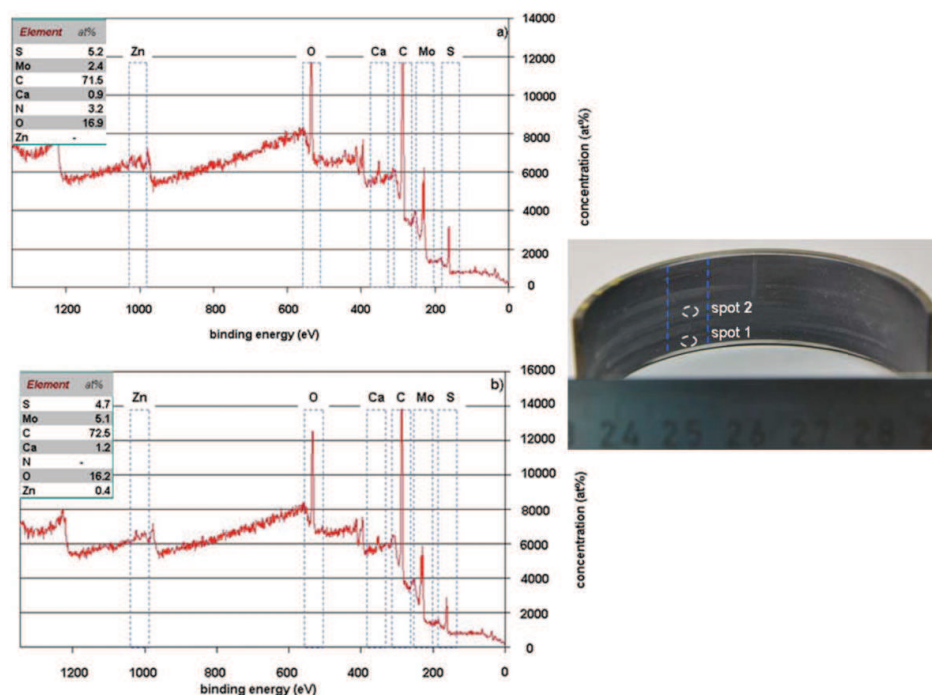


Figure 50 Survey spectra assigned to the spots (photo next to the spectra)

a) spot 1 and b) spot 2. Tables top left show the elemental composition

The amount of MoS₂ is a noticeable difference between surface of the newly produced bearing shell (0.6 at% Mo, reference) and the surfaces obtained by engine bench test (spot 1: 2.4 at% Mo, spot 2: 5.1 at% Mo). In detail, the amounts of molybdenum and sulphur are higher on the stressed surface than on the unaffected surface. This difference is clearly illustrated by two survey spectra (Figure 51). This phenomenon was not observed in the case of the laboratory test (maximum 1.4 at% Mo) which again provides evidence for different wear mechanisms in the engine bench test and laboratory testing.

In the case of the laboratory test, three regions with different appearance were selected. The measurements in spot 1 and spot 2 revealed compositions comparable to the reference surface. Only exception is zinc which was detected in traces in both spots. The spots and corresponding spectra are shown in Figure 52 a) and b).

In spot 3, visual observation already showed that the polymer coating was rubbed off completely.

The corresponding survey spectrum to spot 3 is shown in Figure 52c) and confirms that the substrate material (Al, Sn) is already exposed. In accordance with SEM EDX results, phosphorus was also detected by XPS. Thereby, phosphate (134.3 eV binding energy) was determined as chemical binding state of phosphorus. Zinc (present as ZnSO₄) and sulphur (both sulphide and sulphate) were detected in this region. These three elements can be related to engine oils additives that reacted with the metal surface. The origin of sulphur is not clear (engine oil and/or coating).

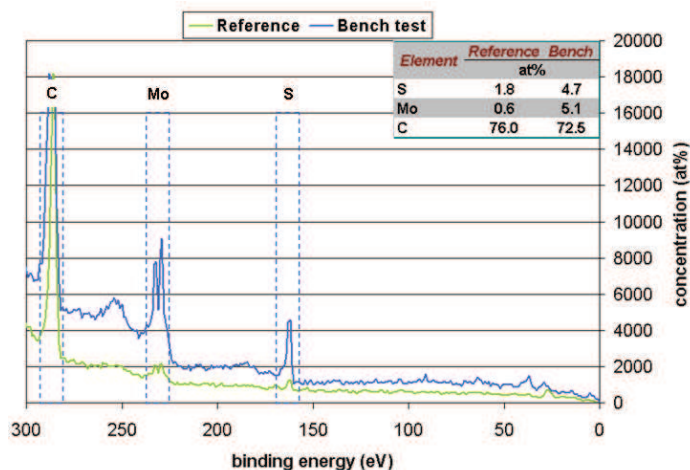


Figure 51 Comparison of surface of the newly produced bearing shell (reference) and the surface obtained by engine bench test. Table top right shows the elemental composition.

Green: newly produced bearing shell, blue: bearing shell after engine bench test

For spot 1, a two colour pattern was observed. This pattern resulted from 'black' and 'grey' spots. These small features were analysed by XPS with a spot resolution reduced to 50 μm to elucidate if the visual difference could be related to a variation in the composition. As shown in Figure 53, there is no particular variation in the composition of these two features as the spectra obtained were widely identical.

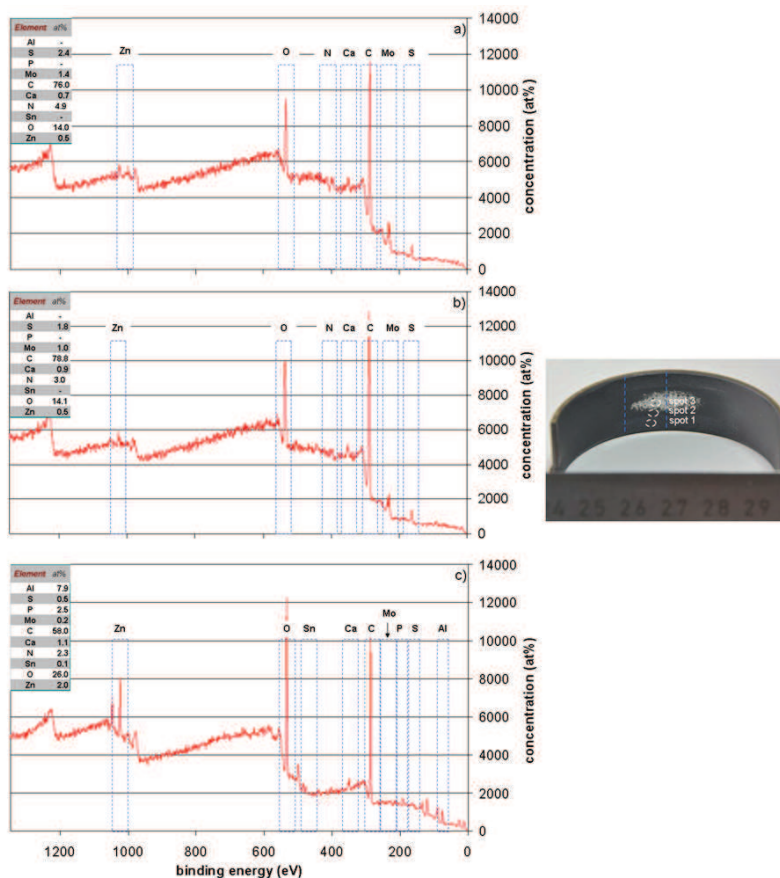


Figure 52 Survey spectra assigned to the spots a) spot 1, b) spot 2 and c) spot 3. Tables top left show the elemental composition and spots on the photo on the right.

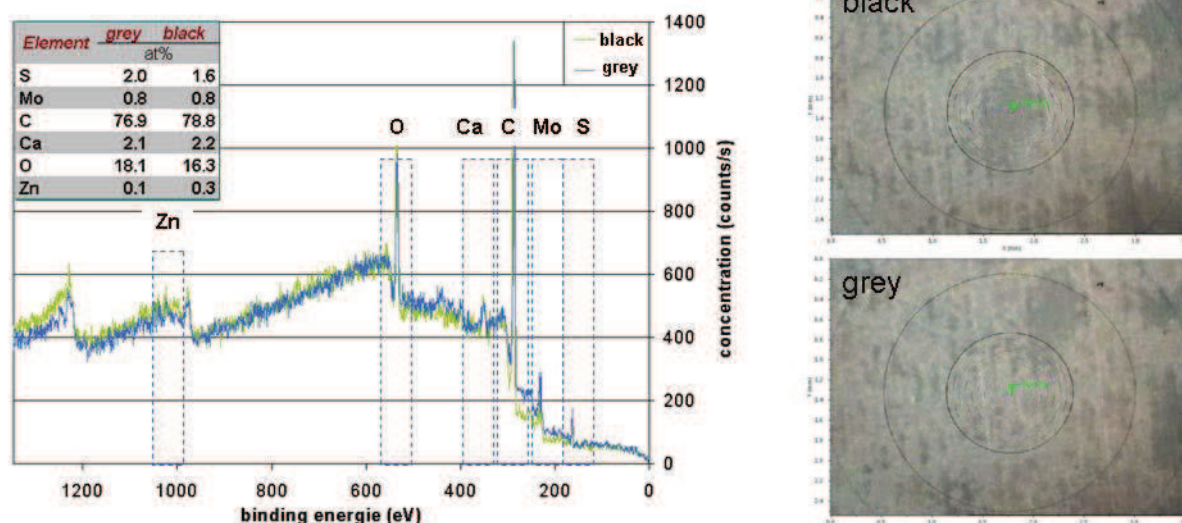


Figure 53 XPS survey measurements in the area of spot 1 (Figure 26) characterised by two colour pattern. The spot diameter was reduced to 50 μm to investigate the “black” and “grey” features. Table top left shows the elemental compositions of ‘black’ and ‘grey’ features.

A depth profile was generated by Ar⁺ sputtering of the exposed substrate material (area comparable to spot 3). In Table 12, three depth levels and the respective elements are illustrated. Sputtering clearly shows, that after a few nanometers (~ 4 nm) of sputtering, phosphor, sulphur and zinc are completely removed from the surface. This suggests that no substantially thick tribolayer is build up in the tribocontact. A typical tribolayer formed by ZDDP would exhibit a thickness of 50 to 200 nm [116].

Table 12 Elemental distribution after sputtering of the exposed substrate material on the bearing half shell after the laboratory test.

| Element | 0 nm | 4 nm | 13 nm |
|---------|------|------|-------|
| | at % | | |
| Al | 8.2 | 45.3 | 57.4 |
| C | 57.8 | 19.1 | 23.2 |
| Ca | 1.1 | 1.3 | - |
| Cu | 0.0 | 0.2 | 0.6 |
| Mo | 0.3 | 0.6 | 0.7 |
| O | 25.7 | 31.0 | 15.1 |
| P | 4.1 | - | - |
| S | 1.4 | - | - |
| Sn | 0.4 | 1.5 | 2.6 |
| Zn | 1.1 | 1.0 | 0.3 |

6.3.4 Surface chemistry by mass spectrometry

After applying both ionization methods, it can be concluded that the LDI approach provided more comprehensive spectra from the bearing shell surface than the MALDI approach (on all samples).

The MALDI approach provided spectra where mainly matrix peaks were observable. For this reason, only spectra obtained by LDI approach are shown.

In general, the area of analysis has significant impact on the ion intensity of the peaks. In this study, the ion intensities at most of the analysed areas showed similar molecule peaks which suggest even distribution over the analysed surface. Unfortunately, intensities of the acquired molecule peaks were too low for performing structural analysis by fragmentation via collision induced dissociation (CID) experiments. Hence, the acquired information is restricted to the accurate mass which was the basis for calculating the sum formula of the respective analyses.

Measurements on the surface of the newly produced bearing shell resulted in spectra with low intensity peaks (Figure 54 top). Thus, no reasonable assignment of a peak to a sum formula was feasible.

This was different in the case of the engine bench test where two homologous series of diphenylamines were detected (Figure 54 bottom). These diphenylamines (antioxidant additive) were already observed in the lubricant by ESI MS. The different alkyl chain lengths lead to different m/z values. The first series starts at 157.08 m/z and ends at 212.14 m/z with delta masses of 14 which correspond to a CH_2 group. The second series start at 220.14 m/z and ends at 276.17 m/z again with delta masses of 14. These series were solely detected on the bearing shell from the engine bench test.

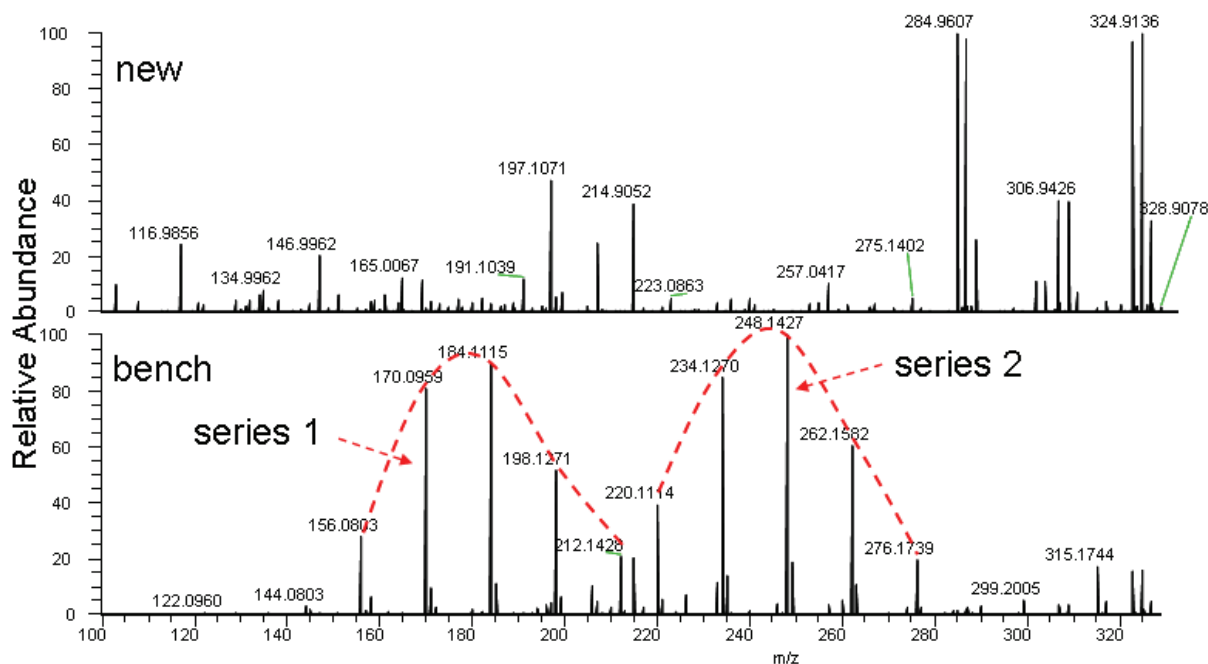


Figure 54 Comparison of the LDI spectra of the surface of the newly produced bearing shell and the bearing shell after the engine bench test. Red dashed lines mark peaks of diphenylamines belonging to series 1 or series 2.

Regarding the bearing shell from the laboratory test, a mass of 233.13 m/z was detected which can be related to a sum formula of $C_{11}H_{22}O_3P$ (Figure 55 bottom). Although the exact structure of this molecule cannot be elucidated, it is suggested that it is a degradation product of ZDDP rather than tris(2,4-di-tert-butylphenyl)phosphite antioxidant. $C_{11}H_{22}O_3P$ compound was solely detected on the bearing shell from the laboratory test.

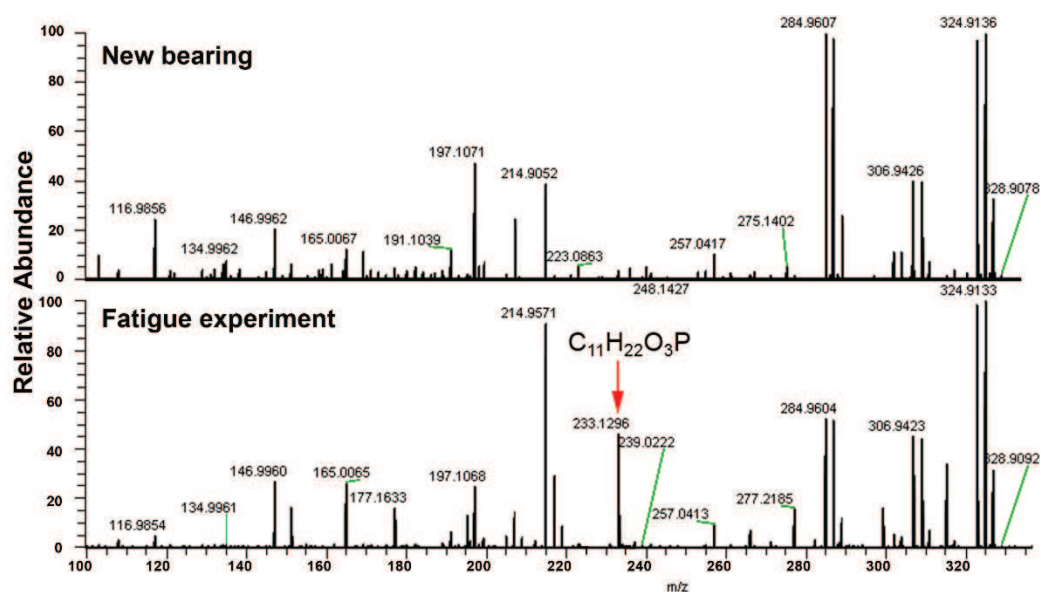


Figure 55 Comparison of the LDI spectra of the surface of the newly produced bearing shell and the bearing shell after the laboratory test. Red arrow marks the peak of the phosphorus-containing compound.

It can be concluded, that the LDI or MALDI approach can provide valuable insight in the surface chemistry composed of additives and their tribochemical reaction products. For the generation of more intense spectra that enable unambiguous compound identification, method development is required for application in the field of lubrication and additive chemistry.

6.4 Implementation of results into surface layer formulation

By the characterisation method, the conventional and advanced surface methodology was developed and put the basis for the material characterisation. Methodology for surface analysis which was developed and the outcome was as follows:

ICP OES, FTIR and other routine analytical methods for lubricants provided general information about composition of unused and used lubricants and the evidence of exact structure of the additives was confirmed by mass spectrometry. This combined method revealed significant additive degradation, e.g. formation of organic phosphates from ZDDP and depletion of tris(2,4-di-tert-butylphenyl)phosphite additive. Within XPS it was possible to reveal elements of P, S and Zn (ZDDP additive elements) were detected on the substrate material although the film thickness was only in the range of few nanometers and therefore this layer was not considered as tribolayer. Depth profiling did not reveal the content. MALDI MS and LDI MS were applied for the first time for such a problem. Especially LDI MS showed its potential by detecting additive molecules (diphenylamines) and degradation products (organic phosphates) on the surfaces of the bearing shells.

The findings revealed that there is no tribolayer formation created and no degradation products of the polymer coating were observed. The degradation of oil and tribolayers are usually connected to metallic surfaces and this could be also the reason. There was small increase of MoS_2 concentration on the polymer layer. There is existing hypothesis that the the polymer matrix is wearing off the aluminium alloy substrate and of the laminar hexagonal character of MoS_2 causing the distribution on the surface. It showed the potential for hexagonal plates of calcium hydroxide.

Aside of MoS_2 , the calcium hydroxide was chosen instead of calcium carbonate as already explained earlier and the outcome of feasibility study gave the methodology and initial insight to the coating sufficiently. PAI succeed in wear performances and as a binder. Results showed no other indication about possible degradation and passed all the tests.

6.5 PAI Characterisation

6.5.1 FTIR of PAIs

The experimental part started with preparation of solution from Torlon and checking the initial composition. It was tried to achieve the same composition as in the Hitachi solution. It was prepared 30 wt.% solution.

As for the chemical composition characterisation, the FTIR was chosen. Resulting comparison can be seen on the following spectra (see Figure 56).

The results show chemical similarity of both paints. It was hard to compare quantitatively. The main difference is in the peak around 1597 cm^{-1} representing benzene. The reason for difference could be associated with addition of xylene towards the solution compared to pure NMP solvent added to Torlon which was carried out in this study. Addition of Xylene is usually for cost reduction towards expensive NMP solvent and that could be the explanation.

To better characterize the chemical differences of PAI quality, Torlon as a powder form was easy to characterize without any additives and solvents. Resulting spectrum is on the picture below (see Figure 57). As can be seen from the results, the FTIR spectrum clearly corresponds to previous spectra where peaks are well understood and correlate to particular chemical bonds.

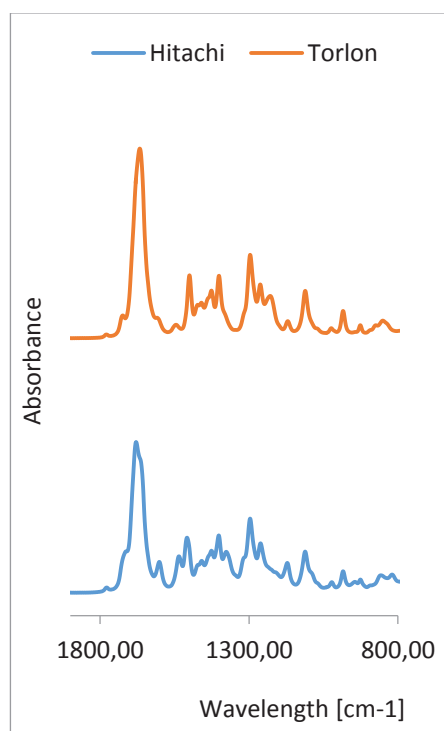


Figure 56 FTIR spectra comparison for Hitachi and Torlon paint mixture

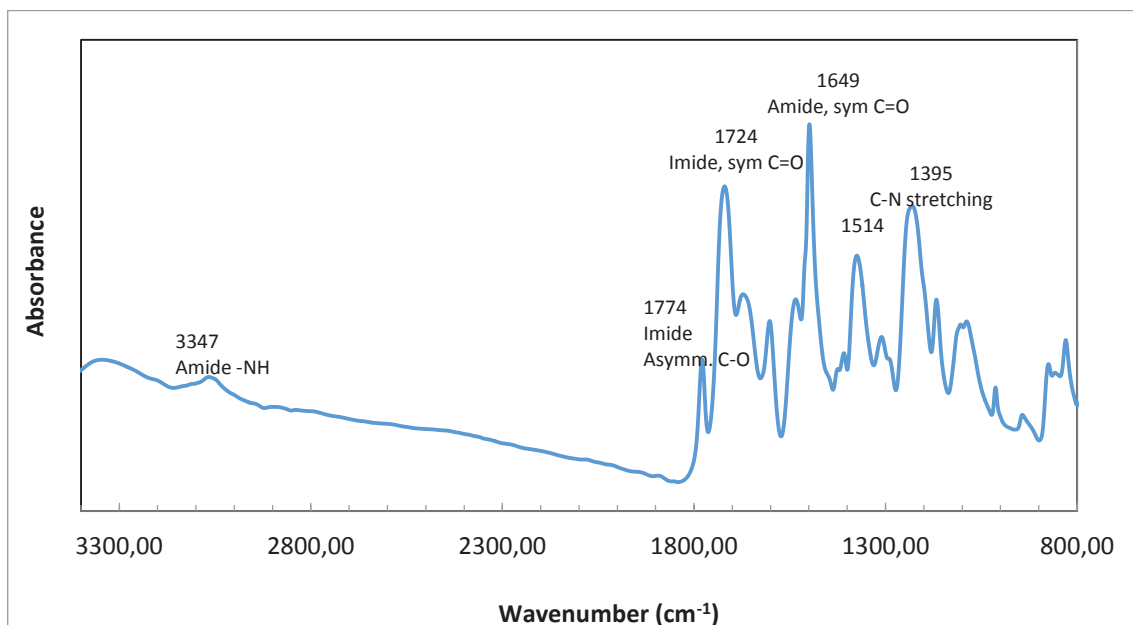


Figure 57 FTIR spectrum of pure PAI powder from Torlon

The peaks at $\sim 1700\text{ cm}^{-1}$ most likely corresponds to a C=O stretch for ketone functional group and at $\sim 1350\text{ cm}^{-1}$ to a C—N stretch functional group. The absorbance seems similar to both from Hitachi as well as from the Torlon paint. What is needed to be mentioned, that there are no stretch vibrations of amide N-H observed on the FTIR spectra of paint mixtures as it is for observed on the powder form. The curing temperature probably varies for resulting mechanical properties of polymer (moulded, sprayed and cured, etc.) and this was taken into the consideration for the preparation of paint.

Torlon polymer was studied in variety of different curing time and observed on the spectrum. The reason of this study was to state the base for curing temperature effect on the other potential additives. Also it was needed for correct preparation of coating. The resulting diagrams can be seen on the figure below Figure 58.

The experiment took part by preparation of PAI solution with NMP and curing in different temperatures for 30 min. The results show that when curing temperature was reaching 240°C , the imide characteristic absorption, particularly around 1724 cm^{-1} characteristic for imide symmetric C=O cyclic imide linkages [117] disappeared.

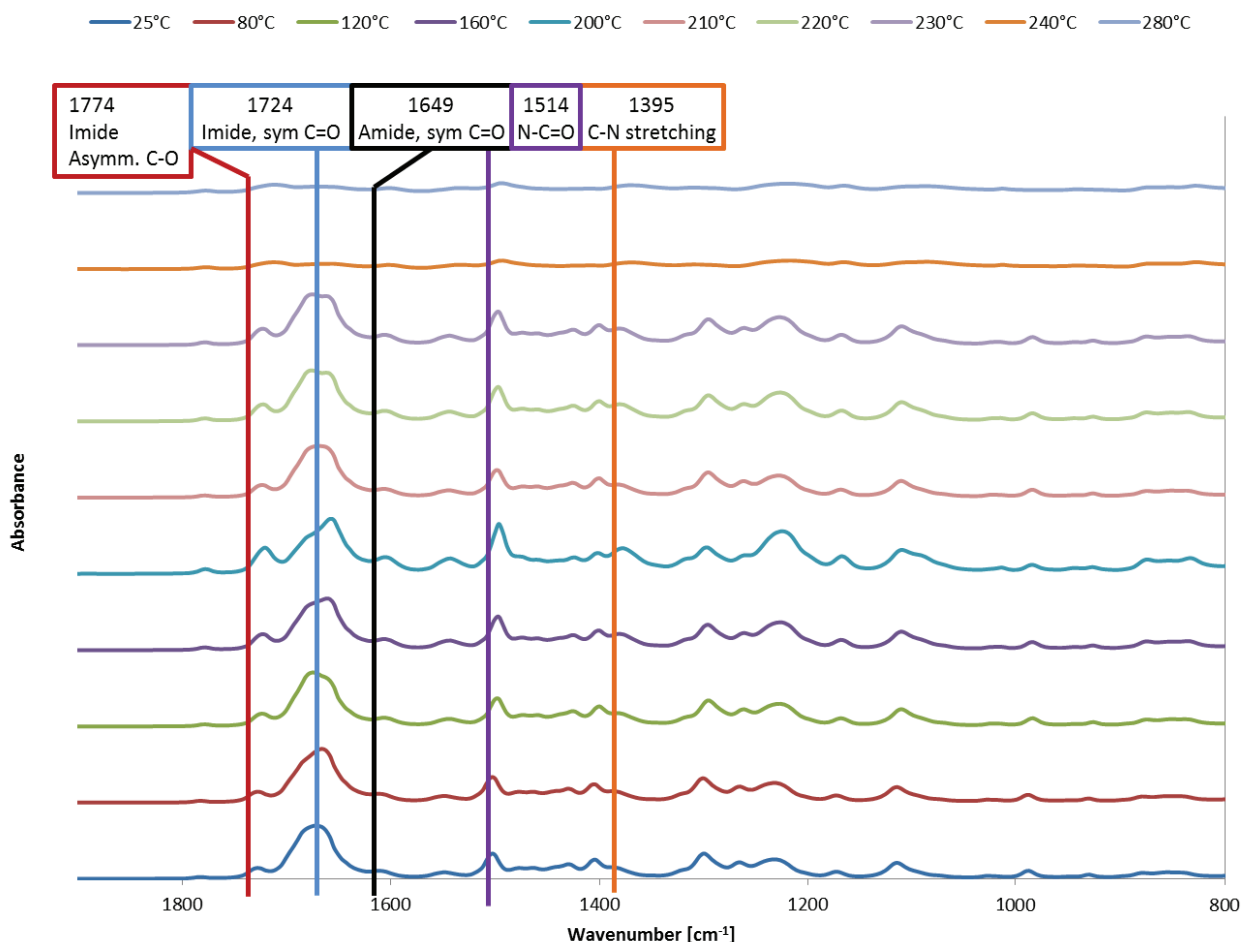


Figure 58 FTIR-ATR spectra of Torlon PAI in different curing temperature.

It indicates the hypothesis that original imide ring in PAI was opened. Similar behaviour was also registered by work of Li et al. when studying polyethyleneimine-functionalized PAI [118]. The similar behaviour was observed also for amide characterized vibrations. The important outcome was that indication of optimal curing temperature which was indicated to above 240°C. Below this temperature no characteristic chemical changes proceeding in the solution of PAI in solvent.

6.6 Coating preparation and characterisation

6.6.1 Shot blasting

The initial preparation was to optimize the process of shot blasting for substrate preparation. By selection of alumina grades was achieved the roughness of the surface from Ra 0.25 μm to 0.27 μm without influencing the bearing thickness. Resulting shot blasted samples are on the Figure 59.

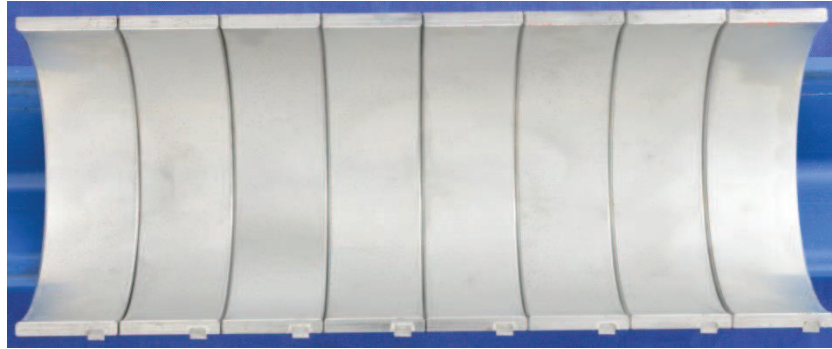


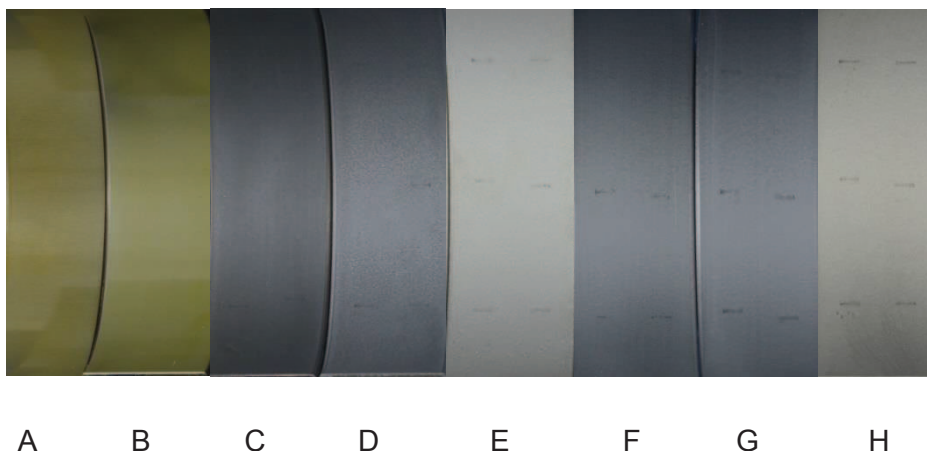
Figure 59 Shot blasted surface appearance

6.6.2 Results of spraying

Prepared surface was cleaned and sprayed by dissolved PAI with variety of additives based on the *Figure 23 Diagram of experimental work flow*, characterised and tested. The prepared solution for each coating was calculated in volume percent as conventional method for coating formulations. The prepared paints were:

- A. Pure PAI Hitachi
- B. Pure PAI Torlon-4000TF
- C. PAI Hitachi 60 vol.% + 40 vol. % MoS_2
- D. PAI Torlon 60 vol.% + 40 vol. % MoS_2
- E. PAI Torlon 50 vol.% + 40 vol. % MoS_2 + 10 vol.% Graphite
- F. PAI Torlon 50 vol.% + 35 vol. % MoS_2 + 15 vol.% Graphite
- G. PAI Torlon 40 vol.% + 40 vol. % MoS_2 + 20 vol.% Graphite
- H. PAI Torlon 50 vol.% + 20 vol. % MoS_2 + 30 vol.% Graphite
- I. PAI Torlon 60 vol.% + 39 vol. % MoS_2 + 1 vol.% Ca(OH)_2
- J. PAI Torlon 60 vol.% + 38 vol. % MoS_2 + 2 vol.% Ca(OH)_2
- K. PAI Torlon 60 vol.% + 37 vol. % MoS_2 + 3 vol.% Ca(OH)_2

The surface appearance of the coated samples of PAI with additives are shown in Figure 60. The appearance was similar grey colour rougher surface compare to the pure polymer which had yellowish appearance and appeared to be very smooth.



A B C D E F G H



I J K

Figure 60 Figure of PAI coating with additives: A) Pure PAI Hitachi, B) Pure PAI Torlon, C) PAI Hitachi 60 vol.% + 40 vol. % MoS_2 , D) PAI Torlon 60 vol.% + 40 vol. % MoS_2 , E) PAI Torlon 50 vol.% + 40 vol. % MoS_2 + 10 vol.% Graphite, F) PAI Torlon 50 vol.% + 35 vol. % MoS_2 + 15 vol.% Graphite, G) PAI Torlon 40 vol.% + 40 vol. % MoS_2 + 20 vol.% Graphite, H) PAI Torlon 50 vol.% + 20 vol. % MoS_2 + 30 vol.% Graphite, I) PAI Torlon 60 vol.% + 39 vol. % MoS_2 + 1 vol.% $\text{Ca}(\text{OH})_2$, J) PAI Torlon 60 vol.% + 38 vol. % MoS_2 + 2 vol.% $\text{Ca}(\text{OH})_2$, K) PAI Torlon 60 vol.% + 37 vol. % MoS_2 + 3 vol.% $\text{Ca}(\text{OH})_2$

6.6.3 EDX analysis

The initial characterisation was carried out on SEM where the EDX mapping was used to find out the distribution of additives into the polymer. Initial focus led to the distribution of MoS_2 in PAI. Results are shown below (it was found out that the additives have tendency to agglomerate in the polymer as can be seen on the following picture).

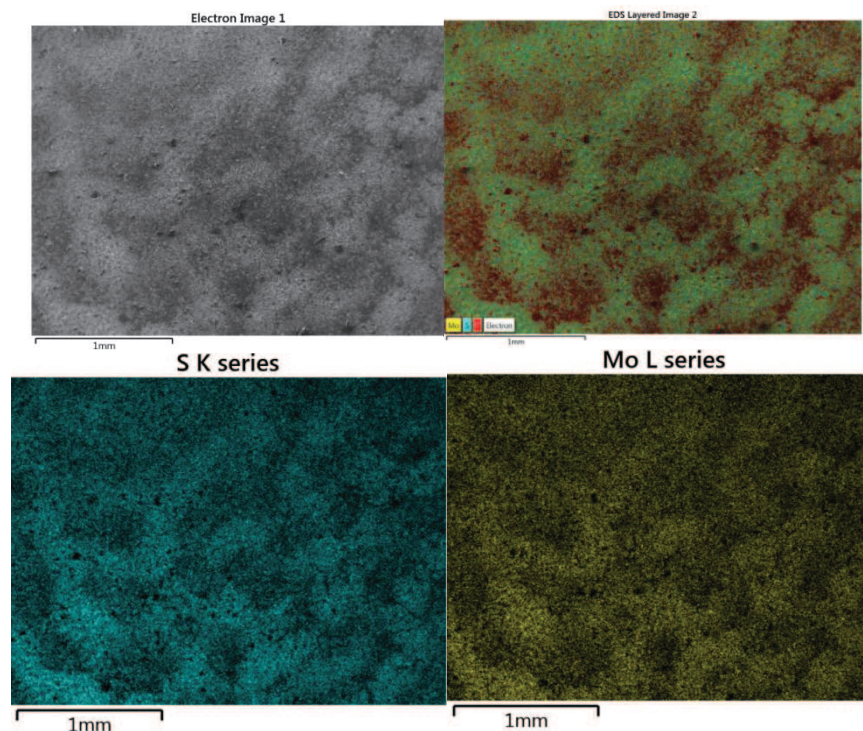


Figure 61 EDX mapping –distribution of MoS_2 in polymer

The distribution of MoS_2 resulting from mapping were not sufficient. It can be seen how MoS_2 was agglomerating in bulk. It was concluded that mixing for this part was not sufficient

and further mechanical dispergation was needed. The same result was achieved with both polymer types.

Other mixing techniques were used and combined to reach target properties. Gyroscopic mixing in combination with mechanical dispergator provided optimal solution as can be seen on the mapping below. MoS_2 is homogeneously distributed over the surface.

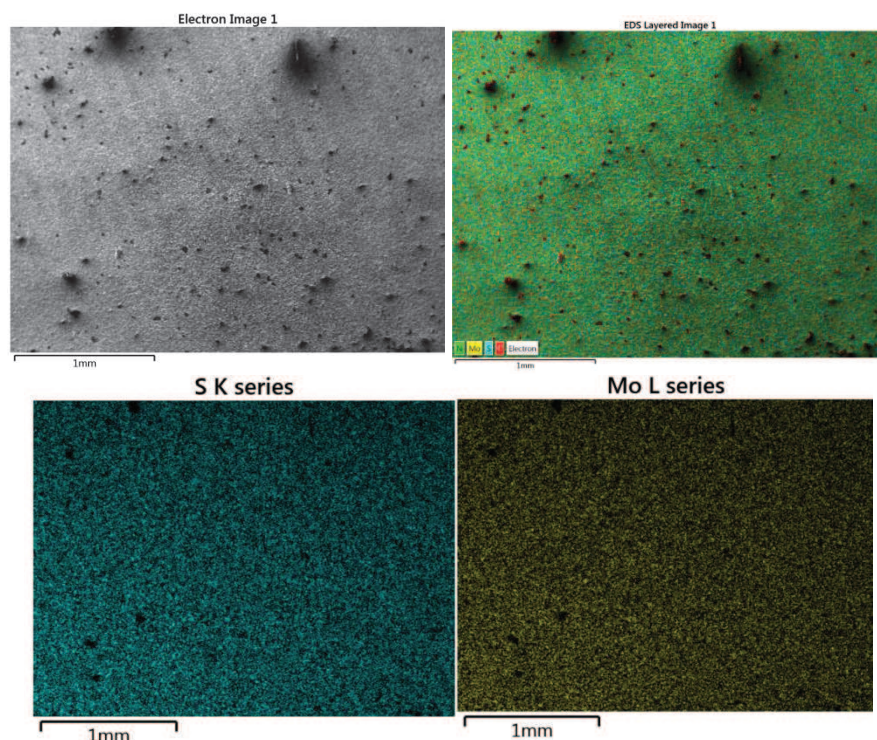


Figure 62 EDX mapping –distribution of MoS_2 in polymer after several

Addition of calcium hydroxide was critical to fulfil the primary ideation phase of hexagonal plates in the PAI matrix. The resulting characteristic structure of the coating is on the Figure 63. The point EDX analysis results indicating particle of $\text{Ca}(\text{OH})_2$ is then summarize in wt. % in the following Table 13.

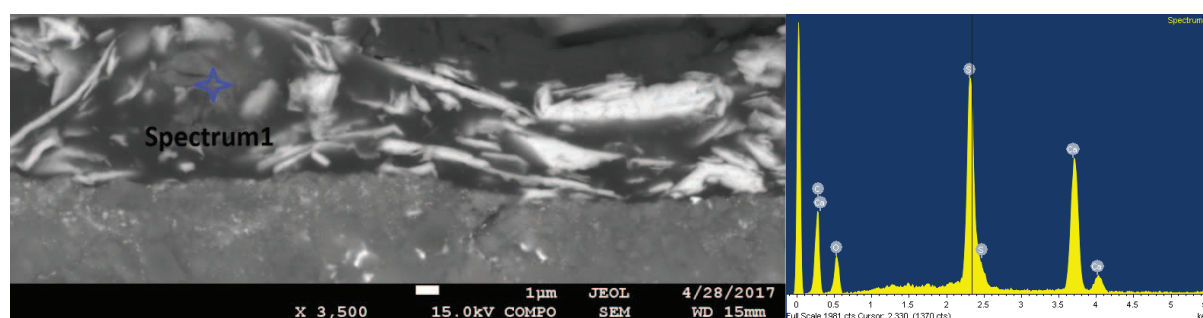


Figure 63 EDX analysis of $\text{Ca}(\text{OH})_2$ distribution in polymer coating

Table 13 All analysed elements by EDX in wt. %

| Spectrum | C | O | S | Ca | Total |
|------------|-------|-------|-------|-------|--------|
| Spectrum 1 | 41.00 | 18.94 | 17.87 | 22.18 | 100.00 |

The higher concentration of carbon and sulphur represents the scatter from MoS₂ particles and polymer matrix respectively. The white particles represent the mentioned MoS₂ lubricants in the dark PAI polymer matrix. The grey substrate represents aluminium alloy where the white parts are associated to tin. Grey particles where the point EDX analysis was performed represents particles of calcium hydroxide.

By this analysis was confirmed that particles of Ca(OH)₂ are formed for the micrometer range in the resulting coating. From the high resolution surface analysis was hard to observe resulting shape structure in the layer of polymer. It was necessary to test the effect as well as characterize it for mechanical properties and effect on adhesion.

6.6.4 Nanoindentation

Nanoindentation was considered as a basic method for comparative study on mechanical properties. The base polymer non-additive coatings were easy to start for testing. The coating roughness was without any surface defects and roughness of the sample was smooth and therefore ideal for nanoindentation. Also the homogeneity of coating did not represent any indentation issues. The results can be found in the following Table 14.

Higher hardness as well as elastic modulus can be found for Torlon as compared to the PAI sample from Hitachi. The load-displacement curve (see Figure 64) shows good repeatability and results are considered as reproducible. Higher hardness is expected also based on the previous selection of the PAI sample from Torlon.

Table 14 Results of Nanoindentation for pure polymer

| | Hitachi | Torlon |
|-----------------------|---|---|
| Hardness | 289.304 MPa 278.970 MPa 297.100 MPa | 420.216 MPa 406.638 MPa 420.333 MPa |
| Mean Std Deviation | 288.458 MPa 9.095 | 415.729 MPa 7.873 |

| | Hitachi | Torlon |
|-----------------------|-------------------------------------|-------------------------------------|
| Elastic Modulus | 6.032 GPa 5.931 GPa 6.174 GPa | 8.477 GPa 8.376 GPa 8.476 GPa |
| Mean Std Deviation | 6.046 GPa 0.122 | 8.443 GPa 0.058 |

Young modulus represents basically the stiffness of the prepared coating. Torlon exhibit higher elastic modulus which was also predicted as was considered as harder material. Torlon's viscoelastic behaviour from this result seems more suitable as the polymer matrix for further additives in consideration of high load applied to conrod half-bearings.

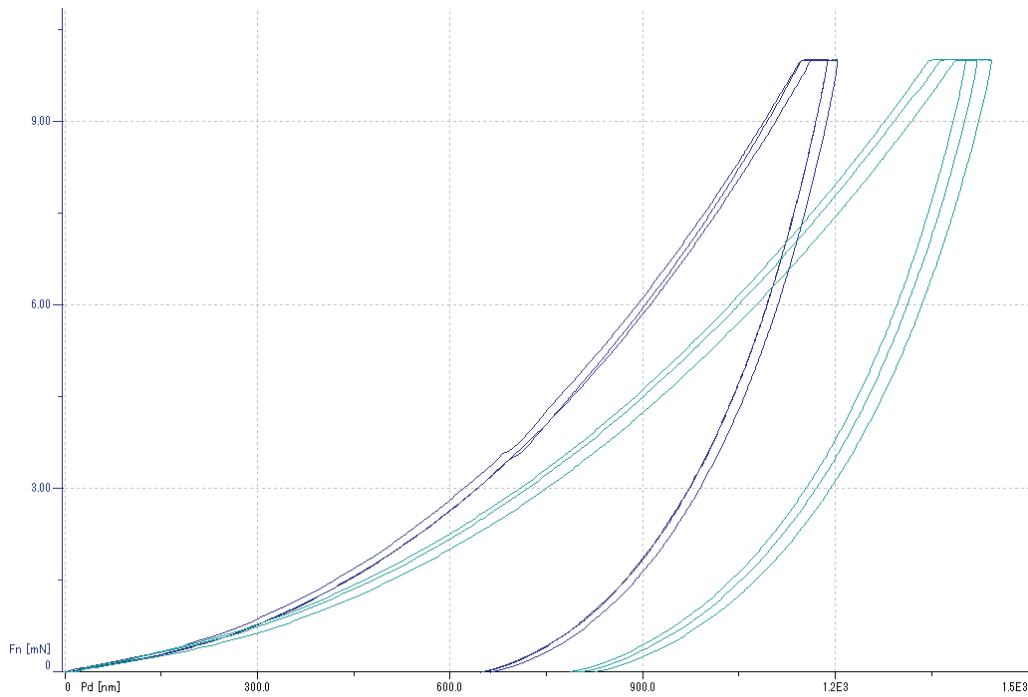


Figure 64 Loading-displacement curve of pure PAI coating from Torlon and Hitachi

Polymer with Additives

The evaluation for the polymer with additives was complicated. Since the Berkovitch type of indent is used for small penetration depths, it was difficult with characterisation of the whole substrate. Table 15 represents the results. As can be seen, the scatter of results is large. The issue is coming with adjusting the position for indentation. Solid lubricants are spread in the PAI matrix and form inhomogeneous mixture for qualified evaluation of formed indent penetrations. The real problem is in the analytical approach. Only option for measuring would be using different type of indent (Vickers e.g.) and use higher loads. Unfortunately coating is too thin for such a solution.

Table 15 Results of Nanoindentation for PAI with MoS₂

| | Hitachi + MoS ₂ | Torlon + MoS ₂ |
|---------------|---|--|
| Hardness | 360.057 MPa 475.266 MPa 368.412 MPa | 3197.222 MPa 4060.177 MPa 1469.512 MPa |
| Mean | 401.245 MPa | 2908.970 MPa |
| Std Deviation | 64.240 | 1319.168 |

| | Hitachi + MoS ₂ | Torlon + MoS ₂ |
|-----------------|--|---|
| Elastic Modulus | 13.547 GPa 22.968 GPa 19.995 GPa | 61.885 GPa 902.515 GPa 27.191 GPa |
| Mean | 18.837 GPa | 330.531 GPa |
| Std Deviation | 4.816 | 495.657 |

The problem with surface roughness and inhomogeneous coating is shown on the loading-displacement curve (see Figure 65).

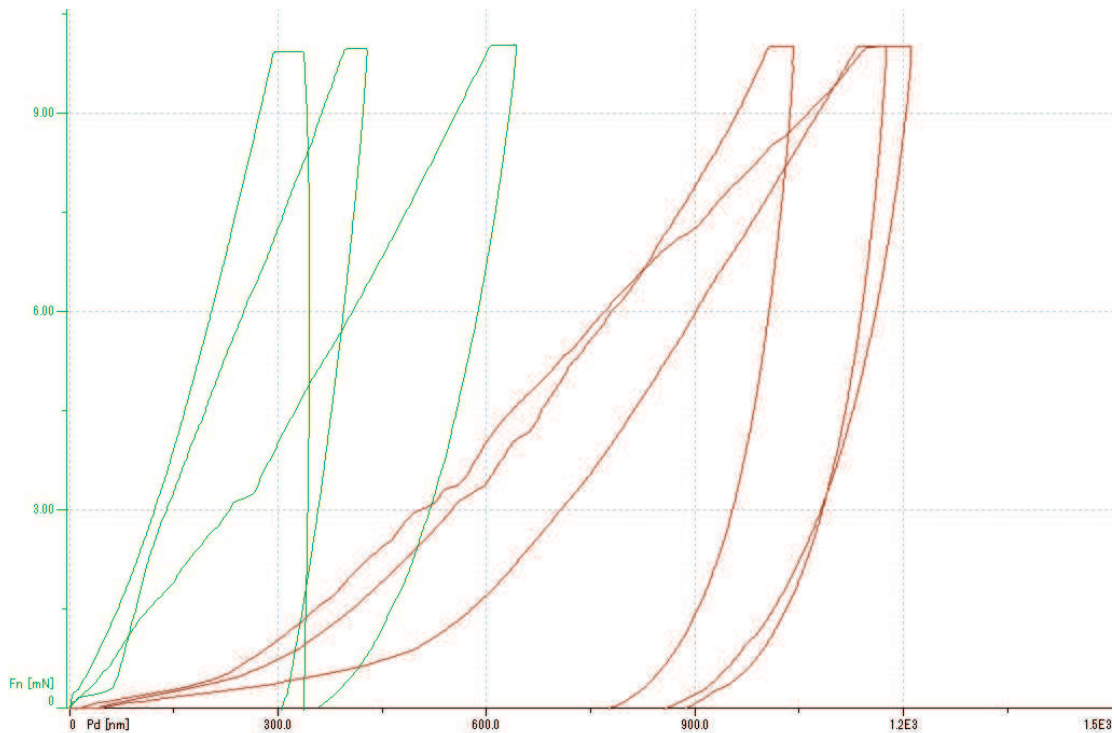


Figure 65 Loading-displacement curve of PAI with MoS₂

It was hard to estimate the mechanical characterisation of the surface with nanoindentation. Changing of the indenter type for Vickers could potentially lead to better results as well as good preparation of the sample. The same results appeared by the cross section since low load needed to be performed in test to avoid influence of the substrate.

At the end, preparation of dogbone samples to investigate mechanical properties by tensile test machines was tried to implement. The difficulty was with preparation from the solution. Polymer supplier indicated problem with preparation thicker bulk PAI samples and was also approved later and therefore other test for indicating mechanical properties were not further implemented.

6.6.5 Adhesion of polymer coatings

As for the benchmarking, it was necessary to test the polymer paint as the pure one and compare the tribological parameters. For the initial testing, the scratch tester was chosen. As regarding the potential delamination, no signal was observed on the acoustic emission. It was considered the adhesion of the coating suitable as well as from further surface profiling. Because of the large amount of images and samples, only results from force sensors were screen in attachment Figure 94 – Figure 102.

As can be seen form the results, there are no significant force resistance of the coating. The expected friction reduction is observed when higher amount of solid lubricant is added to the polymer (see Figure 99). Higher amount of the solid lubricants compare to tough polymer allows the ball to easier penetrate to material is smaller resistivity. Interesting phenomena is observed for results of scratch testing when added Ca(OH)₂. With addition of 3 vol.% of

calcium hydroxide, the rougher surface was more resistant for the penetrated steel ball resulting in increased friction (see Figure 102). This phenomenon was also lately confirmed by the testing.

6.7 Tribotesting

6.7.1 Ball on disc

The easiest way for the frictional performances especially for different lubrication regimes were achieved by testing on mini traction machine, configuration ball on disc.

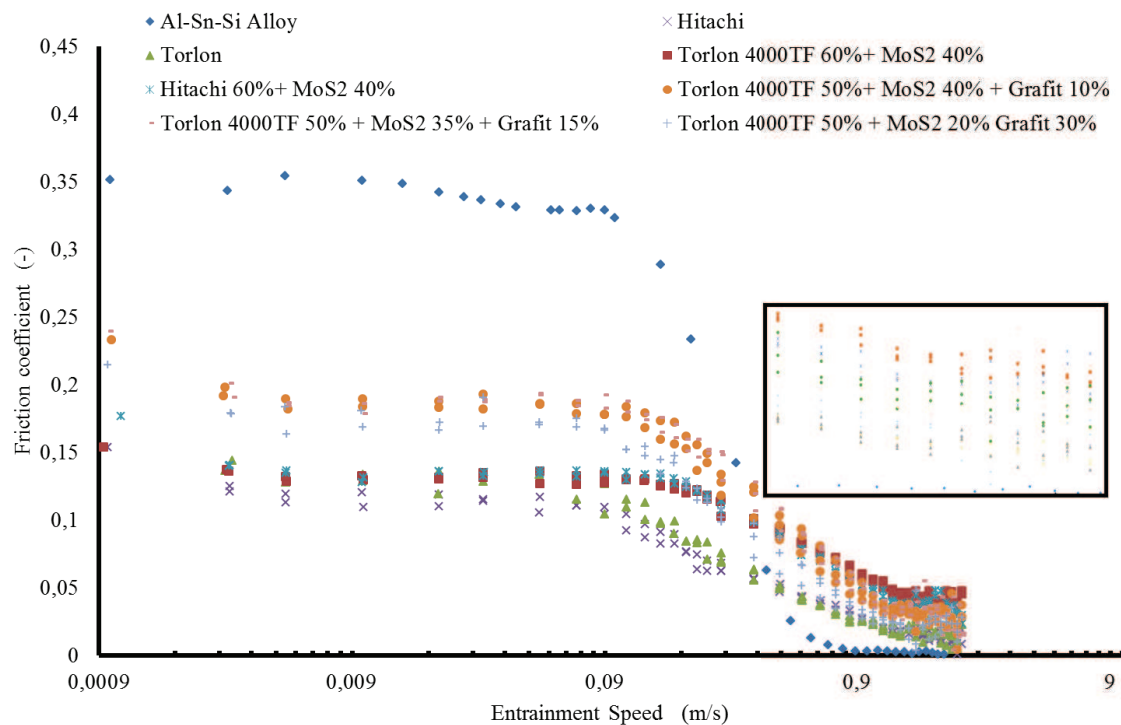


Figure 66 Testing results of PAI pure and with solid lubricants on MTM

As compare to the conventional tests where one counterpart is fixed and there is no sliding velocity, here was implemented method where we controlled the ball as well as the disc independently and achieved the possibility of measuring in the boundary and mixed lubrication regime. The testing was performed with benchmarks as well as the polymers pure and with additives. Initially, only solid lubricants as additives were taken into consideration. The resulting outcome is on the graph below in Figure 66.

The results show as expected generally lower coefficient of friction for polymer coatings compared to the conventional aluminium bearing alloy. This behaviour is observed in low speeds with mixed and boundary lubrication regime. After the formation of the oil film when bearing is in the hydrodynamic lubricational regime, the pure aluminium surface exhibit better frictional behaviour. This phenomenon was already published and explained earlier [119].

Pure PAI polymer exhibits better frictional performance compared to the polymer with solid lubricant, mainly in HD lubrication regime in high speeds of the disc. This behaviour is not expected since solid lubricants should generally decrease the friction. The explanation

could be mainly in physical-mechanical properties of the coatings, especially in hardness of the surface. Commercial polymer coatings from Daido Metal contain solid lubricants resulting in softening of surface. The rotating ball on the disc under the loading more penetrate to the surface and therefore increasing the point contact area. This can results in increased friction.

Regarding lower speeds, we can also observe minor differences of the polymer with MoS₂. The reason for this higher friction could be in the surface profile of each sample. Additives into the polymer caused rougher surface which could be the reason for influencing the friction in boundary conditions.

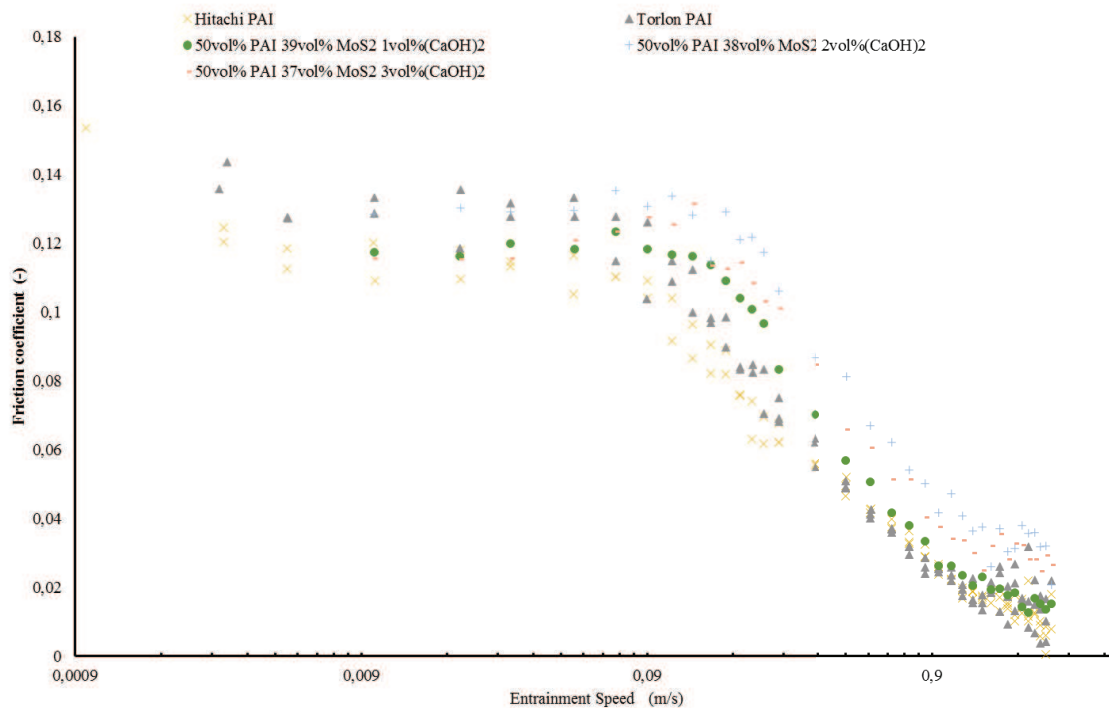


Figure 67 Testing results of PAI with additive Ca(OH)₂ on MTM

Also, what we can see is that polymers in general exhibit higher friction in HD lubrication regime in higher rotation speed as can be seen on the adjusted zooming screen of the Figure 66. It is considered to be also problem associated with low toughness of the coating and increased penetration depth of the ball. Worse friction behaviour can be observed also on the samples of coating with Ca(OH)₂ (please see Figure 67). The wear track was not observed since higher strength and toughness. Higher coefficient of friction is probably caused increased roughness as been checked in advance. The rougher surface caused the same problems also on with following testing.

6.7.2 Block on ring testing

Results of friction measured by pure sliding were achieved with configuration block on ring on Bruker Tribolab system. The experiments were firstly carried out on samples of pure PAI and with solid lubricants (see Figure 68). As it is clear from the results, solid lubricants helping in lower speeds with lubrication of the surface which result in lower friction performance. Wear in higher speeds occurs and although HD regime is already formed,

inhomogeneity and roughness of the surface complicating probably sliding conditions and friction coefficient is increasing.

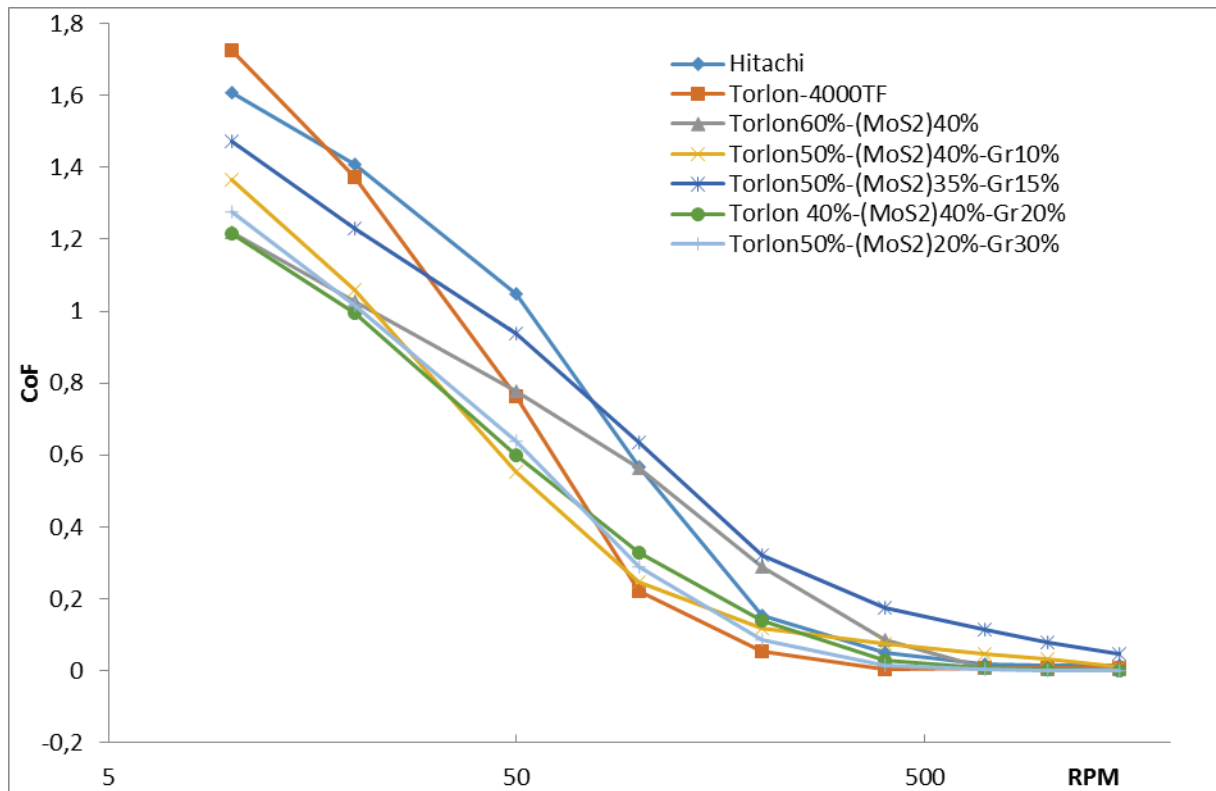


Figure 68 Results of block on ring test for PAI with solid lubricants

Interesting results can be found when addition of $\text{Ca}(\text{OH})_2$. The addition exhibited lower friction in initial stage when lower amount of calcium hydroxide was added (1 and 2 vol. % of $\text{Ca}(\text{OH})_2$). With increased concentration of $\text{Ca}(\text{OH})_2$ (3 vol.%), the higher friction was observed especially when reaching HD regime, in higher speeds. One of the potential reason could be that hydroxide could slowly wash out from the structure near the contact and therefore surface not smoothing up during the wear contact but rather form the surface roughness. This hypothesis was lately studied by topography and morphology. The precipitated form which we prepared obtained not only hexagonal plates as can be seen in Figure 29 and therefore the original idea of laminate structure generated some questions which were lately investigated.

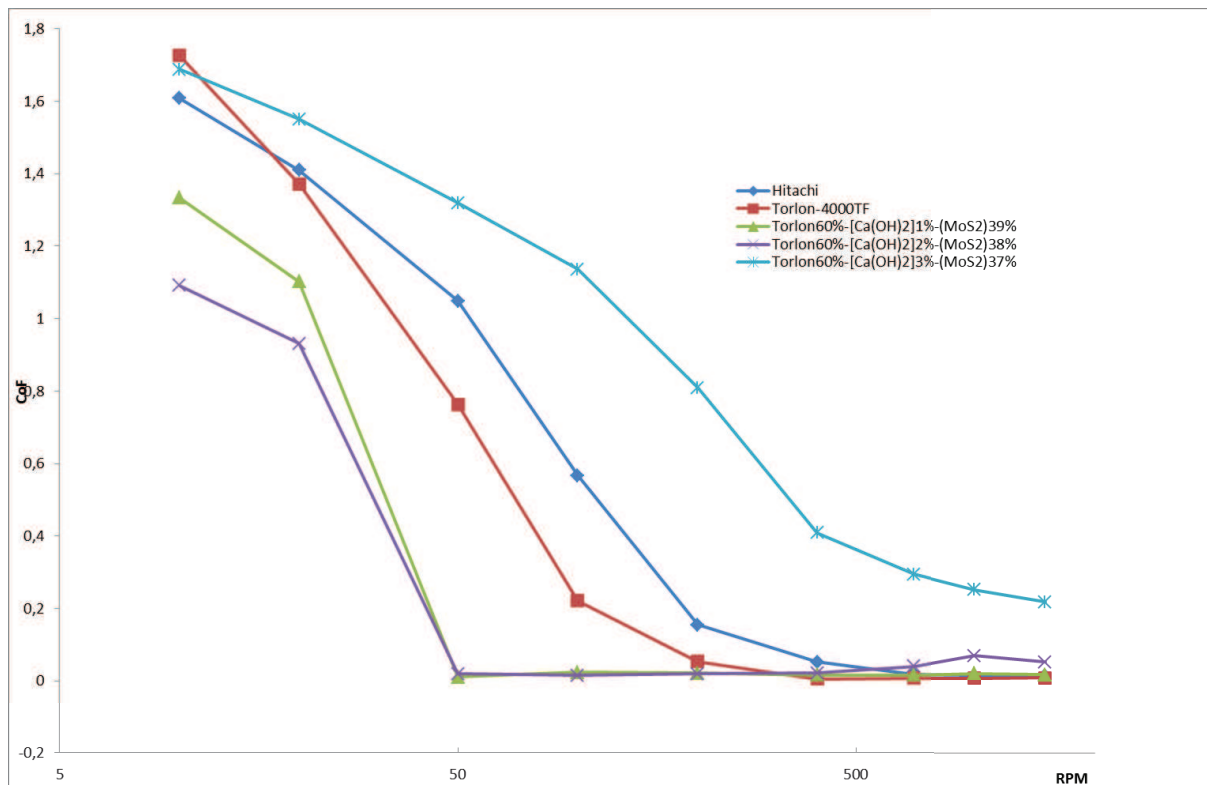


Figure 69 Results of block on ring test for PAI with solid lubricants and $\text{Ca}(\text{OH})_2$

6.7.3 Surface characterisation of tested parts

Topography

As for the start, the topography was observed after the tribotesting to collect information about wear performance of the coating. It was performed by scanning the surface on optical profiler. Study and evaluation was done by measuring the wear amount from the wear track of the contact for both configurations (block on ring on Bruker Tribolab and ball on disc represented by MTM). The studied part covered only the evaluation of the loaded part, in this case coated block and discs and therefore the complete wear volume was hard to . The counterpart was not evaluated. The summary of results can be seen in the following Table 16.

Table 16 Surface profile observation results on samples after the tests

| Coating, Testing method | Width of Wear Track [mm] | Wear Track Depth [μm] | Corresponding Figure |
|---------------------------------------|--------------------------|-----------------------|----------------------|
| Ball on disc | | | |
| PAI Hitachi | 0.2 | 1.20 | Figure 74 |
| PAI Torlon-4000TF | 0.3 | 0.98 | Figure 75 |
| Hitachi60%-(MoS_2)40% | 0.4 | 1.28 | Figure 76 |
| Torlon60%-(MoS_2)40% | 0.4 | 0.58 | Figure 77 |
| Torlon50%-(MoS_2)40%-Gr10% | 1.2 | 15.3 | Figure 78 |

| | | | |
|---|------|-------|-----------|
| Torlon50%-(MoS ₂)35%-Gr15% | 1.0 | 17.2 | Figure 79 |
| Torlon50%-(MoS ₂)20%-Gr30% | 1.0 | 15.59 | Figure 80 |
| Torlon60%-[Ca(OH) ₂]1%-(MoS ₂)39% | 0.4 | 1.27 | Figure 81 |
| Torlon60%-[Ca(OH) ₂]2%-(MoS ₂)38% | 0.4 | 1.17 | Figure 82 |
| Torlon60%-[Ca(OH) ₂]3%-(MoS ₂)37% | 0.4 | 0.25 | Figure 83 |
| Block on ring | | | |
| PAI Hitachi | 0,48 | 0.49 | Figure 84 |
| PAI Torlon-4000TF | 0.4 | 0.46 | Figure 85 |
| Torlon60%-(MoS ₂)40% | 0.4 | 0.28 | Figure 86 |
| Torlon50%-(MoS ₂)40%-Gr10% | 0.6 | 0.69 | Figure 87 |
| Torlon50%-(MoS ₂)35%-Gr15% | 1.2 | 1.6 | Figure 88 |
| Torlon 40%-(MoS ₂)40%-Gr20% | 1.2 | 1.14 | Figure 89 |
| Torlon50%-(MoS ₂)20%-Gr30% | 1.3 | 1.73 | Figure 90 |
| Torlon60%-[Ca(OH) ₂]1%-(MoS ₂)39% | 1.2 | 0.17 | Figure 91 |
| Torlon60%-[Ca(OH) ₂]2%-(MoS ₂)38% | 0.8 | - * | Figure 92 |
| Torlon60%-[Ca(OH) ₂]3%-(MoS ₂)37% | 0.5 | - * | Figure 93 |

** Investigation of depth was hard to determine as can be seen on corresponding Figure 92 and Figure 93 in the appendix.*

All the results are mapping the wear track after the testing. The hypothesis for the effect of Ca(OH)₂ as the reinforcement for resulting paint was confirmed. When higher amount of calcium hydroxide was added, the wear amount achieved almost negligible after the testing by both configurational tests. On contrary, the previous hypothesis with penetration of ball on MTM testing was also confirmed. The results of surface profile showed high wear of samples almost to the substrate of the sample.

Counterparts

Also the counterpart was characterised, this time only by roughness measuring perpendicular to wear track and compared to the original surface before the testing. There were no significant changes. Roughness of the ball before testing on MTM was R_a 0.0197 µm (see the profile in Figure 103) and after the test in the direction perpendicular to wear track was R_a 0.0161 µm (Figure 104). The same observation was achieved with the ring from testing on Bruker Tribolab system. There was roughness before the testing R_a 0.0675 µm and after the testing R_a 0.0660 µm. Both results represents the coating Torlon60%-[Ca(OH)₂]3%-(MoS₂)37%.

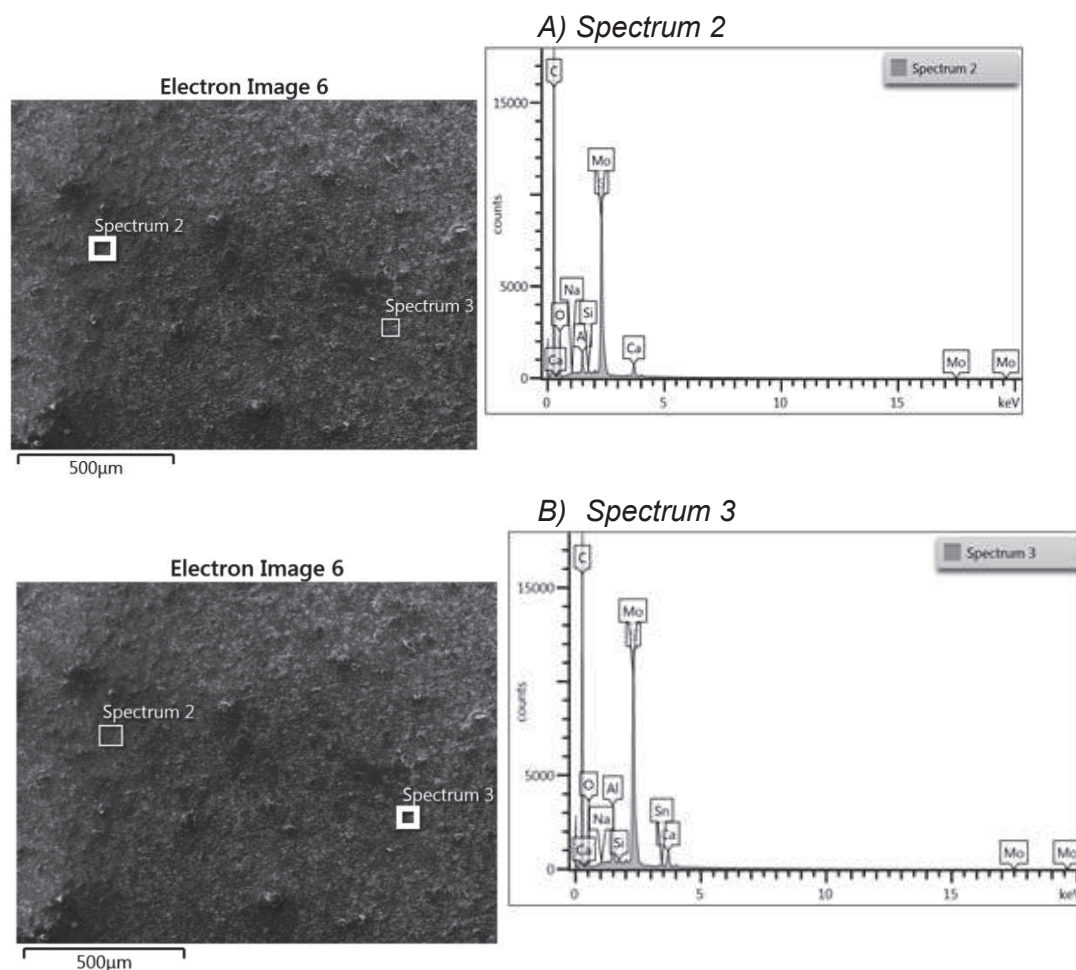
The wear tracks were hardly observed and the results are therefore expected. We observed the similar behaviour also for other coatings and therefore topography of the counterpart surface was not considered.

Surface chemistry

Regarding the study of surface chemistry, the EDX analysis was performed on the samples to investigate the behaviour of the coating and generate answers on already raised hypothesis during the tribotesting on potential degradation products or structural and

morphological changes. First of all, it was needed to prove the hypothesis about the effect of washing out of the $\text{Ca}(\text{OH})_2$ from the structure in wear track.

The EDX point analysis was carried out in the wear track (see Figure 70A) as well as comparatively on the surface (see Figure 70B).



| Spectrum 3 | | | | Spectrum 4 | | | |
|------------|--------|-----------|----------|------------|--------|-----------|----------|
| Element | Wt% | Wt% Sigma | Atomic % | Element | Wt% | Wt% Sigma | Atomic % |
| O | 30.62 | 0.43 | 58.16 | O | 31.22 | 0.39 | 57.65 |
| Na | 0.22 | 0.07 | 0.29 | Na | 0.32 | 0.06 | 0.41 |
| Al | 3.32 | 0.09 | 3.73 | Al | 7.01 | 0.11 | 7.67 |
| Si | 0.37 | 0.06 | 0.40 | Si | 0.40 | 0.05 | 0.43 |
| S | 22.57 | 0.35 | 21.40 | S | 20.99 | 0.30 | 19.34 |
| Ca | 5.49 | 0.14 | 4.16 | Ca | 5.26 | 0.13 | 3.88 |
| Mo | 37.42 | 0.62 | 11.85 | Mo | 33.34 | 0.56 | 10.27 |
| Total: | 100.00 | | 100.00 | Sn | 1.46 | 0.21 | 0.36 |
| | | | | Total: | 100.00 | | 100.00 |

Figure 70 EDX point analysis in the wear track of sampled Torlon PAI with 40 vol% of MoS_2 additive

As can be seen on both results of spectrum 2 and spectrum 3, there were no significant changes in the structure. Calcium is represented on both spectra in quantitatively comparable results. This conclusion could be unfortunately neglected also by hypothesis that some of oil residues may not have been totally removed during cleaning since the samples had been only gently cleaned in the alcohol solvents to not damage the surface before analysis. Some of calcium residues are usually observed also on other samples of bearing materials based on experiences.

Therefore the cross section of the sample was carried out and observed the structure on polished samples in higher magnification. The results of sample PAI coating with 3 vol.% of Ca(OH)_2 and 37 vol% of MoS_2 was characterized after the testing by block on ring. The resulting SEM image of the cross section is on Figure 71.

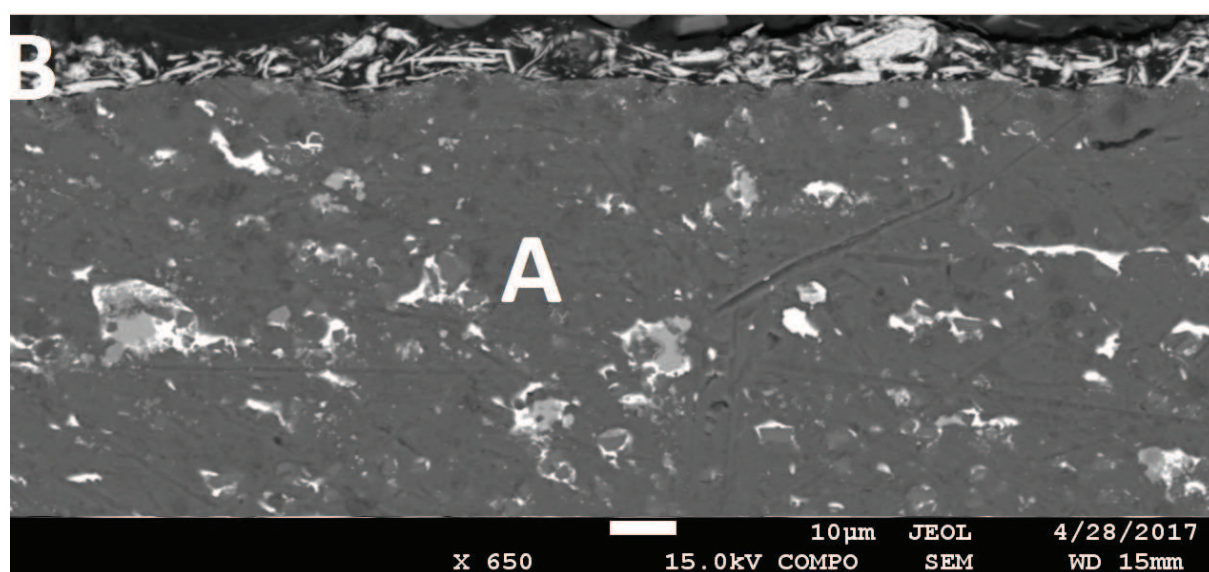


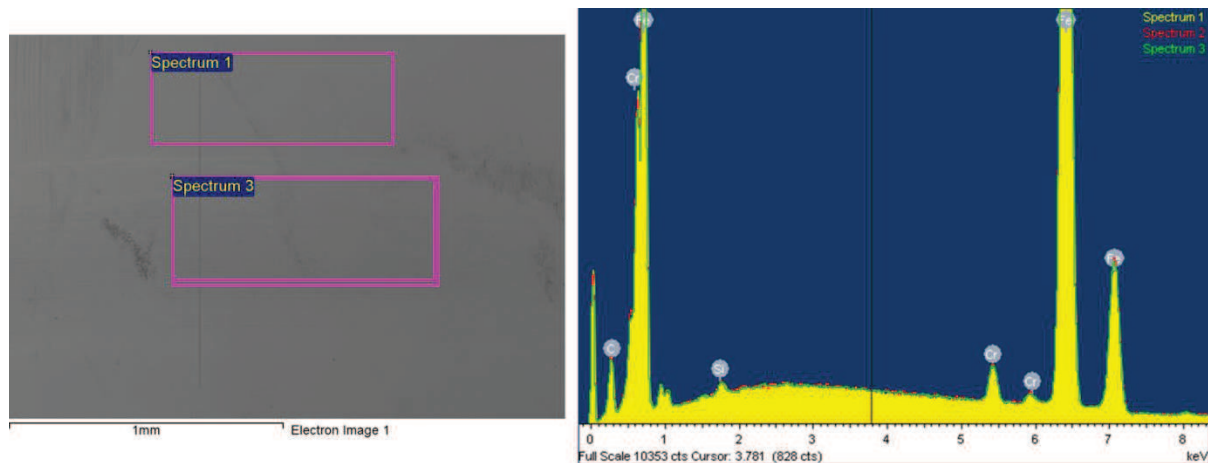
Figure 71 Cross section of PAI coating with 3 vol.% of Ca(OH)_2 and 37 vol% of MoS_2 (B) on the aluminium bearing alloy (A) after block on ring test

The observed part is the where the wear track was and no significant strange appearance was investigated. It indicates that residues of calcium hydroxide which were not properly incorporated into the coating can potentially be removed under the stressing of the surface in wet conditions. The only clear observed particles are the MoS_2 , particularly white plates in the coating (Figure 71B).

The outcome how to avoid the phenomena could be the preparation of the smaller sized hexagonal plates and its distribution in the polymer coating. This could bring another beneficial improvement for mechanical properties of the bearing surface.

Counterpart Surface Chemistry

The surface chemistry on counterparts, respectively on the ball and the ring were investigated by the EDS mapping on the surface of wear track and compared with unstressed area. There were no significant changes. The steel was chromium bearing steel and apart of it, no elements showing the tribolayer or degradation products on the surface were observed (see Figure 72 and Figure 73).



| Element | App | Weight% | Weight% | Atomic% |
|---------|--------|---------|---------|---------|
| C K | 7.80 | 3.82 | 0.11 | 15.54 |
| Si K | 0.48 | 0.15 | 0.02 | 0.27 |
| Cr K | 7.81 | 1.59 | 0.04 | 1.49 |
| Fe K | 378.91 | 94.44 | 0.12 | 82.70 |

Figure 72 EDS mapping on the ball in wear track and out of the wear track.

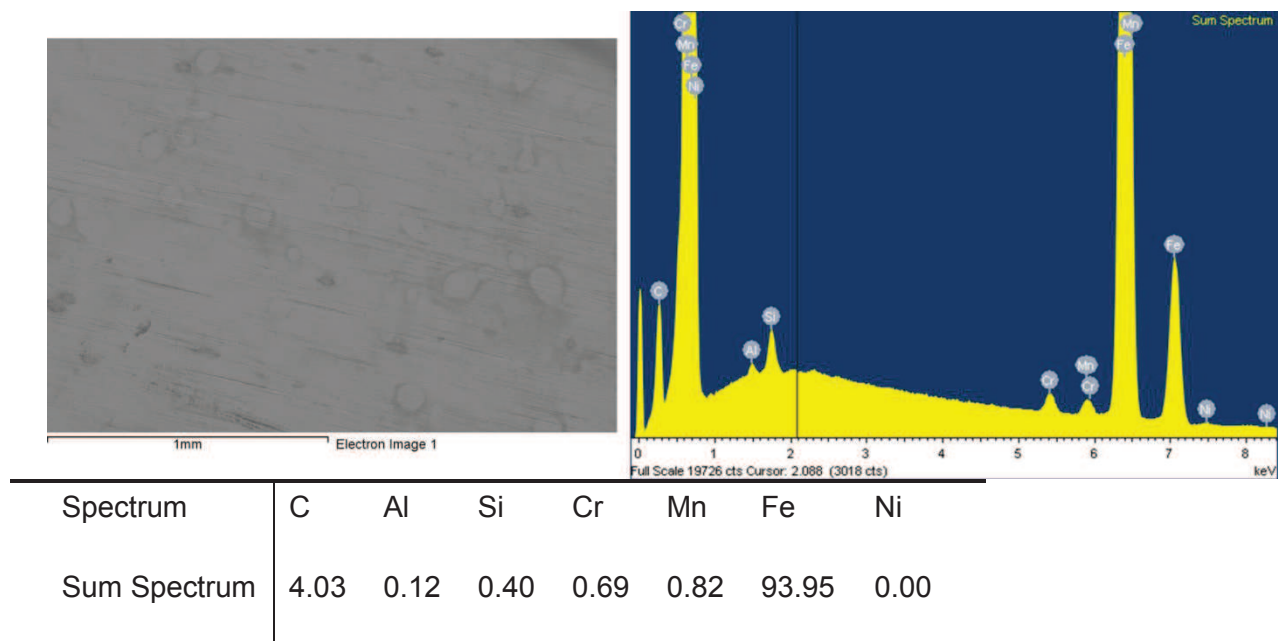


Figure 73 EDS mapping on the block in wear track.

7 CONCLUSION

The aim of the thesis was the study of the bearing overlay with advanced tribological properties. The background for the material composition came from the joint initial expertise of commercial coating layer, respectively its surface observation under boundary operational conditions, oil analysis and effect on the whole tribosystem.

As the first step, the comprehensive description of the chemical and tribochemical behaviour of engine oils and engine half bearings in simulating engine conditions was carried out. A joint approach of conventional and advanced analytical methods for oil and surface characterisation was developed and applied to engine half bearings lubricated with commercial 0W-20 GF5 engine oil.

Lubricant analysis using ICP-OES and FTIR revealed basic information about lubricant composition and was found as essential base for advanced chemical analysis based on high resolution MS to detail especially the degradation mechanism on the molecular level. Overall, only low oil degradation was indicated by conventional oil analysis in the fatigue experiment. However, viscometrical properties were attributed to shear stress that induced substantial polymer cracking during tribotesting.

Regarding surface analysis, oil analytical data were correlated with surface chemistry. XPS revealed different surface chemistries in the real engine bench test compared to the fatigue test machine owing to different tribological processes dominating in the respective tribocontacts. By LDI-MS, the main analytical findings related to a phosphorus-containing moiety detected in the mainly loaded area of the fatigue experiment which correlates to alkyl phosphates that were also identified as degradation products in the used engine oil.

The overall methodology led to promising findings although a significant protective tribofilm was not observed and therefore could not bring more into the further correlation with paint formulation. The findings revealed no tribolayer formation which is sometimes reported mainly with metallic surfaces. Small increase of MoS_2 concentration on the polymer layer was observed. The existing hypothesis is that the lubricant has the tendency to release from the polymer matrix and lubricate the contact because of his laminar hexagonal character. It indicated hypothesis for possible success of hexagonal plates of calcium hydroxide.

Although the results of advanced analytical techniques showed potential in surface characterisation and some of them were indicated for this application for the first time (MALDI and LDI MS), for further formulation were not needed to apply. All the subsequent testing was carried out with non-additive base oil and in laboratory testing conditions.

Second part of the thesis studied effect of hexagonal plates of Ca(OH)_2 in polymer coating in according to form the laminate composite structure and to stiffen the PAI coating. Secondary supposed effect of Ca(OH)_2 addition was its lubrication potential at the coating surface. At the beginning, the research and development of paint solution preparation and application to the surface took place. Novel solution for application was developed together with paint preparation and was successfully introduced.

The last part focused on the characterisation of the effect of calcium hydroxide and solid lubricants in PAI polymer matrix on the tribological properties. Prepared coated samples were tested on two different configurations of tribotesting to achieve basic characterisation on friction and lately by surface topography measurements for the wear performances.

From the results was concluded that calcium hydroxide has positive effect on the surface. It helps to increase the strength of polymer layer and can withstand high specific load to the

surface without wear. The effect on the friction was also positively investigated. Basic phenomena have been studied and investigated towards the limitations mainly associated with potential removal of surface particles of calcium hydroxide in wet conditions. It is suggested to proceed with finer powder form of solid lubricants as well as the calcium hydroxide.

The main contribution of this work is that PAI with solid lubricants and Ca(OH)_2 was formulated and characterized for the first time for this application. Thanks to this work, the preparation methods and application methods has been designed and developed as well as the testing procedures in laboratory conditions. The gained knowledge from initial expertise and further formulations and conclusions put the base for ongoing research and showing the promising way of new coating for real applications in tribology field.

8 FUTURE WORK

Although Ca(OH)_2 showed potential in tribological applications, the further tests under real engine conditions were not performed. The laboratory tribotesting provide initial evaluation of the surface after tests, but further in-depth evaluation could be certainly performed to gain better understanding of the mechanism for the effect of Ca(OH)_2 on the sliding properties of the bearing overlay.

Further research topics are associated with hypothesis of finer particles of used additives. The comparative study could be additionally proceeded and prove the theoretical background which this thesis put down. Used additives were commercially available (graphite, MoS_2) or laboratory prepared where the particle size distribution exceeded microns. Lower particle size could improve surface roughness and exhibit lower friction in running conditions.

Advanced analysis could be carried out also for the surface of newly developed bearing surface after application tests.

9 APPENDIX

9.1 Appendix 1 Surface profile analysis

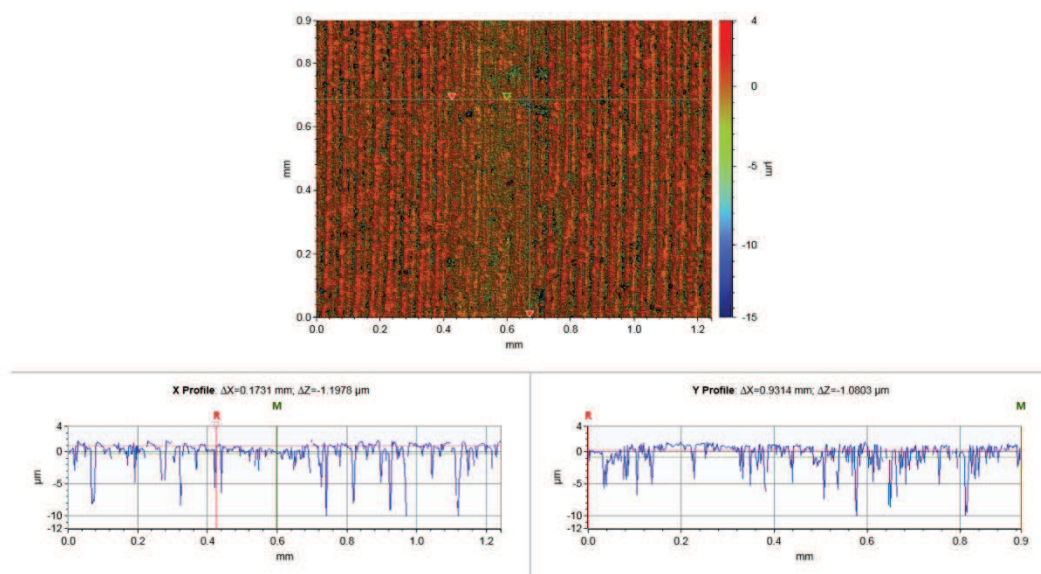


Figure 74 Surface profile of the pure PAI from Hitachi after the testing on MTM machine

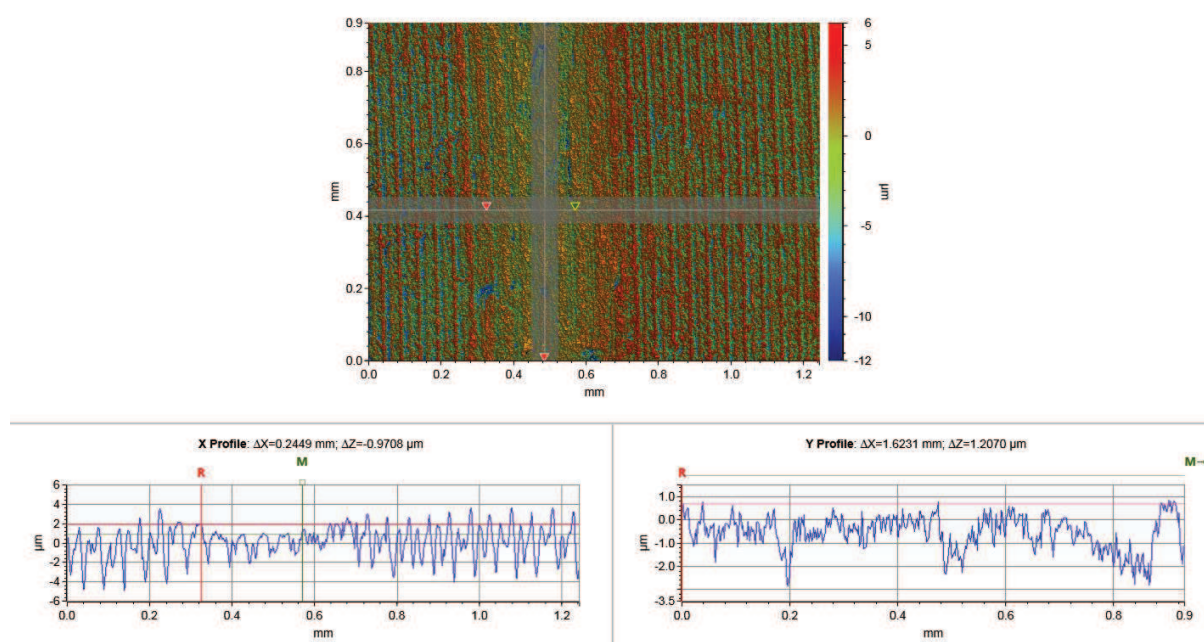


Figure 75 Surface profile of the pure PAI from Torlon after the testing on MTM machine

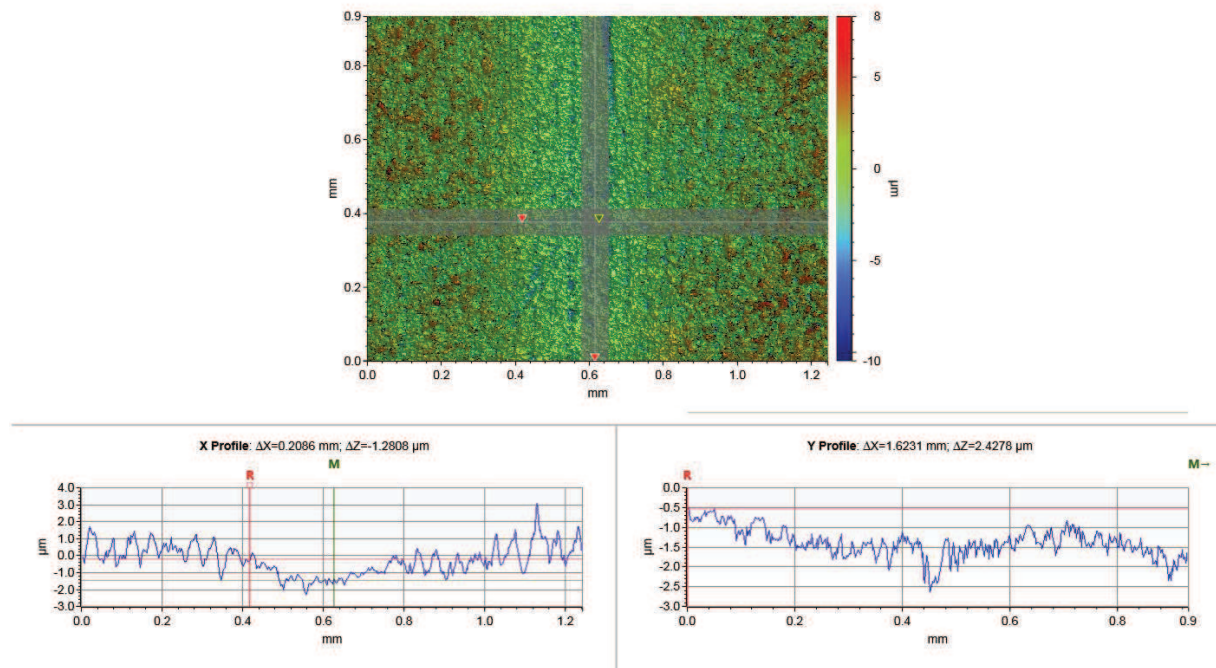


Figure 76 Surface profile of PAI from Hitachi with 40vol % MoS₂ after the testing on MTM machine

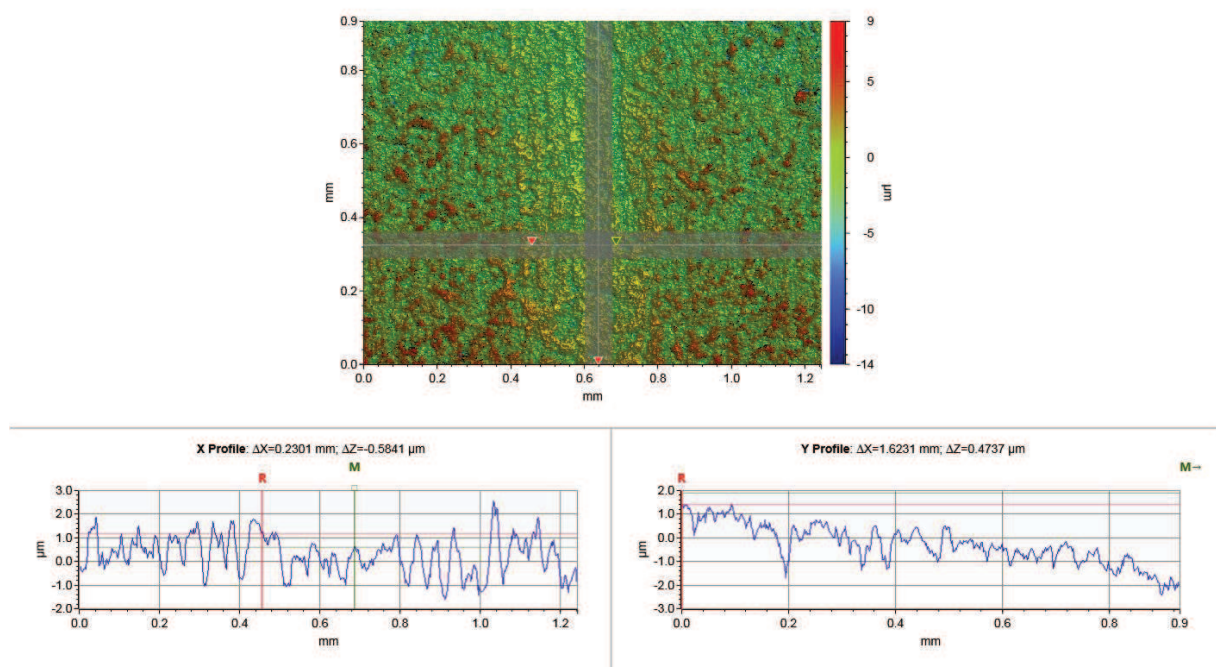


Figure 77 Surface profile of PAI from Torlon with 40vol % MoS₂ after the testing on MTM machine

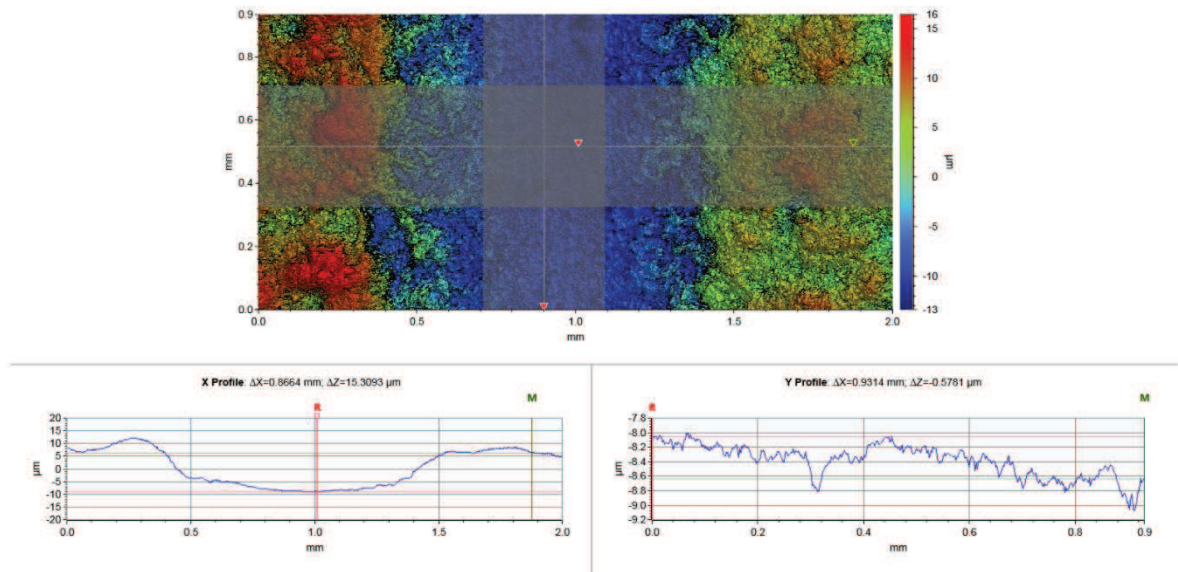


Figure 78 Surface profile of PAI from Torlon with additives 40vol % MoS₂ and 10 vol% of Graphite after the testing on MTM machine

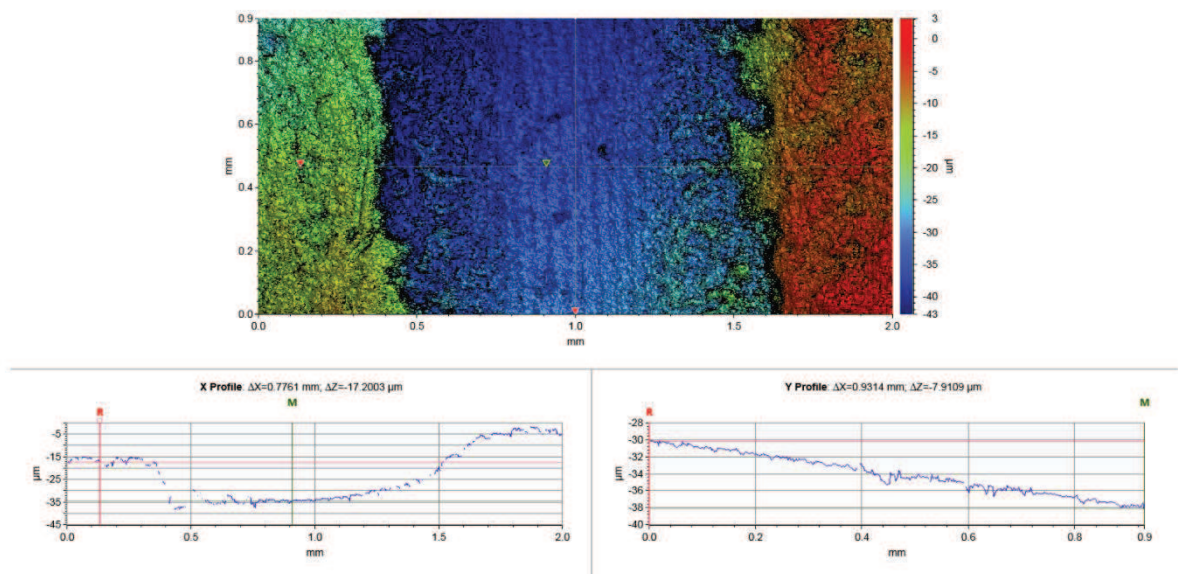


Figure 79 Surface profile of PAI from Torlon with additives 35vol % MoS₂ and 15 vol% of Graphite after the testing on MTM machine

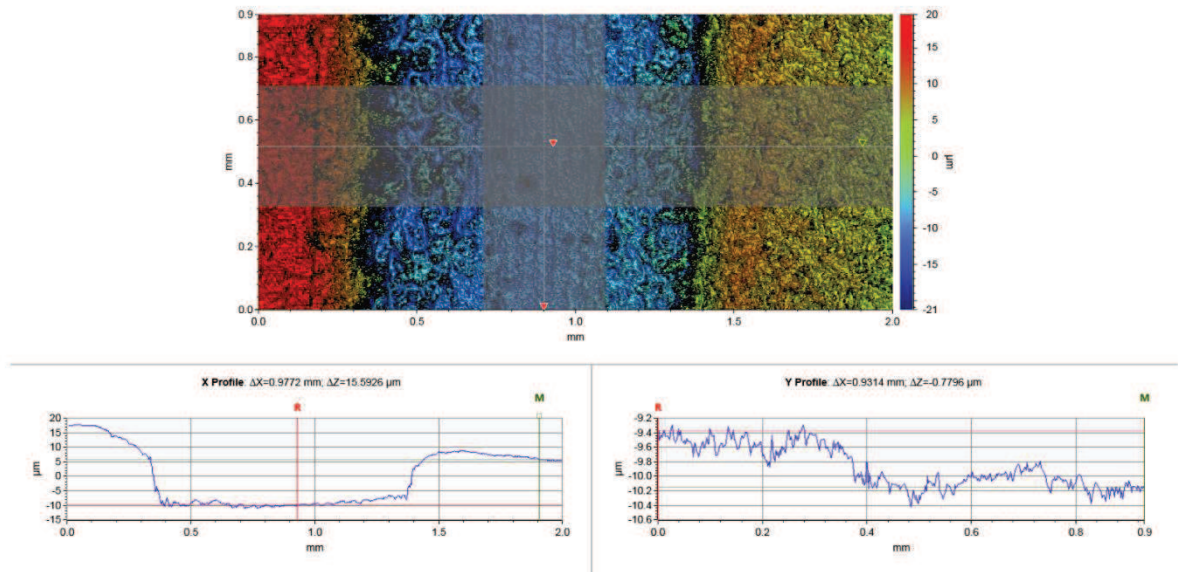


Figure 80 Surface profile of PAI from Torlon with additives 20vol % MoS₂ and 30 vol% of Graphite after the testing on MTM machine

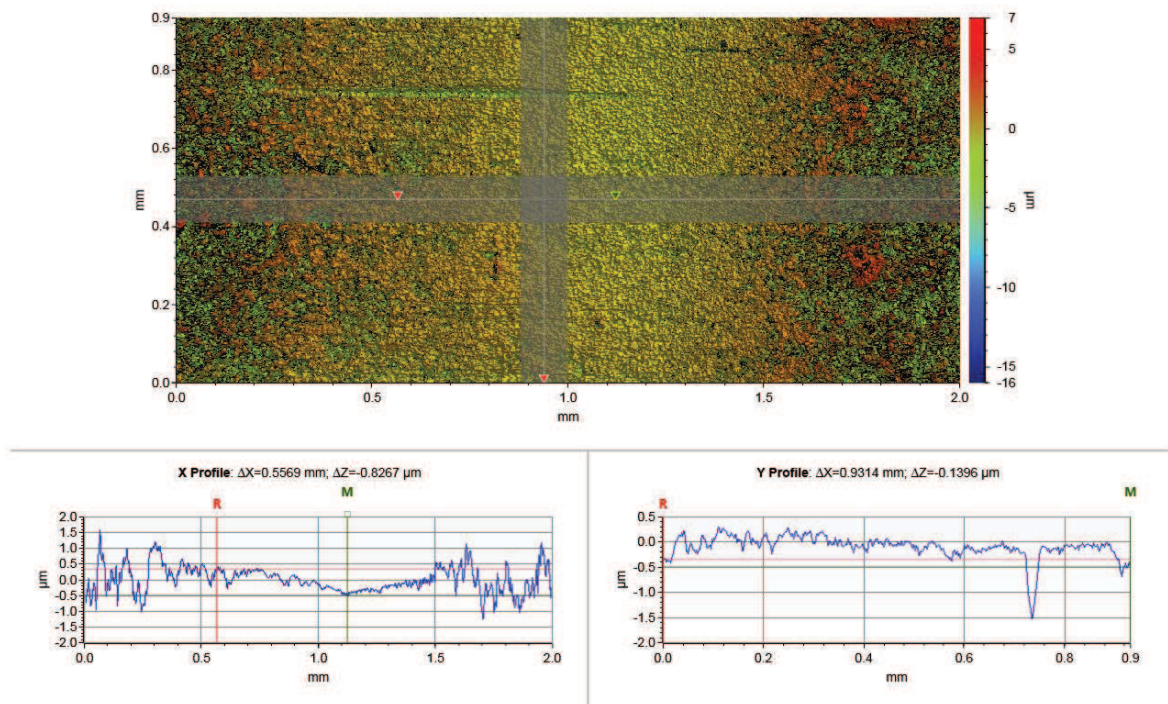


Figure 81 Surface profile of PAI from Torlon with additives 39vol % MoS₂ and 1 vol% of Ca(OH)₂ after the testing on MTM machine

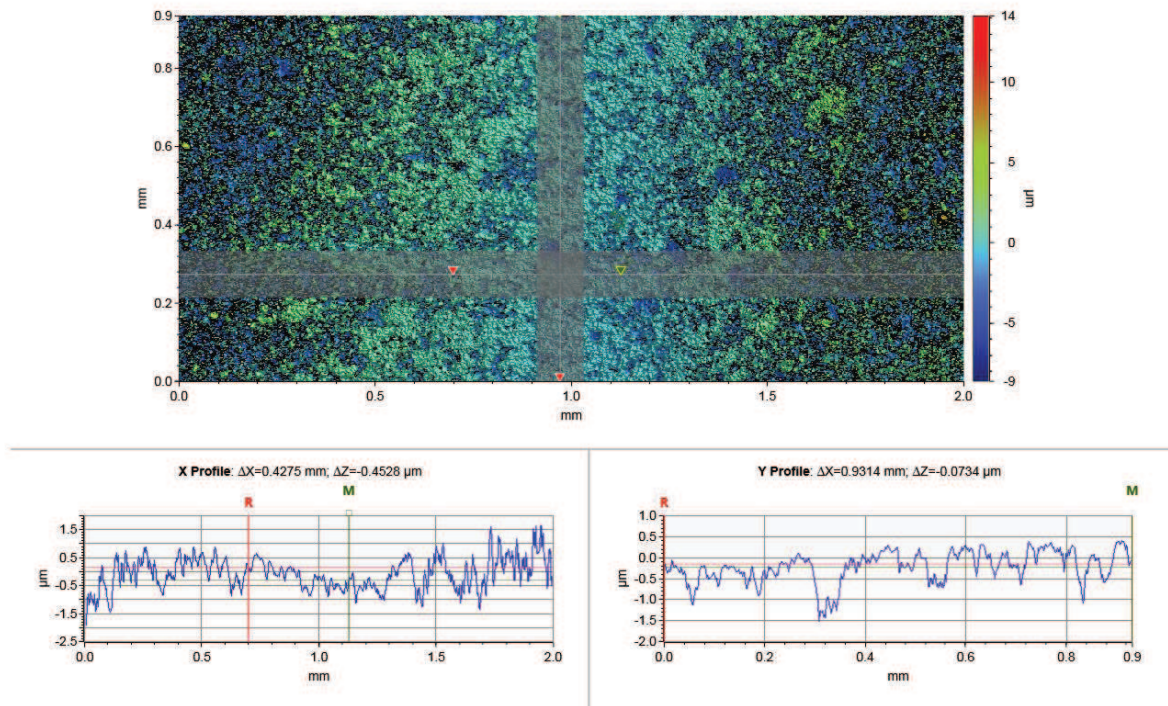


Figure 82 Surface profile of PAI from Torlon with additives 38vol % MoS_2 and 2 vol% of $\text{Ca}(\text{OH})_2$ after the testing on MTM machine

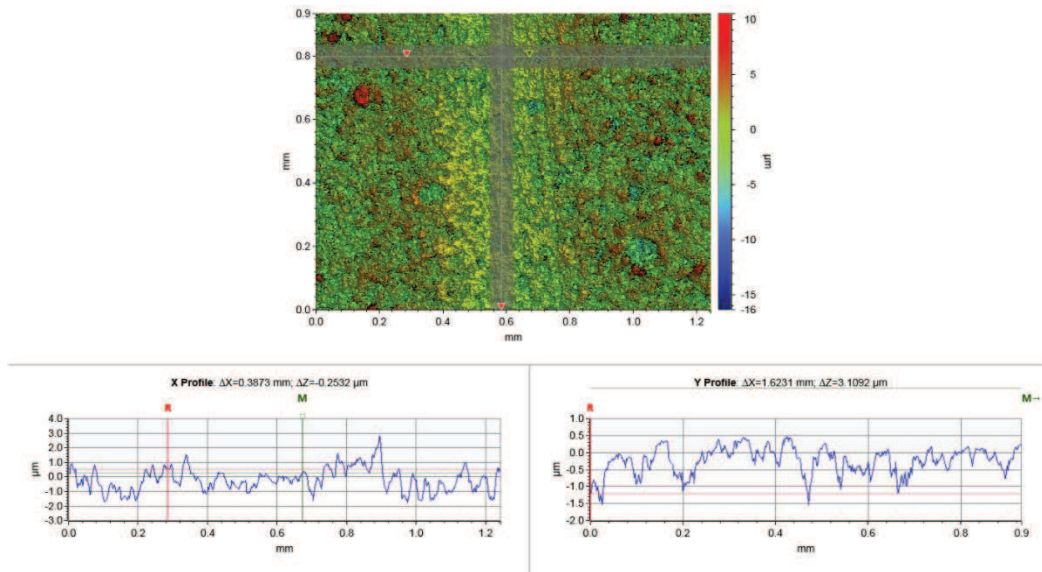


Figure 83 Surface profile of PAI from Torlon with additives 37vol % MoS_2 and 3 vol% of $\text{Ca}(\text{OH})_2$ after the testing on MTM machine

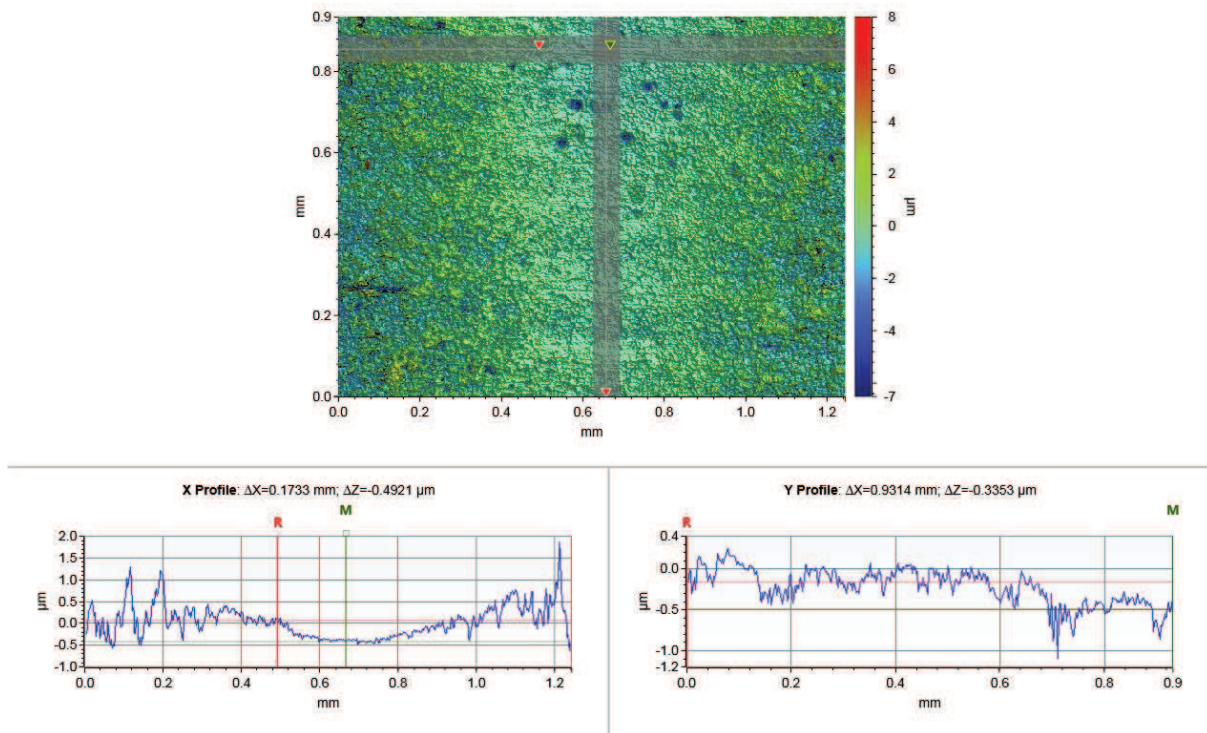


Figure 84 Surface profile of the pure PAI from Hitachi after the testing on BoR Tribolab system

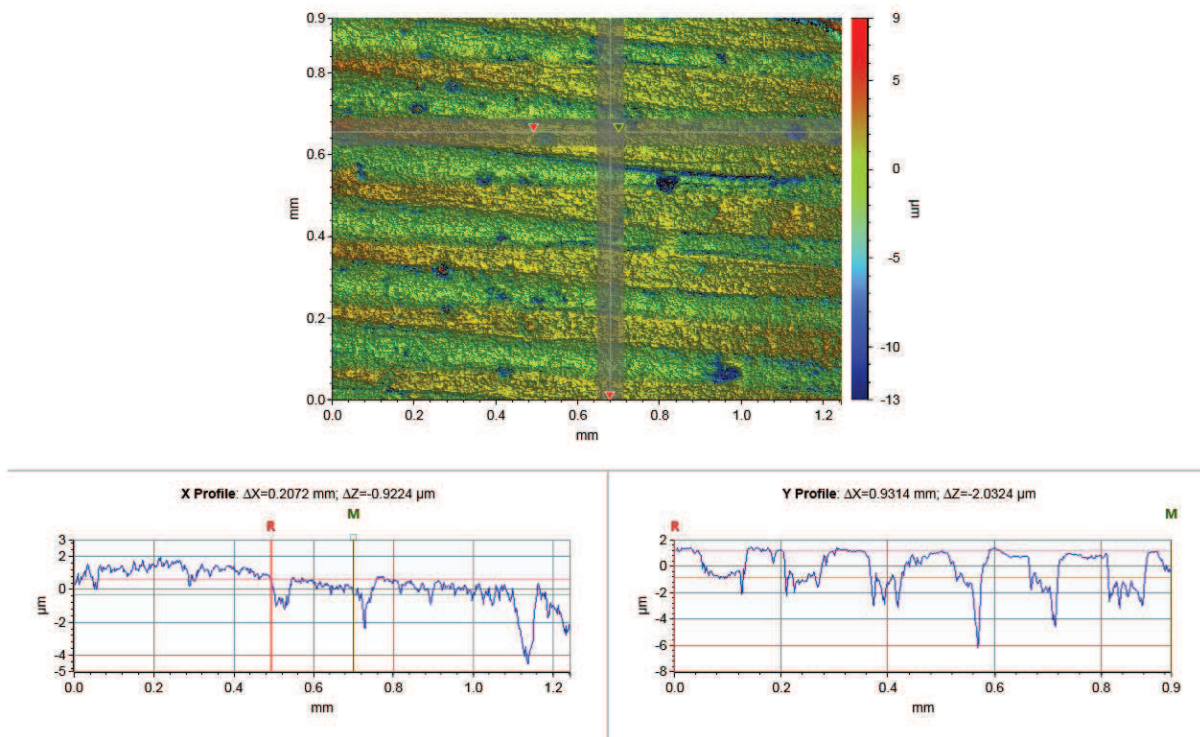


Figure 85 Surface profile of the pure PAI from Torlon after the testing on BoR Tribolab system

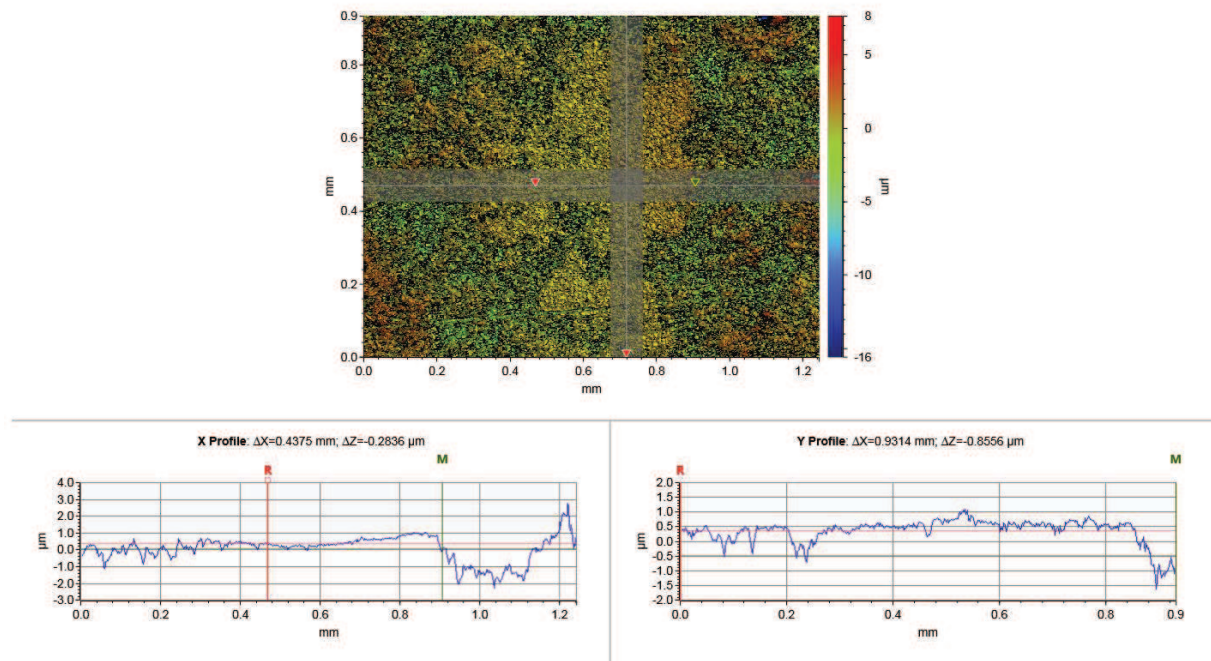


Figure 86 Surface profile of coating from PAI from Torlon (60 vol %) with 40vol % MoS₂ after the testing on BoR Tribolab system

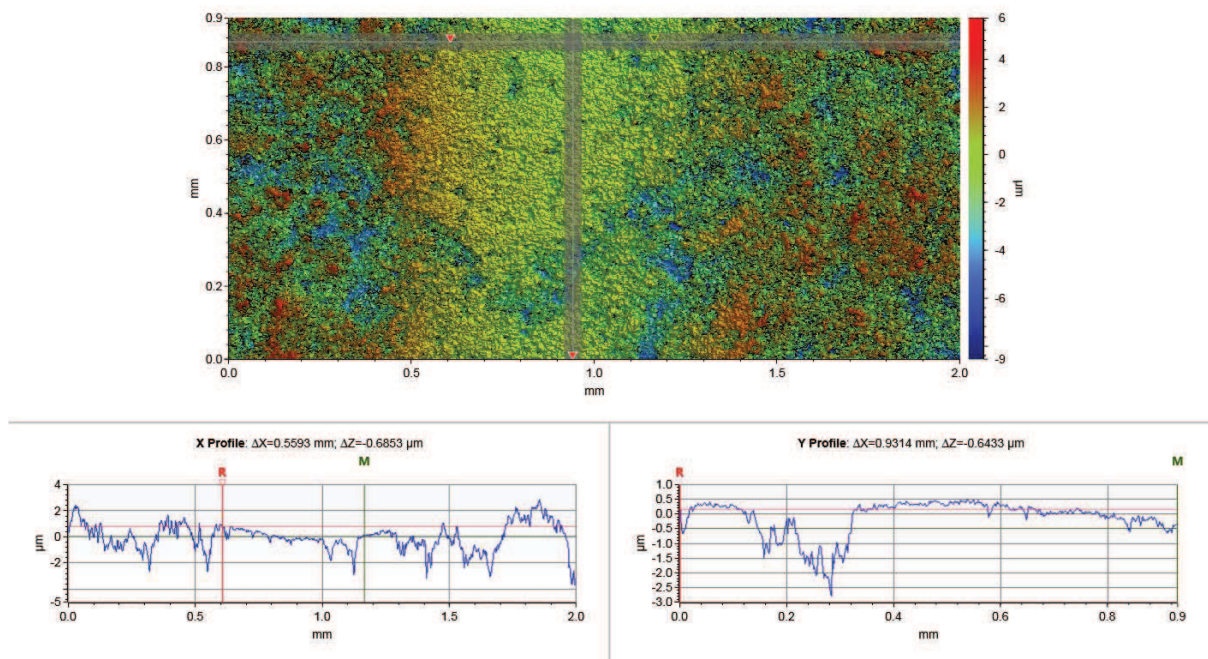


Figure 87 Surface profile of PAI from Torlon with additives 40vol % MoS₂ and 10 vol% of Graphite after the testing on BoR Tribolab system

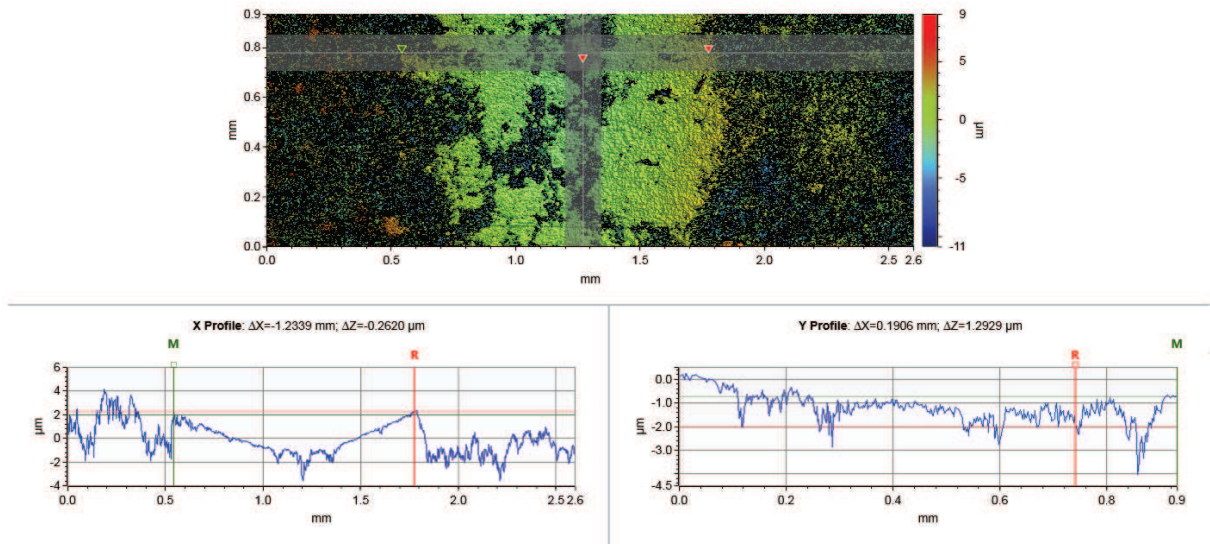


Figure 88 Surface profile of PAI from Torlon with additives 35vol % MoS2 and 15 vol% of Graphite after the testing on BoR Tribolab system

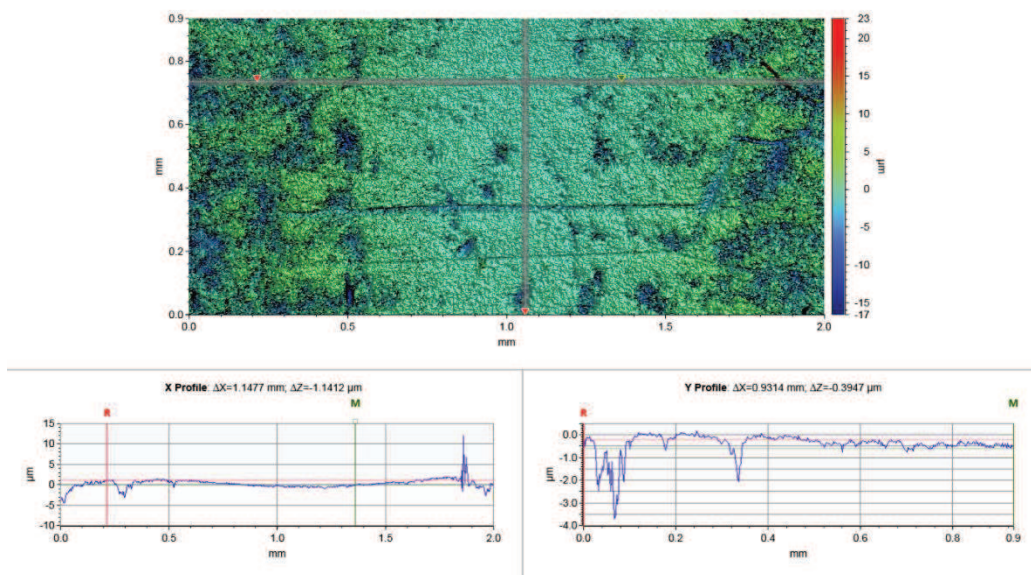


Figure 89 Surface profile of PAI from Torlon (40 vol. %) with additives 40vol % MoS2 and 20 vol% of Graphite after the testing on BoR Tribolab system

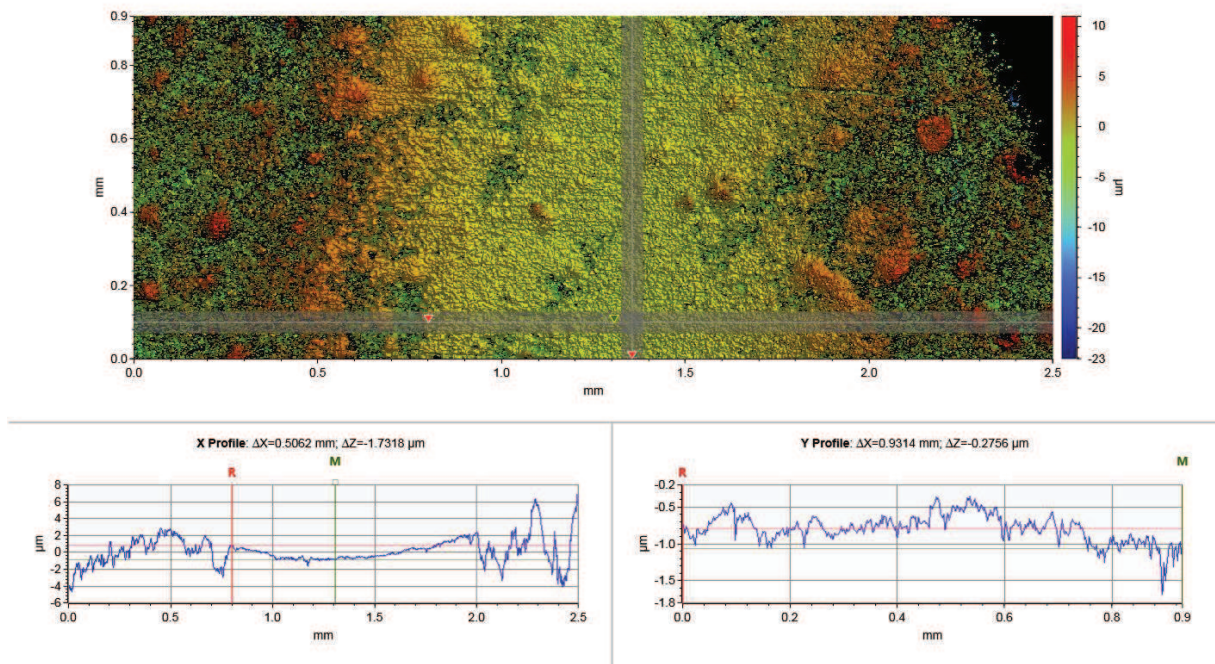


Figure 90 Surface profile of PAI from Torlon with additives 20vol % MoS₂ and 30 vol% of Graphite after the testing on BoR Tribolab system

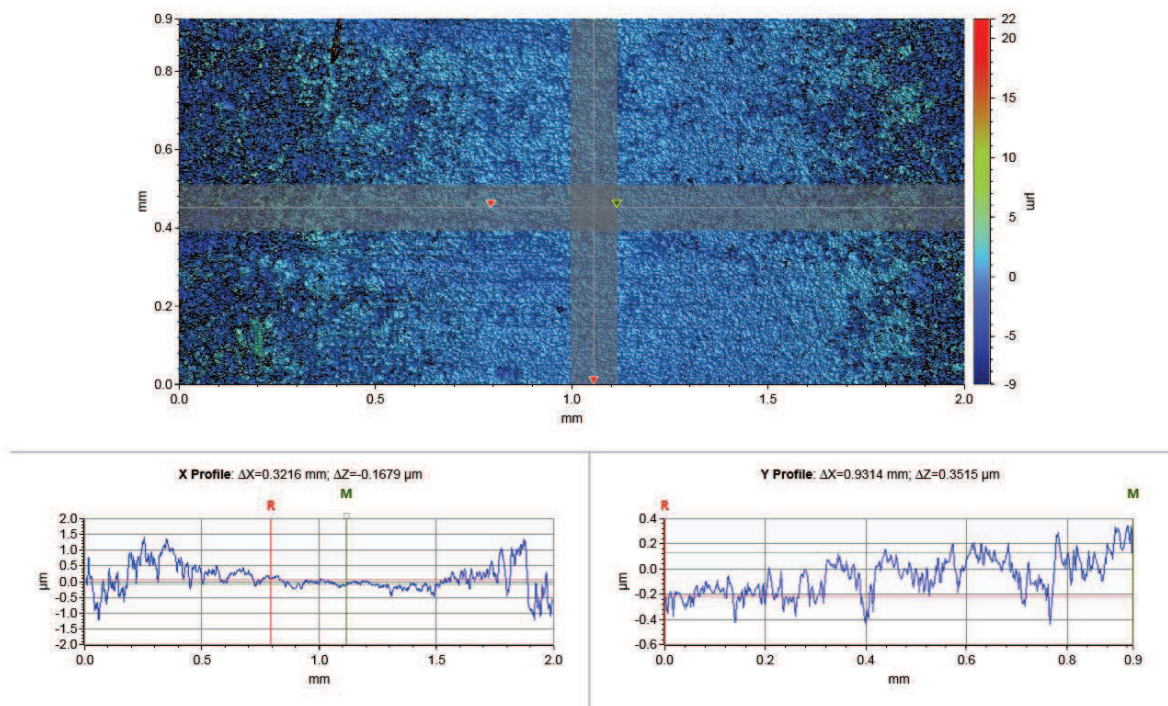


Figure 91 Surface profile of PAI from Torlon with additives 39vol % MoS₂ and 1 vol% of Ca(OH)₂ after the testing on BoR Tribolab system

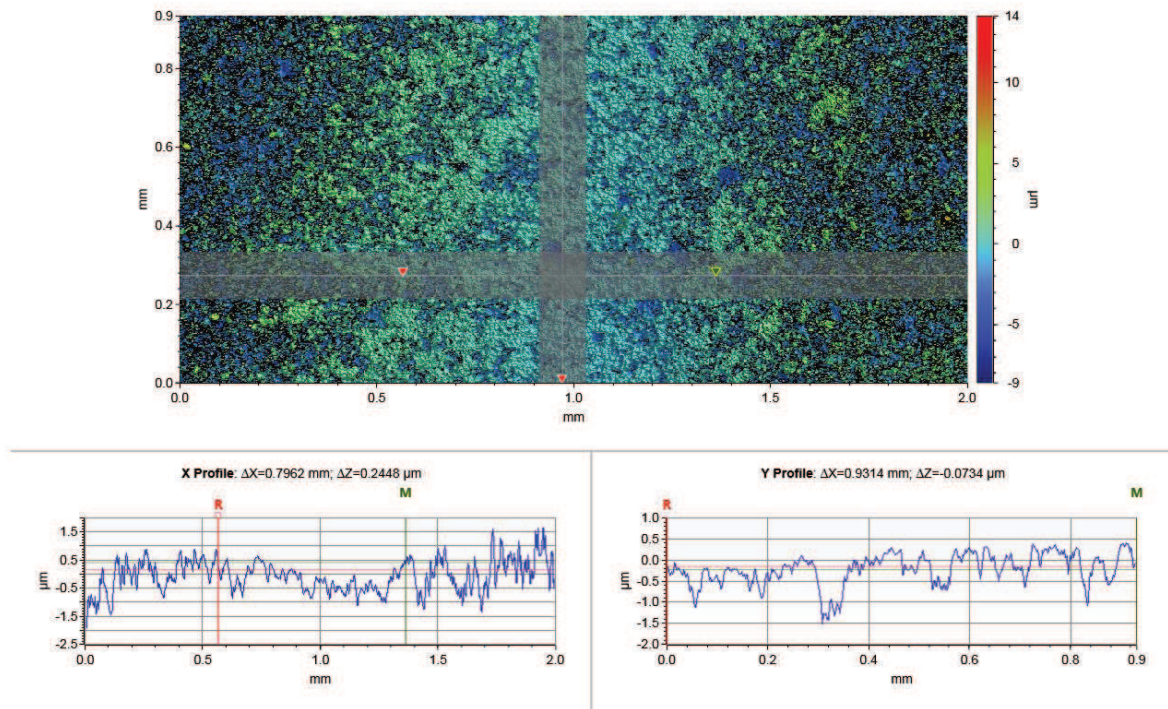


Figure 92 Surface profile of PAI from Torlon with additives 38vol % MoS_2 and 2 vol% of Ca(OH)_2 after the testing on BoR Tribolab

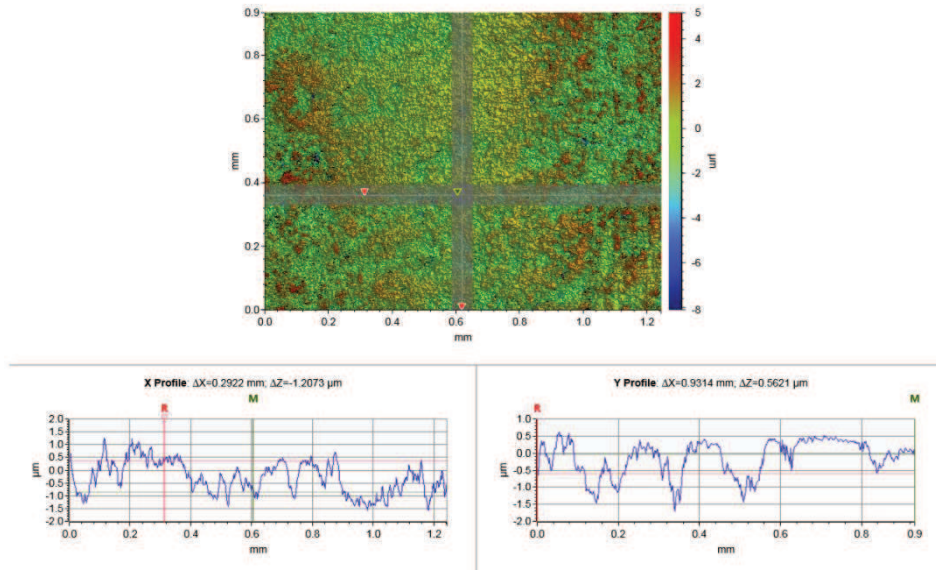


Figure 93 Surface profile of PAI from Torlon with additives 37vol % MoS_2 and 3 vol% of Ca(OH)_2 after the testing on BoR Tribolab

9.2 Appendix 2 Micro-scratch testing

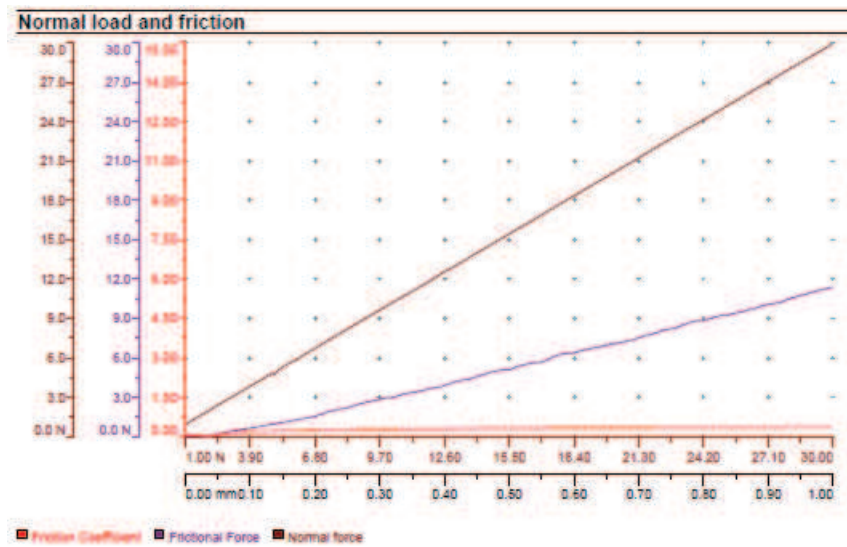


Figure 94 Scratch Testing of the pure PAI from Hitachi

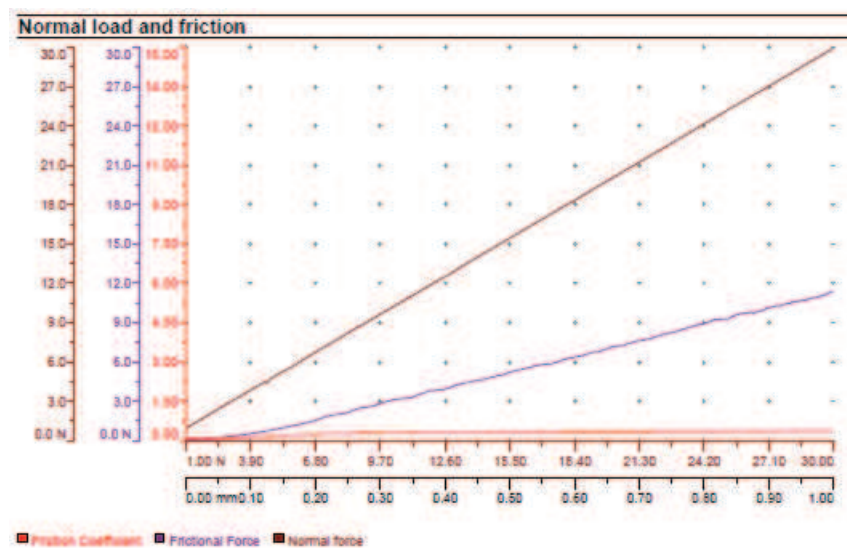


Figure 95 Scratch testing of the pure PAI from Torlon

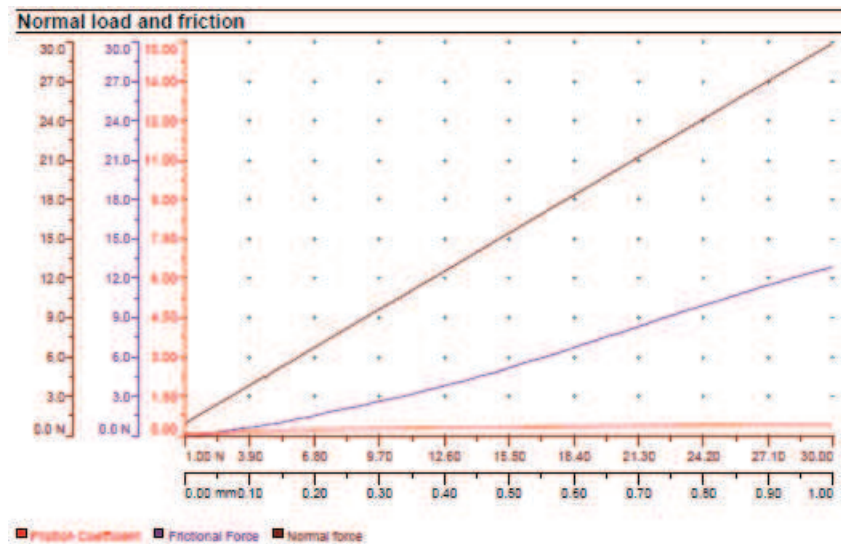


Figure 96 Scratch testing of PAI from Torlon with 40vol % MoS₂

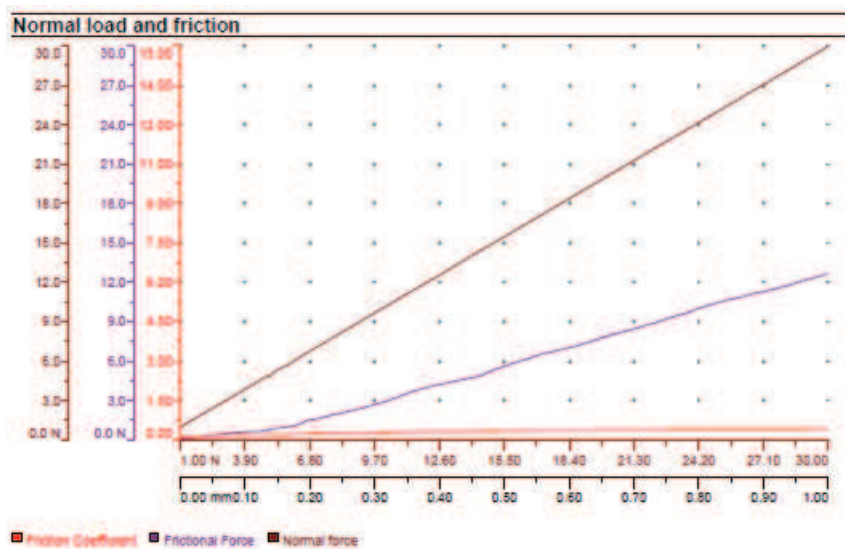


Figure 97 Scratch testing of PAI from Torlon with additives 40vol % MoS₂ and 10 vol% of Graphite

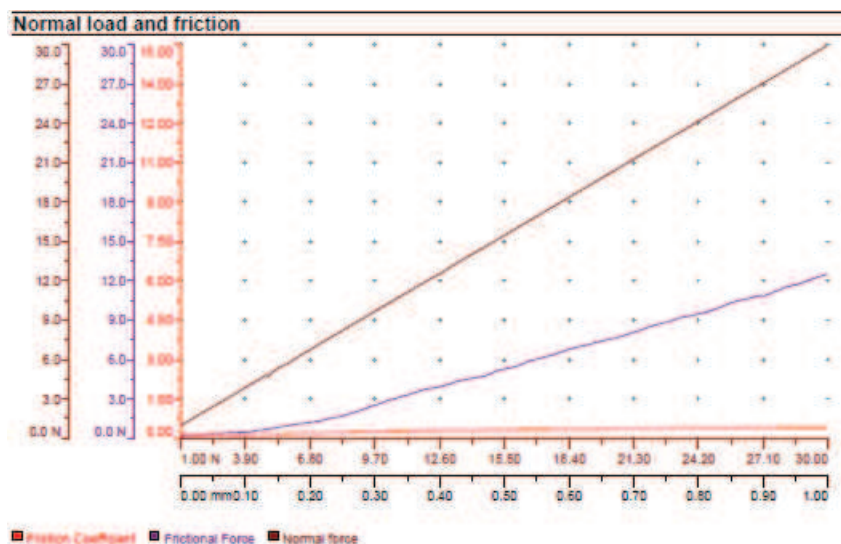


Figure 98 Scratch testing of PAI from Torlon with additives 35vol % MoS₂ and 15 vol% of Graphite

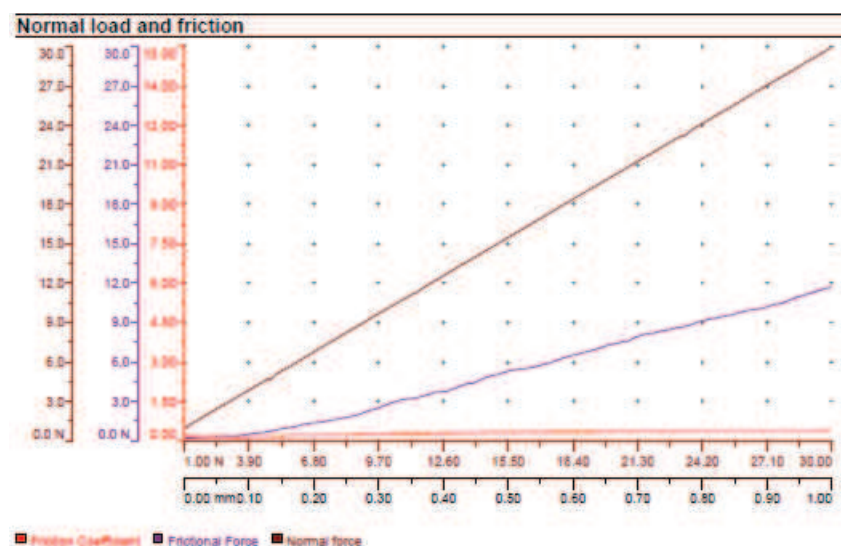


Figure 99 Scratch Testing of PAI from Torlon with additives 20vol % MoS₂ and 30 vol% of Graphite

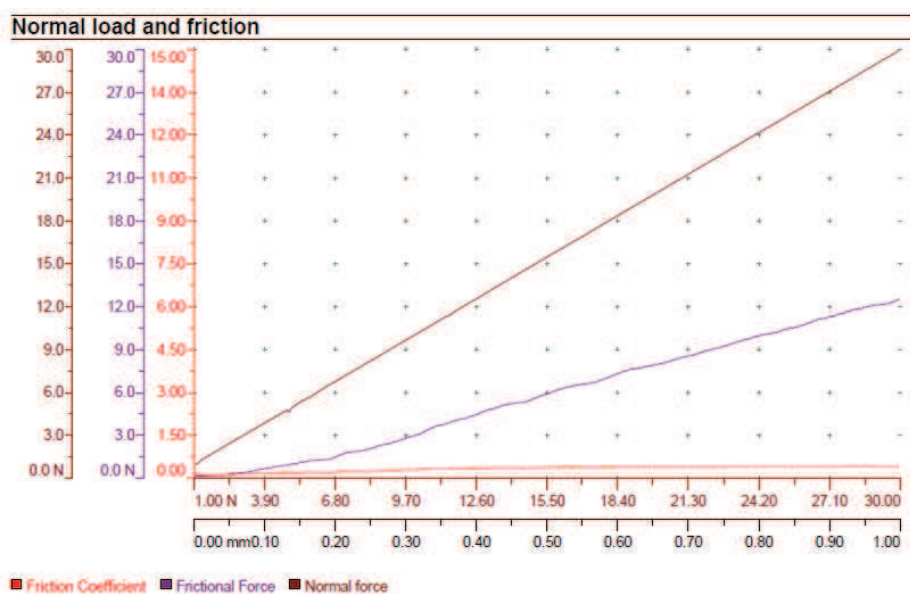


Figure 100 Scratch testing of PAI from Torlon with additives 39vol % MoS_2 and 1 vol% of Ca(OH)_2

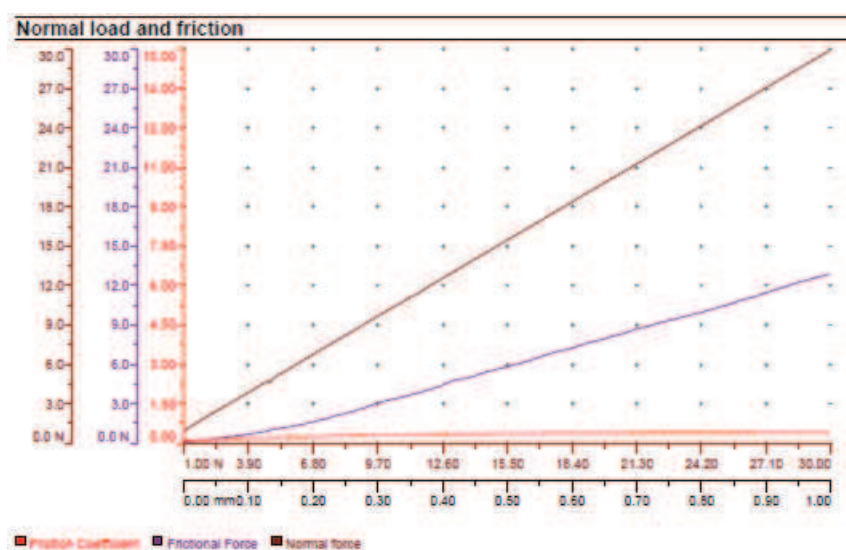


Figure 101 Scratch Testing of PAI from Torlon with additives 38vol % MoS_2 and 2 vol% of Ca(OH)_2

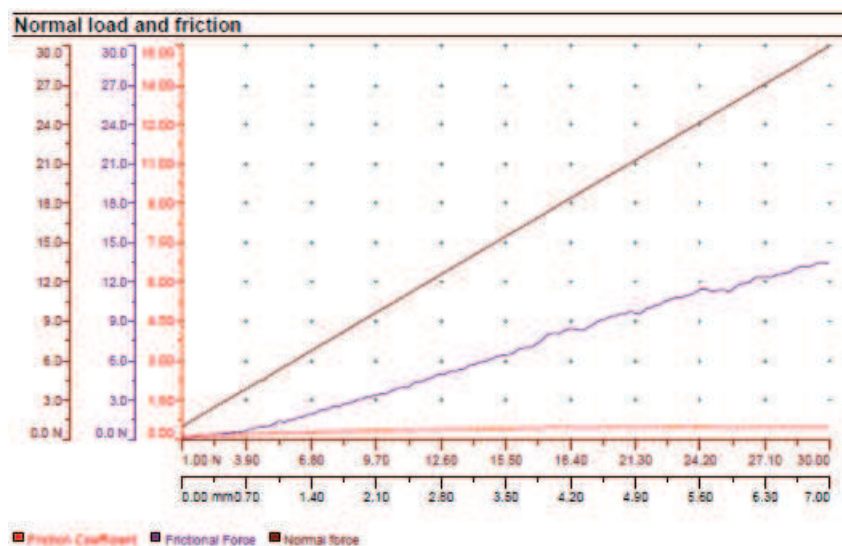


Figure 102 Scratch Testing of PAI from Torlon with additives 37vol % MoS_2 and 3 vol% of $\text{Ca}(\text{OH})_2$

9.3 Appendix 3 Roughness on the counterparts

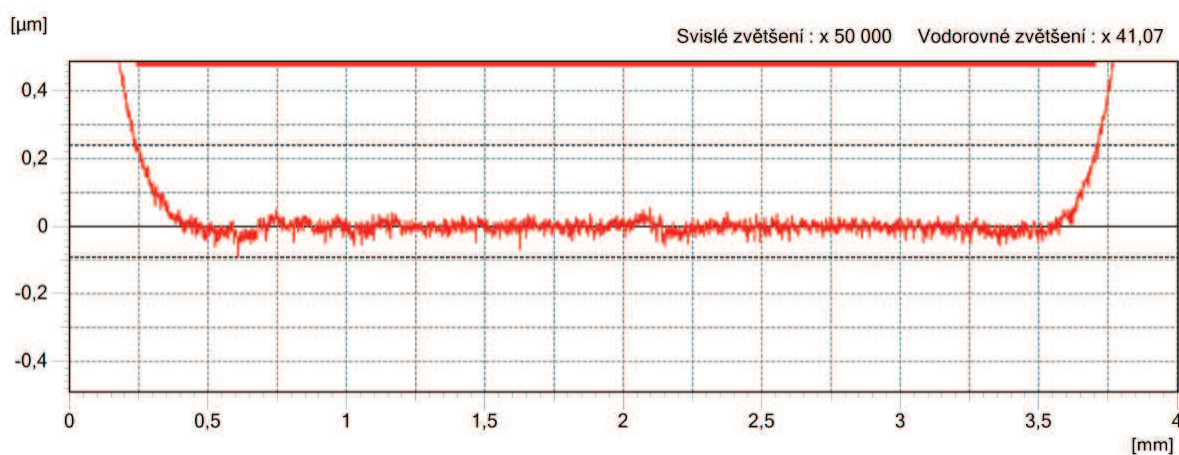


Figure 103 Roughness of the ball before testing on MTM



Figure 104 Roughness of the ball after the testing on disc coated by PAI from Torlon with additives 37vol % MoS_2 and 3 vol% of $\text{Ca}(\text{OH})_2$

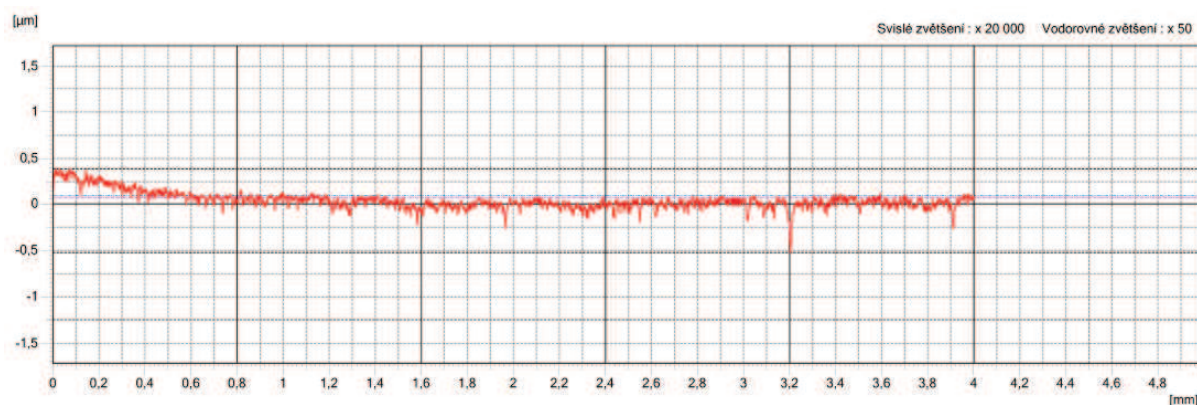


Figure 105 Roughness of the ring before testing on Bruker Tribolab

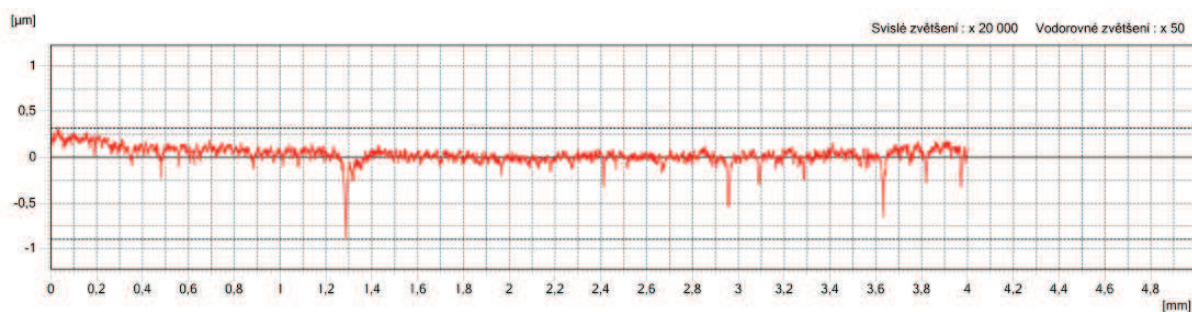


Figure 106 Roughness of the ring after the testing with block coated by PAI from Torlon with additives 37vol % MoS_2 and 3 vol% of $\text{Ca}(\text{OH})_2$

10 LIST OF ABBREVIATIONS

| | |
|---------------------|---|
| BoR | Block-on-ring |
| CaCO ₃ | Calcium carbonate |
| Ca(OH) ₂ | Calcium hydroxide |
| CID | Collision induced dissociation |
| CNT | Carbon nanotubes |
| DIDA | Diimide dicarboxylic acid |
| E | Modulus of elasticity |
| EDX | Energy-dispersive X-ray spectroscopy |
| FTIR | Fourier transform infrared spectroscopy |
| GNP | Graphene nanopowder |
| HD | Hydrodynamic |
| ICP-OES | Inductively coupled plasma atomic emission spectroscopy |
| LDI | Laser desorption ionization |
| MALDI | Matrix-assisted laser desorption/ionization |
| MoS ₂ | Molybdenum disulphide |
| MS | Mass spectrometry |
| MTM | Mini-traction-machine |
| NN | Neutralization number |
| NMP | N-methyl pyrrolidone |
| ODA | 4,4'-oxydianiline |
| PAI | Polyamide-imide |
| PVD | Physical Vapour Deposition |
| PEEK | Polyether ether ketone |
| PTFE | Polytetrafluoroethylene |
| RPM | Rotation per minute |
| SCF | Short Carbon Fiber |
| SEM | Scanning electron microscope |
| TBN | Total Base Number |
| TMA | Trimellitic anhydride |
| TMAc | Trimellitic anhydride chloride |
| TPP | Triphenyl phosphite |
| VI | Viscosity index |
| WS ₂ | Tungsten (IV) sulphide |
| WS ₂ F | Tungsten (IV) sulphide fullerene-like |
| WS ₂ N | Tungsten (IV) sulphide needle-like |
| XPS | X-ray photoelectron spectroscopy |
| ZDDP | Zinc dithiophosphate |

11 REFERENCES

- [1] KOBAYAKAWA, H.; TSUJI, H.; KAWAKAMI, N.; MCALEESE, C. et al. *A Study of Resin Overlay Bearing Material for Recent Automotive Engines*. SAE Technical Paper 2013-01-1394. SAE International, 2013.
- [2] ZHANG, Y. et al. High strength tin-based overlay for medium and high speed diesel engine bearing tribological applications. *Tribology International*. 2016, vol. 93, pp. 687-695.
- [3] PRATT, G. C. Bearing materials: plain bearings. In: *Encyclopedia of materials: science and technology*. Oxford: Elsevier Science Ltd., 2004, pp. 488-96.
- [4] EASTHAM, D. R.; CROOKS, C. S. Plating for bearing applications. *Aston university metals engineering congress*. September 1981, pp. 9-13.
- [5] GEBRETSADIK, D. W. et al. Tribological performance of tin-based overlay plated engine bearing materials. *Tribology International*. 2015, vol. 92, pp. 281-289.
- [6] KATSUKI, H. et al. *Friction and wear properties of low friction plain bearing materials by a ball on disk test*. JAST Tribology Conf., Fukui, Japan, September 2010, pp.247-248.
- [7] NAKADA, M. Trends in engine technology and tribology. *Tribology International*. 1994, vol. 27, pp. 3-8.
- [8] ZALAZNIK, M.; KALIN, M.; NOVAK, S.; JAKŠA, G. Effect of the type, size and concentration of solid lubricants on the tribological properties of the polymer PEEK. *Wear*. 2016, vol. 364-365, pp. 31-39.
- [9] TANAKA, T.; NAKA, I. et al. *Studies on lead-free resin overlay for engine bearings*. SAE Technical Paper 2006-01-1104. SAE International, 2006.
- [10] SAKAI, K.; ZUSHI, K. et al. *Development of lead free copper based alloys for three layers bearings under higher load engines*. SAE Technical Paper 2004-01-1600. SAE International, 2004.
- [11] GRUN, F.; GODOR, I.; GARTNER, W.; EICHLSEDER, W.: *Influence of overlays on the tribological behavior of journal bearing materials*. World Tribology Congress, Kyoto, Japan, September 2009, Paper F-131.
- [12] TSUJI, H.; KAWAKAMI, N.; MCALEESE, C.; KATSUKI, H.; KATO, K. *A study of resin overlay bearing material for recent automotive engines*. SAE Technical Paper. 2013-01-1394. SAE International, 2013.
- [13] BARBISA, M. V. et al. Physicochemical characterisation of tribolayers by micro-Raman and GDOES analyses. *Tribology International*. 2015, vol. 81, pp. 223-230.
- [14] BISWAS, S. K. Some mechanisms of tribofilm formation in metal/metal and ceramic/metal sliding interactions. *Wear*. 2000, vol. 245, pp. 178-189.
- [15] FISCHER, T. E. Tribochemistry. *Annual Review of Materials Science*. 1988, vol. 18, pp. 303-323.
- [16] DUMPALA, R.; KUMAR, N. et al. Characterization of tribo-layer formed during sliding wear of SiC ball against nanocrystalline diamond coatings. *Materials Characterization*. 2014, vol. 95, pp. 252-258.
- [17] FISCHER, T. E.; TOMIZAWA, H. Interaction of tribochemistry and microfracture in the friction and wear of silicon nitride, *Wear* 1985, vol. 105, pp. 29-45.
- [18] MAHATHANABODEE S. et al.: Dry sliding wear behavior of SS316L composites containing h-BN and MoS₂ solid lubricants. *Wear* 2014, vol. 316, pp. 37-48
- [19] Bruce, W. R.: *Handbook of Lubrication and Tribology, Volume II, Theory and Design, 2nd edition*. Suite: CRC Press, 2012.
- [20] DOWSON, D.: *History of Tribology*. London: Longman Group Limited, 1979.
- [21] STACHOWIAK, G. W.; BATCHELOR, A. W. *Engineering Tribology*. London: Elsevier Inc., 1993
- [22] ZHANG, Y.; TUDELA, I. et al. High strength tin-based overlay for medium and high speed diesel engine bearing tribological applications. *Tribology International*. 2016, vol. 93, pp. 687-695.
- [23] PRIESTER, J. et al. *Klzné ložiská*. Bratislava/Praha: ALFA/SNTL, 1980.
- [24] Internal documentation Daido Metal.
- [25] VINŠ, J. *Kluzná ložiska*. Praha: SNTL, 1971.
- [26] HAMROCK, B. J.; SCHMID, S. R.; JACOBSON, B. O. *Fundamentals of Fluid Film Lubrication*. Boca Reton: CRC Press, 2004.
- [27] TOMIMOTO, M. Experimental verification of a hard particle induced friction model in journal bearings. *Wear*. 2003, vol. 254, pp. 749-762.
- [28] LIGIER, J.-L.; NOEL, B. Friction Reduction and Reliability for Engines Bearings. *Lubricants*. 2015, vol. 3, pp. 569-596.

-
- [29] KUMAR, N.; GAUTAM, G. et al. Wear, friction and profilometer studies of insitu AA5052/ZrB2 composites. *Tribology International*. 2016, vol. 97, pp. 313-326.
 - [30] STACHOWIAK, G. W.; BATCHELOR, A. W. *Engeneering Tribology*. New York: Elsevier Inc., 2014.
 - [31] NEALE, M. J.; GEE, M. *Wear Problems and Testing for Industry*. New York: Elsevier Inc., 2001.
 - [32] VENCL, A.; RAC, A. Diesel engine crankshaft journal bearings failures: Case study. *Engineering Failure Analysis*. 2014, vol. 44, pp. 217-228.
 - [33] *Pall Corporation: Why is Filtration Important?* [online]. Pall Corporation: ©2014, [cit. 2.8.2014]. Available in: <http://www.pall.de/main/industrial-manufacturing/why-is-filtration-important-3779.page>
 - [34] LIGIERA, J. L.; DUTFOY, L. Modeling and prediction of a simplified seizure mechanism occurring in conrod bearings. *Mécanique & Industries*. 2011, vol. 12, no. 4, pp. 265-273.
 - [35] PRIESTER, J. et al. *Klzné ložiská*. Bratislava: Vydavateľstvo Technické a ekonomickej literatúry Bratislava, 1983.
 - [36] SHARMA, A.; RAJAN, T. V. Bearing characteristics of cast leaded aluminium-silicon alloys. *Wear*. 1996, vol. 197, pp. 105-114.
 - [37] PRAZZ, G. C.: Materials for Plain Bearings. *International Materials Review*. 1973, vol. 18, pp. 62.
 - [38] NIIR BOARD OF CONSULTANTS AND ENGINEERS. *The Complete Technology Book on Aluminium And Aluminium Products*. Delhi: Asia Pacific Business Press Inc., 2007.
 - [39] COPPER DEVELOPLMENT ASOCIATION. *Cost-Effective Manufacturing: Copper Alloy Bearings* [online]. CDA Publication, 1992. [cit.] Available in: <http://www.nationalbronze.com/pub-45-copper-alloy-bearings-pdf.pdf>
 - [40] KOPELIOVICH, D. *Manufacturing bi-metal strips for copper bearings* [online]. [cit.] Available in: http://www.substech.com/dokuwiki/doku.php?id=manufacturing_bi-metal_strips_for_copper_bearings
 - [41] HOLMBERG, K.; MATTHEWS, A. *Coatings Tribology: Properties, Mechanisms, Techniques and Applications in Surface Engineering*. New York: Elsevier Inc., 2009.
 - [42] HOLLECK, H. Material selection for hard coatings. *Journal of Vacuum Science and Technology A: Vacuum, Surfaces, and Films*. 1986, vol. 4, pp. 6
 - [43] MATTHEWS, A.; RICKERBY, D. S. eds. *Advanced Surface Coatings: A Handbook of Surface Engineering*. Glasgow: Springer, 1991.
 - [44] KOROSCHETZ, F.; HOKE, E.; GRASSERBAUER, M. Diffusionsvorgänge an galvanisch abgeschiedenen PbSnCu-Gleitlayerschichten. *Mikrochimica Acta*. 1981, vol. 9, pp. 139-52.
 - [45] GRUN, F.; GODOR, I. et al. Tribological performance of thin overlays for journal bearings. *Tribology International*. 2011, vol. 44, pp. 1271-1280.
 - [46] ADAM, A. et al. *The progression of engine bearing overlays*. SAE Technical Paper 2002-01-1316. SAE International, 2002.
 - [47] ISHIKAWA, H.; NOMURA, K.; MIZUNO, Y.; MICHIOKA, H. et al. *Development of bearing with composite overlay for high-performance engines*. SAE Technical paper 960988. SAE International, 1996.
 - [48] GEBRETSADIK, D. W.; HARDELL, J.; PRAKASH, B. Tribological performance of tin-based overlay plated engine bearing materials. *Tribology International*. 2015, vol. 92, pp. 281-289.
 - [49] ROSA, H.; CARDUS, G.; BROITMAN, E.; ZIMMERMAN, R. Structural properties of Al-Sn thin films deposited by magnetron sputtering. *Journal of Materials Science Letters*. 2001, vol. 20, pp. 1365-1367.
 - [50] HAMROCK, B. J.; SCHMID, S. R.; JACOBSON, B. O. *Fundamental of Ftuid Fitm Lubrication*. New York: Marcel Dekker, Inc., 2004.
 - [51] KHEDKAR, J.; NEGUELSC, I.; MELETIS, E. I. Sliding wear behavior of PTFE composites. *Wear*. 2002, vol. 252, pp. 361-369.
 - [52] LEE, L. H.: *Polymer Wear and its Control*. Washington: American Chemical Society, 1985.
 - [53] TANAKA, K.; UCHIYAMA, Y.; TOYOOKA, S. The Mechanism Of Wear Of Polytetrafluoroethylene. *Wear*. 1973, vol. 23, pp.153-172.
 - [54] GGB INC. Sliding layer for multilayer bearing material. Inventors: Y. H. PENG and M. KIM. European patent application. EP 2710273 A1. 26.4.2014.
 - [55] KOLBENSCHMIDT AG. Material for use in the manufacture of composite bearings for crankshafts. Inventors: W. BICKLE and H. PFESTORF. US patent application. US4666792 (A). 19.5.1987.

-
- [56] PARKER D. et al. Polymers, High-Temperature. In: *Ullman's Encyclopedia of Industrial Chemistry* [online]. Wiley-WCH Verlag GmbH & Co. KGaA, 2002 [cit.] Available in: http://onlinelibrary.wiley.com/doi/10.1002/14356007.a21_449.pub3/abstract
 - [57] RODRIGUEZ, V.; SUKUMARAN, J.; SCHLARB, A. K.; DE BAETS, P.: Influence of solid lubricants on tribological properties of polyetheretherketone (PEEK). *Tribology International*. 2016, vol. 103, pp. 45-57.
 - [58] LAUX, K. A.; JEAN-FULCRAND, A et al. The influence of surface properties on sliding contact temperature and friction for polyetheretherketone (PEEK). *Polymer*. 2016, vol. 103, pp. 397-404.
 - [59] KALIN, M.; ZALAZNIK, M.; NOVAK, S. Wear and friction behaviour of poly-ether-ether-ketone (PEEK) filled with graphene, WS₂ and CNT nanoparticles. *Wear*. 2015, vol. 332-333, pp. 855-862.
 - [60] ZHANG G.; WETZEL, B.; WANG, Q. Tribological behavior of PEEK-based materials under mixed and boundary lubrication conditions. *Tribology International*. 2015, vol. 88, pp. 153-161.
 - [61] ROBERTSON, G. P.; GUIVERA, M. D.; YOSHIKAWA, M.; BROWNSTEIN, S. Structural determination of Torlonw4000T polyamide – imide by NMR spectroscopy. *Polymer*. 2004, vol. 45, pp. 1111-1117.
 - [62] DODDA, J. M.; BĚLSKÝ, P. Progress in designing poly(amide imide)s (PAI) in terms of chemical structure, preparation methods and processability. *European Polymer Journal*. 2016, vol. 84, pp. 514-537.
 - [63] VINOGRADOVA, S. V.; VYGODSKII, Y. S. Cardopolymers (Loop polymers). *Russian Chemical Reviews*. 1973, vol. 42, pp. 551-569.
 - [64] HAMICUC, E.; SAVA, I. et al. New poly(amide-imide)s containing cinnamoyl and azobenzene groups. *Polymers for Advanced Technologies*. 2006, vol. 17, pp. 641-646.
 - [65] BEHNIAFAR, H.; SAEED, A. B.; HADIAN, A. Novel heat-resistant and organosoluble poly(amide-imide)s containing laterally-attached phenoxy phenylene groups. *Polymer Degradation and Stability*. 2009, vol. 94, pp. 1991-1998.
 - [66] HSIAO, S. H.; GUO, W. et al. Synthesis and characterization of electrochromic poly(amide-imide)s bearing methoxy-substituted triphenylamine units. *Materials Chemistry and Physics*. 2011, vol. 130, pp. 1086-1093.
 - [67] MEHDIPOUR-ATAEI, S.; ZIGHEIMAT, F. Soluble poly(amide imide)s containing oligoether spacers. *European Polymer Journal*. 2007, vol. 43, pp. 1020-1026.
 - [68] BELL TELEPHONE LABOR INC. Linear polymer cycling imide groups. Inventor: C. J. FROSCHE. US patent application. US2421024 A. 27.5.1947.
 - [69] MARK, J. E. *Polymer Data Handbook*. New York: Oxford University Press, 1999.
 - [70] *Torlon PAI* [online]. Solvay: © 2017 [cit.] Available in: <http://www.solvay.com/en/markets-and-products/featured-products/torlon.html>
 - [71] CHITOSE, T.; KAMIYA, S.; KABEYA, Y.; DESAKI, T. *Friction and Wear Reduction of Engine Bearings with Solid Lubricant Overlay*. SAE Technical Paper 2014-01-0955. SAE International, 2014.
 - [72] SHABANIAN, M. et al. Synthesis of a novel CNT/polyamide composite containing phosphine oxide groups and its flame retardancy and thermal properties. *New Carbon Materials*. 2015, vol. 30, no. 5, pp. 397-403.
 - [73] GEBRETSADIK D. W.; HARDELL J.; PRAKASH, B. Friction and wear characteristics of different Pb-free bearing materials in mixed and boundary lubrication regimes. *Wear*. 2015, vol. 340-341, pp. 63-72.
 - [74] FEDERAL-MOGUL CORPORATION. Coated Sliding Element. Inventors: K. TROY, J. R. TOTH, R. R. AHARONOV. US patent application. US20160312891 A1. 27. 10. 2016.
 - [75] DAIDO METAL COMPANY LTD. Bearing Structure. Inventors: H. NOBUTAKA, S. MITSURU, M. YOSHIKATU, S. TAKAYUKI. US patent application. US005700093A. 23. 12. 1997.
 - [76] FORTUNE CONSTRUCTION ENGINEERING LTD. Sliding Bearing for Structural Engineering Applications. Inventor: F. ABET. European patent application. WO2015059610 A1. 30.4.2015.
 - [77] KOLBENSCHMIDT AG. Composite material for sliding surface bearings. Inventors: J. BRAUS, H.-P. BAUREIS, W. BICKLE. US patent application. US4847135A. 11. 7. 1989.
 - [78] MBA GLEITLAGER GMBH. Bearing element. Inventor: H. LANG. European patent application. EP1717469A2. 2.11.2006.
 - [79] MBA GLEITLAGER AUSTRIA GMBH. Sliding bearing element. Inventor: G. LEONARDELLI. European patent application. WO2016079133 A1. 26.5.2016.

-
- [80] MAHLE METAL LEVE S/A. Bearing for an internal combustion engine. Inventors: S. LIMA et al. US patent application. US2015139579 A1. 21.5.2015.
- [81] PARK, K. H.; WATANABE, S.; KAKIMOTO, M. A.; IMAI, Y. Synthesis and properties of new aromatic noncyclic poly(imide-amide)s from N,N-bis(aminobenzoyl) anilines and aromatic dicarboxylic acids. *Macromolecular Chemistry and Physics*. 1998, vol. 199, pp. 409-413.
- [82] NIETO, J. L.; DE LA CAMPA, J. G.; ABAJO, D. Aliphatic-aromatic polyamide-imides from diisocyanates, 2. Study of the influence of the reaction conditions on polymer structure. *Macromolecular Chemistry and Physics*. 1982, vol. 183, pp. 571-578.
- [83] YAMAZAKI, N.; MATSUMOTO, M.; HIGASHI, F. Studies on reactions of the N-phosphonium salts of pyridines. XIV. Wholly aromatic polyamides by the direct polycondensation reaction by using phosphites in the presence of metal salts. *Journal of Polymer Science Part A: Polymer Chemistry*. 1975, vol. 13, pp. 1373-1380.
- [84] HSIAO, S. H.; YANG, C. P. Preparation of poly(amide-imide)s by direct polycondensation with triphenyl phosphite, 3. Poly(amide-imide)s based on bis (trimellitimide)s. *Macromolecular Chemistry and Physics*. 1990, vol. 19, pp. 155-167.
- [85] YANG, C. P.; HSIAO, S. H. Preparation of poly(amide-imide)s by means of triphenyl phosphite, 1. Aliphatic-aromatic poly(amide-imide)s based on trimellitimide, *Macromolecular Chemistry and Physics*. 1989, vol. 190, pp. 2119-2131.
- [86] IMAI, Y.; MALDAR, N. N.; KAKIMOTO, M. A. Synthesis and characterization of aromatic polyamide-imides from 2,5-bis(4-aminophenyl)-3,4- diphenylthiophene and 4-chloroformylphthalic anhydride. *Journal of Polymer Science Part A: Polymer Chemistry*. 1985, vol. 23, pp. 2077-2080.
- [87] STANDARD OIL CO. Foam resins prepared from aromatic anhydrides and isocyanates. Inventor: H. E. FREY. US patent application. US3300420A. 24.1.1967.
- [88] AVELLA, N.; MAGLIO, G.; PALUMBO, R.; VIGNOLA, M. C. Poly(amideimide)s based on diamines containing bisaryloxy groups: structure-properties relationships. *Polymer*. 1996, vol. 37, pp. 4615-4619.
- [89] PATIL, P. S.; PAL, et al. Synthesis of aromatic poly(amide-imide)s from novel diimide-diacid (DIDA) containing sulphone and bulky pendant groups by direct polycondensation with various diamines. *European Polymer Journal*. 2007, vol. 43, pp. 5047-5054.
- [90] DIXON GROUP. Bearing Compositions. Inventors: H. T. CHILDS and E. J. MACK. US patent application. US3652409 A. 28.3.1972.
- [91] XING, X.S.; LI, R. K. Y. Wear behavior of epoxy matrix composites filled with uniform sized sub-micron spherical silica particles. *Wear*. 2004, vol. 256, pp. 21-26.
- [92] RONG, M. Z.; ZHANG, M. et al. Microstructure and tribological behavior of polymetric nanocomposites. *Industrial Lubrication and Tribology*. 2001, vol. 53, pp. 72-77.
- [93] XUE, Q.; WANG, Q. Wear mechanisms of polyetheretherketone composite filled with various kinds of SiC. *Wear*. 1997, vol. 213, pp. 54-58.
- [94] ZHANG, J.; CHANG, L. et al. Some insights into effects of nanoparticles on sliding wear performance of epoxy nanocomposites. *Wear*. 2013, vol. 304, pp. 138-143.
- [95] KABUSHIKI KAISHA SANKYO SEIKI SEISAKUSHO. Bearing Material And Plastic Bearin. Inventors: T. KOBAYASHI et al. US patent application. US005236784A. 17.8.1993.
- [96] TAIHO KOGYO CO LTD. Sliding bearing. Inventors: K. ASIHARA et al. US patent application. US2016333922 A1. 17.11.2016.
- [97] MAHLE INT GMBH; MAHLE ENGINE SYSTEMS UK LTD. Bearing materil. Inventor D. LATHAM. European patent application. JP2016074892. 12.5.2016.
- [98] MAHLE INT GMBH; MAHLE ENGINE SYSTEMS UK LTD. Sliding engine component. Inventor: N-. FISHER. US patent application. US20160273582A1. 22.9.2016.
- [99] FEDERAL-MOGUL WIESBADEN GMBH. Plain bearing material and a plain bearing composite material, comprising zinc sulphide and barium sulphate. Inventors: A. ACHIM and N. FLEISCHHACKER. US patent application. US2016319867. 3.11.2016.
- [100] ALEXANDRE, M.; DUBOIS, P. Polymer-layered silicate nanocomposites: preparation, properties and uses of a new class of materials. *Material Science and Engeneering: R: Reports*. 2000, vol. 28, pp. 1-63.
- [101] RAY, S. S.; OKAMOTO, M. Polymer/layered silicate nanocomposites: a review from preparation to processing. *Progress in Polymer Science*. 2003, vol. 28, pp. 1539-1641.
- [102] Fu, S. Y.; LAUKE, B. Characterization of tensile behaviour of hybrid short glass fibre calcite particle ABS composites. *Composites Part A*. 1998, vol. 29A, pp. 575-583.

-
- [103] EIRICH, F. R. Some mechanical and molecular aspects of the performance of composites. *Journal of Applied Polymer Science*. 1984, vol. 39, pp. 93-102.
 - [104] FUA, S.-Y.; FENGB, X.-Q.; LAUKEC, B.; MAI, Y.-W. Effects of particle size, particle/matrix interface adhesion and particle loading on mechanical properties of particulate–polymer composites. *Composites Part B: Engineering*. 2008, vol. 39, pp. 933-961.
 - [105] Bartczak, Z. et al. Toughness mechanism in semi-crystalline polymer blends: II. High-density polyethylene toughened with calcium carbonate filler particles. *Polymer*. 1999, vol. 40, pp. 2347-2365.
 - [106] DEKKERS, M. E. J.; HEIKENS, D. The effect of interfacial adhesion on the tensile behavior of polystyrene–glass-bead composites. *Journal of Applied Polymer Science*. 1983, vol. 28, pp. 3809-3815.
 - [107] HLAVÁČ, J.: *Základy technologie silikátů*. Praha: SNTL, 1988.
 - [108] DAIDO METAL COMPANY LTD. Sliding bearing. Inventors: H. KOBAYAKAWA, C. MCALEESE et al. European patent application. EP2762736 B1. 2.11.2016.
 - [109] TAGLIERI, G. et al. Synthesis and X-Ray Diffraction Analyses of Calcium Hydroxide Nanoparticles in Aqueous Suspension. *Advances in Materials Physics and Chemistry*. 2003, vol. 3, pp. 108-112.
 - [110] DANIELE, V.; TAGLIERI, G.; QUARESIMA, R.: The nanolimes in Cultural Heritage conservation: Characterisation and analysis of the carbonatation process. *Journal of Cultural Heritage*. 2008, vol. 9, pp. 294-301.
 - [111] TAGLIERI, G. et al. Synthesis, Textural and Structural Properties of Calcium Hydroxide Nanoparticles in Hydro-Alcoholic Suspension. *Advances in Materials Physics and Chemistry*. 2014, vol. 4, pp. 50-59
 - [112] PISAROVA L. et al.: Insight into degradation of ammonium-based ionic liquids and comparison of tribological performance between selected intact and altered ionic liquid. *Tribology International*. 2013, vol. 65, pp. 13-27.
 - [113] WIDDER L. et al.: Ristic A, Brenner F, Brenner J, Hutter H. Modified-Atmospheric Pressure-Matrix Assisted Laser Desorption/Ionization Identification of Friction Modifier Additives Oleamid and Ethoxylated Tallow Amines on Varied Metal Target Materials and Tribologically Stressed Steel Surfaces. *Analytical Chemistry*. 2015, vol 87, pp. 11375-11382.
 - [114] HU, J.-Q. et al. Tribological behaviors and mechanism of sulfur- and phosphorus-free organic molybdate ester with zinc dialkyldithiophosphate. *Tribology International*. 2008, vol. 41, pp. 549-55.
 - [115] RUDDNICK, L. R.: *Lubricant additives chemistry and applications*. New York: Marcel Dekker Inc., 2003.
 - [116] ZHANG, J., SPIKES, H. On the Mechanism of ZDDP Antiwear Film Formation. *Tribol Lett*. 2016, vol. 2, pp. 63-24.
 - [117] SAEDI, H. Intercalated Polyamide-Imide Nanocomposite with Montmorillonite. *American Journal of Polymer Science*. 2015, vol. 5, pp. 47-53.
 - [118] LI, F. S.; QIU et al. Polyethyleneimine-Functionalized Polyamide Imide (Torlon) Hollow-Fiber Sorbents for Post-Combustion CO₂ Capture. *ChemSusChem*. 2013, vol. 6, pp. 1216-1223.
 - [119] KATSUKI, H. Et al. *Mixed and Boundary Lubrication Characteristics of Resin Overlay for Plain Bearing Materials*. World Tribology Congress 2013, Torino, Italy. September 2013, pp. 8-13.